University of Alberta

In-situ Stress Magnitude and Core Disking

by

Seong Sik Lim

A thesis submitted to the Faculty of Graduate Studies and Research
in partial fulfillment of the requirements for the degree of

Doctor of Philosophy

in

Geotechnical Engineering

Department of Civil and Environmental Engineering

Dedication

To my daughter Seohyun, my son Doeon and my wife Jooyeon.

ABSTRACT

Accurate measurement of *in situ* stress using surface-drilled deep boreholes is a challenge in high stress regimes in which both horizontal stresses exceed the vertical stress. For such stress regimes core damage and core disking is often observed and these observations were used to constrain the stress state.

Digital image analysis was used to examine the characteristics of microcracks and volumetric strain measurement technique used to quantify stress-induced microcracks in granite-cored samples, obtained in the depth range from ground surface to 1000 m. The results indicate that at depths of less than 200 m, the dominant mode of microcracks can be classed as naturally occurring. The volume of stress-induced microcracks was found to increase linearly with sampling depth with the proportion of grain-boundary, intragranular and transgranular microcracks remaining relatively constant. Moreover it was observed that most of the stress-induced transgranular microcracks formed in a plane perpendicular to the core axis.

Disked cores from boreholes drilled from underground excavations in massive unfractured granite at AECL's Underground Research Laboratory, where the stress magnitudes are known with confidence, were used to establish a relationship between core disk thickness and the stress magnitude. Relationships were established three disk thickness categories; (1) thin (t/D<0.2), (2) medium (0.2<t/D<0.4) and (3) thick (0.4<t/D<2.2) and partial disking. The data suggests that core disking initiates when the maximum principal stress normalized to the tensile strength is 6.5. Stress path analyses indicated that tensile stress controlled the onset of disking.

Three dimensional numerical analyses were carried out to determine the distribution of tensile stresses in the vicinity of the advancing drill bit. A methodology was developed to examine the spatial distribution of the maximum, minimum, and average, maximum tensile stress. A criterion based on the Averaged Maximum Tensile Stress (AMTS) was found to give good agreement with the thickness of field core disks. This approach was then used to establish general core disking nomograms

using site specific geometry, the Brazilian tensile strength, and the AMTS. The approach was applied to two sites and found to be in agreement with field observations.

ACKNOWLEDGEMENT

Table of Contents

List of Tables

List of Figures

Chapter 1

Introduction

Accurate estimation of *in situ* stress for underground development is necessary, whether for development of dam foundations, hydraulic power plants, nuclear waste repositories, underground oil and gas storage facilities, mines, or petroleum extraction sites. As Amadei and Stephansson (1997) note in the case of geological storage design, *in situ* stress could mandate changes in location, excavation method, alignment of underground openings, and associated supporting safety systems.

Various methods have been developed to investigate *in situ* stress, with hydraulic fracturing (Haimson and Fairhurst, 1967) and overcoring (Leeman, 1967) being the most widely used. Over the past twenty years, the technology for both methods has advanced such that each can be used in small diameter boreholes to depths exceeding 500 m. Each method assumes that the rock behaves as a linear, elastic, continuous, homogeneous material. However, many geological environments defy that assumption. For instance, in a thrust fault environment in which the minimum principal stress is vertical, hydraulic fracturing can provide only the weight of the overburden (data that can be calculated from the weight of rock mass), but not the magnitude of either horizontal *in situ* stress. Additionally, once stress magnitudes exceed critical values during coring, the results are core damage, including stress-induced microcracking and core disking. Drilling-induced core damage undermines the reliability of overcoring tests for *in situ* stress (Doe et al., 2006; SKB, 2005). Such situations, therefore, require additional information to constrain stress

1

magnitudes and directions.

Stress-estimation techniques based on core damage may be used in the early stages of a project. The most common stress-estimation methods using damaged core samples are strain recovery techniques and core disking analysis (Amadei and Stephansson, 1997; Ljunggren et al., 2003). Anelastic strain recovery (ASR) and differential strain curve analysis (DSCA) employ the amount of strain recovery to estimate the *in situ* stress state. These methods measure strain behavior from microcrack opening and closing in the extracted cores, and are useful in the early stage (at high stress regions and at great depth) where the direct stress measurement methods are either inapplicable or unreliable. One of the main assumptions of those methods is that the stress induced microcracks are primarily aligned with the direction of original *in situ* stress (Strickland and Ren, 1980; Teufel, 1982). Thus, the magnitude and direction of principal stresses are coincident with the amount of microcrack opening and closing. It is well known that stress-induced microcracks align perpendicular to the drill core axis and hence, these stress induced microcracks may easily limit the reliability of this method (Martin and Stimpson, 1994).

Since the 1960s, researchers have extensively investigated core disking. Previous studies significantly illuminated the core disking mechanism, demonstrating the possibilities for applying the technique to *in situ* stress estimation. However, those studies were restricted to laboratory tests and/or numerical analysis. The laboratory tests often used small diameter cores and showed large scale effects while the numerical analysis were limited by the assumptions made regarding the disking process and the numerical software.

This dissertation investigates the relationship between the magnitude of *in situ* stress and stress-induced core damage using field observations, and will establish:

- the characteristics of natural and stress-induced microcracks from microscopic image analysis, and

- the relationship between the amount of stress-induced microcracks and *in situ* stress magnitude in a thrust fault stress environment.

This dissertation will also investigate:

- the relationship between core disk thickness and the magnitude of *in situ* stress using the field core disking data, and

- the core disking criteria based on the numerical stress analysis in conjunction with field observations.

1.1 *In situ* stress

Unlike artificial materials such as concrete and steel, natural materials such as rock and soil are subject to natural (virgin) stresses called *in situ* stresses, which fall into four categories named for their causes (Amadei and Stephansson, 1997):

1. Gravitational, a mass of overburden material,

2. Tectonic, divided into two classes based on the timing of tectonic events: active tectonic stresses due to current tectonic activity, and remnant tectonic stresses due to past tectonic events,

3. Residual, a remaining stress in a material after the external force is removed, and

4. Terrestrial, induced by diurnal and seasonal variations of temperature, lunar pull, and the Coriolis force.

Because geologic materials face combinations of the above *in situ* stresses, determining the stress history can be difficult. The distribution of *in situ* stress is complicated by depth and location due to different generation history. Brown and Hoek (1978) summarized *in situ* stress measurement data obtained from various geological environments. Figure 1.1 shows the proposed relation of vertical stress (σ_v) and the average horizontal stress (σ_{ha}) against depth. Equation (1.1) and (1.2) represent the trend of those two relationships respectively.
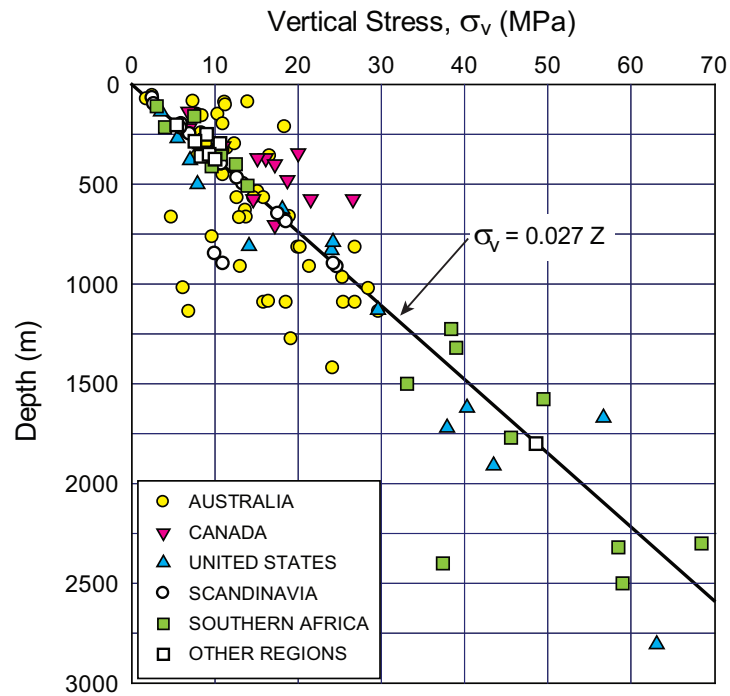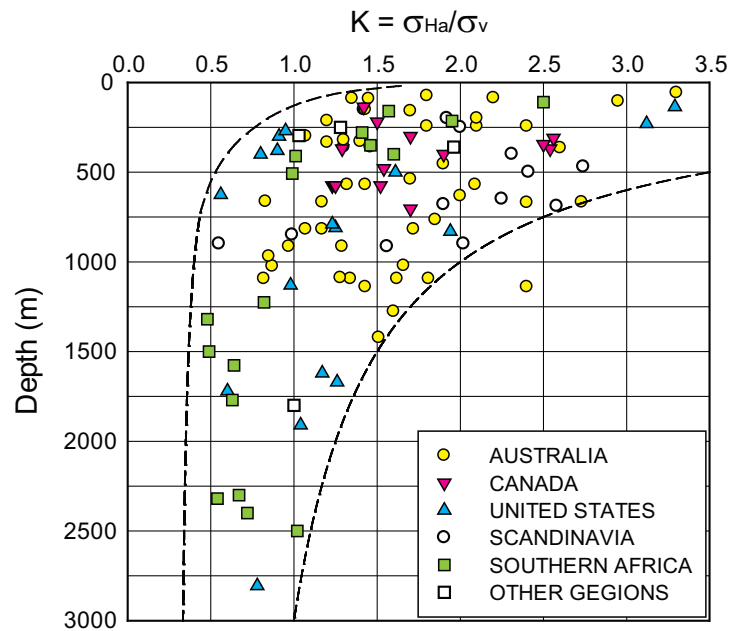
Figure 1.1: The vertical and average horizontal stress ratio versus depth (after Brown and Hoek (1978)).

$$\sigma_v = 0.027Z \tag{1.1}$$

$$\sigma_1 = \frac{100}{Z} + 0.30 \leq K \leq \frac{1500}{Z} + 0.50 \tag{1.2}$$

Z: depth (m)

K: the ratio of average horizontal to vertical stress

1.2   *In situ* stress measurement methods in rock

Over the last fifty years, researchers have developed and applied various methods for estimation of *in situ* rock stress in the field (Amadei and Stephansson, 1997). Ljunggren et al. (2003) categorized rock stress measurement techniques based on operational type as shown in Table 1.1. The volume associated with each method is also given in Table 1.1. Because of these different approaches, measurement techniques and associated rock mass volumes, there is often no correlation between the different methods.

The *in situ* stress measurement categories describe in Table 1.1 can be classed into two main groups. Techniques in the first group include the two common traditional direct methods (hydraulic fracturing and overcoring) performed in boreholes and are carried out when the stress magnitudes and orientations need to be established with confidence for the design of underground excavations. Techniques in the second group can only estimate *in situ* stress states based on observations of rock behavior and these techniques are referred to as stress indicators. Borehole breakout is the stress indicator measured from damage to the borehole wall; strain recovery methods and core disking analysis are the stress indicators interpreted from core damage. The indirect techniques are typically employed when the traditional direct methods meet their limitations. However, it should be noted that the confidence in the magnitudes derived from these indirect methods is typically very low as there is seldom field verification of the magnitude estimates made by these methods and the actual *in situ* stress magnitudes.

Table 1.1: Methods for rock stress measurement classified by operational type (after Ljunggren et al. (2003))

Category	Method	Rock Volume (m^3)
Methods performed in boreholes	Hydraulic fracturing	$0.5 - 50$
	Overcoring	$10^{-3} - 10^{-2}$
	HTPF	$1 - 10$
	Borehole breakouts	$10^{-2} - 100$
Methods performed using drill cores	Core disking	10^{-3}
	Strain recovery methods	10^{-3}
	Acoustic methods (Kaiser effect)	10^{-3}
Methods performed on rock surfaces	Jacking methods	$0.5 - 2$
	Surface relief methods	$1 - 2$
Analysis of large-scale geological structures	Earthquake focal mechanism	10^9
	Fault slip analysis	10^8
Other	Relief of large rock volumes	$10^2 - 10^3$

1.3 Difficulties of *in situ* stress measurement

There are uncertainties associated with all stress measurement techniques, and these uncertainties make precise and accurate *in situ* stress measurements impossible. The uncertainties can be categorized into three types based on their source: 1) natural (intrinsic), 2) measurement-related, and 3) data-analytical (Amadei and Stephansson, 1997).

Natural uncertainty arises primarily from local variations of mechanical properties, geological structures, and fabric and grain size of rock mass. This local variation is closely related to the volume of the rock mass which must be considered for stress measurement. For example, Aytmatov (1986) reported that the Young′s modulus of granitic rock changed up to 25% over a 5 m borehole length, which would change the stress magnitude from the overcoring method by a similar amount.

Measurement-related errors occur because of the measuring instruments themselves and/or from the experimental procedure. The main errors, for overcoring tests, arise from strain gauge deterioration due to microcrack damage or breaks of borehole walls or cores, poor glue quality causing creep, yield of the adhesive and detachment of gauges from pilot hole walls, temperature change due to drilling water, and

drill bit induced heat affecting the measuring sensors, and other various technical problems (Hakala et al., 2003; Cai and Thomas, 1993; Irvin et al., 1987). Martin and christiansson (1991) found that the magnitude of principal stress could be changed about 25% with 8^oC of temperature variation.

Uncertainty related to data analysis usually occurs during data selection among extensive data sets or components which may include exceptional measurement values. Errors may also arise during data analysis based on assumptions that the rock is a linear, elastic, isotropic, continuous, and homogeneous material, which many geological regimes violate.

Amadei and Stephansson (1997) suggest three methods to reduce uncertainties: (1) conduct laboratory tests to identify the limitations, accuracy, and performance of instruments, (2) discard bad data outside statistical deviations to constrain the range of proper measurements, and (3) compare stress measurements in the same borehole obtained with the same method, or compare parallel measurements obtained with different methods. This process could constrain the *in situ* stress magnitude and orientation.

1.4 Research objectives

During core drilling in a stressed rock mass, stress is concentrated at the drilling point, generating microcracks in the core samples. Stress-induced microcracking increases with depth due to elevated *in situ* stress magnitude, and eventually causes core disking - the extreme form of microcracking. Martin and Stimpson (1994) noted that stress-induced core damage is a progressive phenomenon as a function of *in situ* stress magnitude.

This research seeks to establish the relationship between *in situ* stress magnitude and the degree of stress-induced microcracking and core disking, by investigating: 1) the quantification of stress-induced microcrack volume, 2) the correlation between field core disking data and *in situ* stress magnitude, and 3) the establishment of core disking criteria from numerical analysis. The detailed research objectives

7

are:

1. Quantification of stress-induced microcracks

   - Explore the characteristics of natural and stress-induced microcracks.

   - Explore the aspect of microcrack closure during the compression testing.

   - Establish a correlation between microcrack volumetric strain and *in situ* stress magnitude.

2. Analysis of field core disking data

   - Establish a correlation between core disk thickness and stress magnitude.

   - Characterize the core disking fracture in terms of disk thickness, fracture persistence, rock types, and observed zone.

3. Numerical modeling for core disking

   - Explore the core disking mechanism and disking initiation stress by using the numerical analysis in conjunction with field core disking data.

   - Establish the core disking criteria applicable to the relevant fields.

1.5 Thesis outline

The dissertation, presented in paper-based format, consists of three main chapters, supplemented by two appendices. Each main chapter is an article prepared for submission to a peer reviewed journal and includes an independent literature review and citations. Chapter 3 was published in Engineering Geology Journal (Lim et al., 2012), Chapter 4 was published in International Journal of Rock Mechanics and Mining Sciences (IJRMMS) (Lim and Martin, 2010), and Chapter 5 was submitted to Rock Mechanics and Rock Engineering Journal in December 2012. Two other papers published in conference proceedings appear in the Appendices (Lim et al., 2006, 2007).

Chapter 1 introduces the motive and objectives for the research, and outlines the organization of the dissertation.

Chapter 2 provides the literature background of research interest. Definitions and characteristics of natural and stress-induced microcracks and analysis appear with discussion of the origin and types of those microcracks. The chapter also illustrates the quantification method for microcrack volume. For core disking studies, it includes definitions and explanations of failure mechanisms, failure criteria, and issues relevant to core disking, followed by discussion of the limitations of previous approaches.

Chapter 3 presents the quantification work of the stress-induced microcracks, by 1) measuring microcrack volumes from the initial loading stages of the extracted cores, 2) establishing *in situ* stress profiles at the investigated sites, 3) attempting correlation work between stress-induced microcrack volume and *in situ* stress magnitude, 4) using included microscopic image analysis to discern the origin and characteristics of natural and stress-induced microcracks, and 5) measuring and analyzing microcrack type, density, length, orientation, as well as grain size.

Chapter 4 presents the investigation process for establishing the relationship between core disk thickness and *in situ* stress magnitude. The study includes: 1) the characterization of core disk thickness, surface geometry, and fracture persistence, 2) the 3D numerical stress analysis for estimating stress magnitude in which the core disks are observed, 3) the correlation work between maximum principal stress and core disk thickness for Lac du Bonnet granite and granodiorite, and 4) the categorization work based on the characteristics of the core disk and the established correlation.

Chapter 5 analyzes the numerical modeling of core disking, by 1) discussing the discrepancy between observed field core disking data and the estimated core disking thickness of the existing tensile stress criterion, 2) introducing core disking criteria based on the averaged maximum tensile stress (AMTS) in conjunction with field core disking data, and 3) applying the introduced criterion to the fields to estimate

in situ stress from core disking observation.

Chapter 6 summarizes and concludes the entire research project including the suggestion of future works.

The Appendices are two papers published in conference proceedings. The first paper (Lim et al., 2007) discusses the study of stress-induced microcracks using crack closure energy, explaining the purpose of Chapter 3. The second paper (Lim et al., 2006) discusses core disking analysis and its implications for a field, and forms the beginning of the work for Chapter 4 and Chapter 5.

Bibliography

Amadei, B., Stephansson, O. 1997. *Rock Stress and Its Measurement*. First ed. Chapman & Hall, London.

Aytmatov, I.T. 1986. On virgin stress state of a rock mass in mobile folded areas. In: *Proc. Int. Symp. on Rock Stress and Rock Stress Measurements*, *Stockholm*, pp. 55–59.

Brown, E.T., Hoek, E. 1978. Trends in relationships between measured and *in situ* stresses and depth. *Int. J. Rock Mech. Min. Sci.* 15: 211–215.

Cai, M., Thomas, L.J. 1993. Performance of overcoring stress measurement device in various rock types and conditions. *Timm*. 102: 134–140.

Doe T.W., Zieger M, Enachescu C., Cohner J.B. 2006 In-situ stress measurements in exploratory boreholes. *Felsbau*. 24 (4): 39–47.

Haimson, B., Fairhurst, C. 1967. Initiation and extension of hydraulic fractures in rocks. *Socitey of Petroleum Engineers Journal*. 310–318.

Hakala, M., Hudson, J.A., Christiansson, R. 2003. Quality control of overcoring stress measurement data. *Int. J. Rock Mech. Min. Sci.* 40(7-8): 1141–1159.

Irvin, R.A., Garritty, P., Farmer, I.W. 1987. The effet of boundary yield on the results of *in situ* stress measurements using overcoring techniques. *Int. J. Rock Mech. Min. Sci.* 24(1): 89–93.

Leeman, E.R. 1967. The borehole deformation type of rock stress measuring instrument. *Int. J. Rock Mech. Min. Sci.* 4(1): 23–44.

Lim, S.S., Martin, C.D. 2010. Core disking and its relationship with stress magnitude for Lac du Bonnet granite. *Int. J. Rock Mech. Min. Sci.* 47(2): 254–264.

Lim, S.S., Martin, C.D., Akesson, U. 2012. In-situ stress and microcracking in granite cores with depth. *Engineering Geology* 147: 1–13.

Lim, S.S., Martin, C.D., Christiansson, R. 2006. Estimating in-situ stress magnitudes from core disking In: *Proceedings of International Symposium on In-situ Rock Stress*, *Trondheim*. Lu, M., Li, C.C., Kjorholt, H., Dahle, H. *editors*. A.A. Balkema, Rotterdam, pp. 159–166.

Lim, S.S., Martin, C.D., Christiansson, R. 2007. In-situ stress estimation using crack closure energy in crystalline rock. In: *Proceedings 1st Canada-U.S. Rock Mechanics Symposium*, *Vancouver*. Eberhardt, E., Stead, D., Morrison, T. *editors*. Taylor & Francis Group, London, pp. 683–689.

Ljunggren, C., Changa, Y., Janson, T. 2003. An overview of rock stress measurement methods. *Int. J. Rock Mech. Min. Sci.* 40(7-8): 975–989.

Martin, C.D., Christiansson, R. 1991. Overcoring in highly stressed granite – The influence of microcracking. *Int. J. Rock Mech. Min. Sci.* 28(1): 53-70.

Martin, C.D., Stimpson, B. 1994. The effect of sample disturbance on laboratory properties of Lac du Bonnet granite. *Can. Geotech. J.* 31(5): 692–702.

SKB 2005. Preliminary site description Forsmark area - version 1.2. *SKB-R-05-18*, Swedish Nuclear Fuel and Waste Management Co., Stockholm.

Strickland, F.G., Ren, N.K. 1980. Prediction of hydraulic fracture azimuth from anelastic strain recovery measurements of oriented core. In: *Proc. 21th U.S. Symp. on Rock Mechanics*, *Rolla*. Amadei, Kranz, Scoot, *editors*. University of Missouri, pp. 523–532.

Teufel, L.W. 1982. Prediction of hydraulic fracture azimuth from anelastic strain recovery measurements of oriented core. In: *Proc. 23th U.S. Symp. on Rock Mechanics*, *Berkeley*. Amadei, Kranz, Scoot, *editors*. SME/AIME, pp. 238–245.

Chapter 2

Background

2.1 Microcracks

Extracting core from deep boreholes can lead to significant increases in microcrack porosity commonly referred to as sample disturbance or stress-induced core damage (Chernis, 1984; Martin and Stimpson, 1994). These microcracks affect the physical properties of intact rock such as strength, compressibility, elastic wave velocities, permeability and electrical conductivity (Chernis, 1984; Martin and Stimpson, 1994; Kranz, 1983; Simmons and Richter, 1976; Wang and Simmons, 1978). Chernis (1984) examined samples of Lac du Bonnet (LdB) granite using a Scanning Electron Microscope (SEM) to determine the types of microcracks, i.e., grainboundary, intragranular, and transgranular, and concluded that the origins and types of microcracks strongly affect the physical properties of the rock samples.

2.1.1 Origin and types of microcracks

Microcracks in crystalline rocks nucleate when local stresses exceed the local strength, and can be classed as: 1) natural microcracks existing over geological time that are formed by natural processes, and 2) drilling-induced (stress-induced) microcracks produced by stress changes associated with coring (Nur and Simmons, 1970). Naturally-formed microcracks in granitic rocks arise from stress changes associated with isobaric cooling and isothermal decompression of rock from its original

hydrostatic stress condition (Vollbrecht et al., 1991; Nadan and Engelder, 2009). In contrast, drilling-induced (stress-induced) microcracks are nucleated by artificial stress change generated when rock is removed from its original subterranean environment.

Natural microcracks

Thermal cooling and decompression as rock mass evolves over geological time are the primary causes of these local internal stresses (Nur and Simmons, 1970; Vollbrecht et al., 1991; Nadan and Engelder, 2009). Nadan and Engelder (2009) examined microcracking mechanisms in New England granites and suggested that during solidification, rock mass experienced initial isobaric cooling under laterally constrained boundaries, creating deviatoric stress conditions. This lateral unloading and high vertical compressive stress produces vertically aligned microcracks. After isobaric cooling, the rock mass will be exhumed, removing the overburden stress. Nadan and Engelder (2009) suggest that the latter process causes additional cooling and decompression of rock, generating high horizontal stresses and horizontally aligned microcracks. Figure 2.1a illustrates both processes leading to the formation of natural microcracks. As Brace et al. (1972) note, natural microcracks seldom form sharp fracture surfaces. The contact surfaces of such fractures are serrated with rounded contact points, likely reflecting their formation over geological time (see Figure 2.1b).

Stress-induced microcracks

The thin slot produced during drilling concentrates and redistributes *in situ* stresses. Any magnitude of concentrated stresses exceeding the stress required to initiate microcracking will generate the stress-induced fractures (Obert and Stephenson, 1965; Stacey, 1982; Dyke, 1988; Martin and Stimpson, 1994; Lim and Martin, 2010). Figure 2.2a illustrates the origin of stress-induced microcracks and core disking, the extreme form of microcracking in a drilling context. Wang and Simmons (1978) also suggested that intact rocks are essentially crack-free *in situ*, and that microc-

14

(a)

(b)
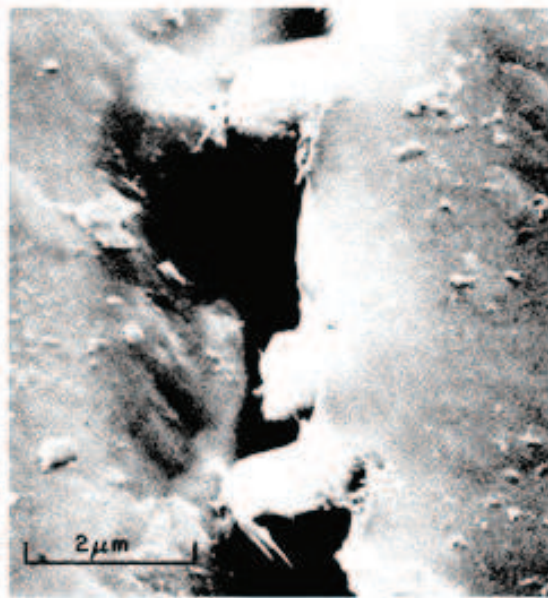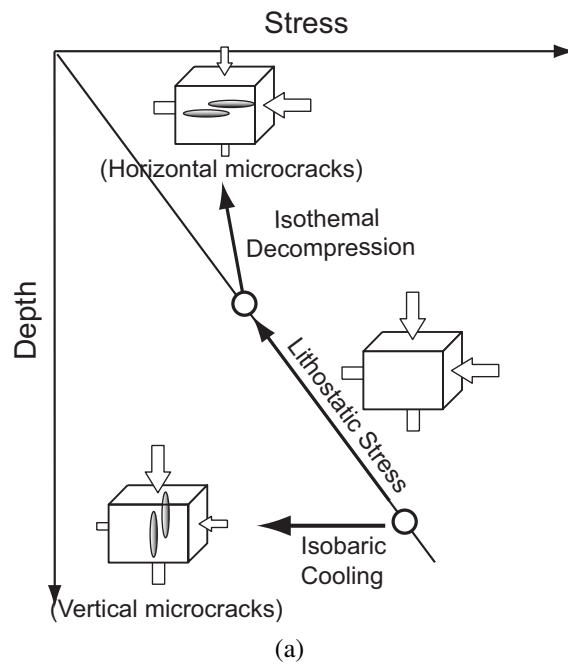
Figure 2.1: Illustration of the origin of natural microcracks: (a) Geological processes involved in the formation of natural microcracks (modified from Nadan and Engelder (2009)) and (b) an example of a natural microcracks, taken with a Scanning Electron Microscope (SEM) (after Chernis (1984)).
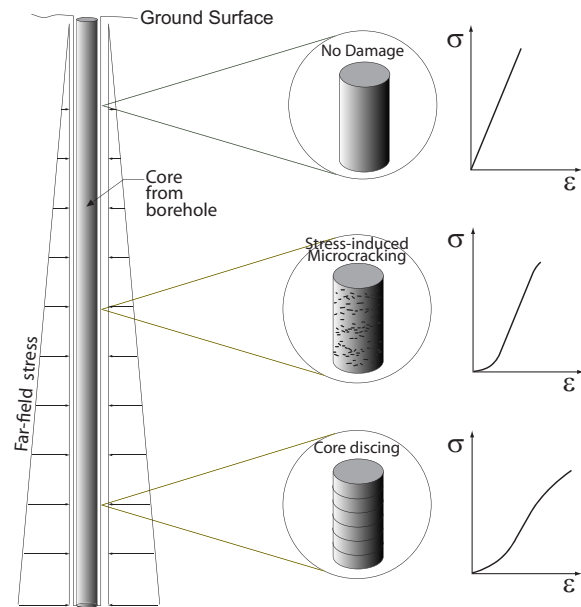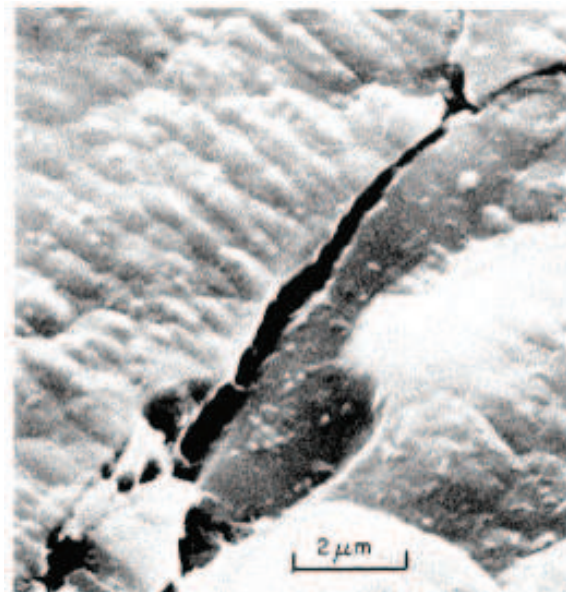
Figure 2.2: Illustration of the origin of stress-induced microcracks. (a) Formation of stress-induced core damage during drilling (modified from Martin and Stimpson (1994) and (b) An example of stress-induced microcrack taken with a SEM (after Chernis (1984)).

racks open during stress-relief coring. Their laboratory findings and *in situ* studies support their suggestion by showing that *in situ* seismic velocities were nearly constant, whereas the measured laboratory velocities decreased with sampling depth.

Stress-induced microcracks show different physical characteristics from natural microcracks. From the optical and scanning electron microscope observations of Illinois granite, Kowallis and Wang (1983) found that stress-induced microcracks are long and narrow, and lack alteration and secondary mineralization. In their study, stress-induced microcracks developed primarily along the pre-existing healed cracks and cleavage planes in feldspar. Based on microscopic observation of rock samples from different depths, Chernis (1984) noted that while natural microcracks have irregular walls, rounded edges, and small infillings, stress-induced microcracks show sharp-ended, parallel-walled, and echelon features (see Figure 2.1b and Figure 2.2b).

Many researchers observed stress-induced microcracking and core damage (Chernis, 1984; Wang and Simmons, 1978; Carlson and Wang, 1986; Martin and Stimpson, 1994). Chernis (1984) observed that granite core samples extracted from about 800 m contained more than double the number of stress-induced microcracks compared with the samples obtained from 400 m depth. Chernis (1984) found that stress-induced microcracks in deep samples increased porosity and permeability, and decreased elastic wave velocity of core samples. Figure 2.3 shows the clear indication of sample damage affecting laboratory properties of rock. Martin and Stimpson (1994) also noted that core sample strength in high-stress regions does not reflect their *in situ* strength. Uniaxial compressive and tensile strengths were reduced up to 30% and 60% respectively, with significant cohesion loss (up to 70%) among the damaged samples.

Stress-induced transgranular microcracks increase the porosity and permeability of rock while reducing its strength, but the natural grain boundary microcracks had little effect on these properties. Martin and Stimpson (1994) investigated the sample disturbance caused by the stress-induced microcracks using the laboratory mechanical properties for LdB granite cores extracted from depths ranging from

17
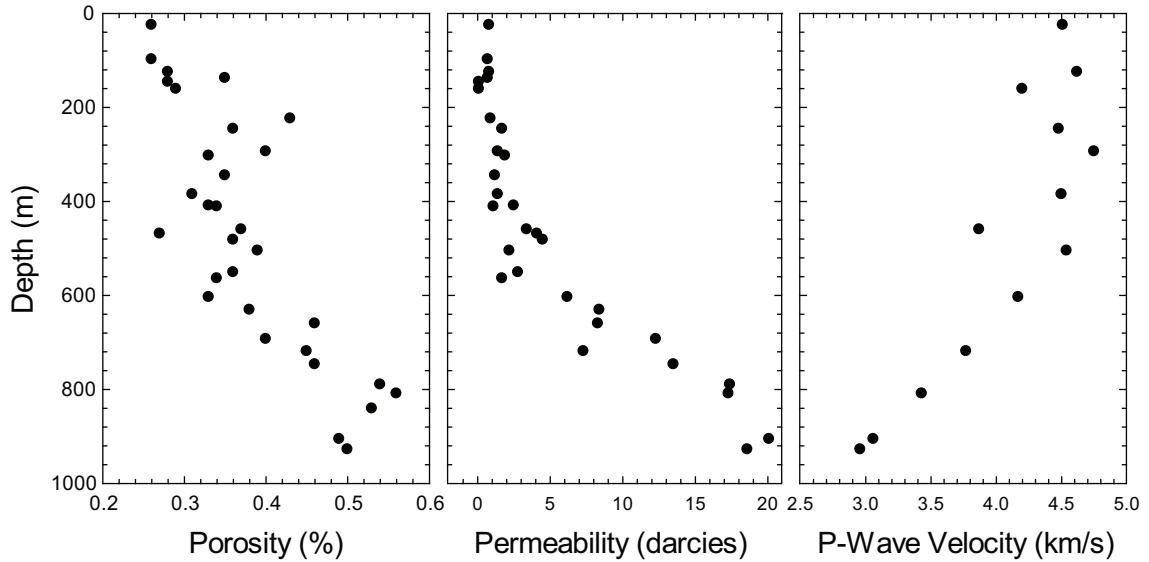
Figure 2.3: Laboratory properties versus depth at URL, Canada (data from Chernis (1984))

ground surface to 1000 m. They found that the strength, P-wave velocity, and tangent Young's modulus of the granite samples decrease as the magnitude of *in situ* stresses increases. Martin and Stimpson (1994) suggested that the stress-induced microcracking affecting laboratory properties begins when maximum stress reaches a critical threshold.

Microcracks can also influence *in situ* stress results from overcore measurements. Martin and christiansson (1991) found that microcracks induced during overcore drilling create modulus anisotropy in overcore samples, influencing both the orientations and magnitudes of the *in situ* principal stresses. On the other hand, techniques such as anelastic strain recovery (ASR) and differential strain curve analysis (DSCA) use microcracks and the rate of microcracking to estimate *in situ* stress magnitudes (Amadei and Stephansson, 1997). The characteristics and quantity of microcracks measured in core samples may provide indirect evidence of *in situ* stress magnitudes.

2.1.2 Measurement of microcrack volume

Numerous researchers attempted to quantify the microcrack volume for low porosity rock core samples (Stephens, 1964; Walsh, 1965; Brace, 1965; Simmons and Siegfried, 1974; Siegfried and Simmons, 1978; Ren and Roegiers, 1983; Martin and Stimpson, 1994; Jacobsson et al., 2007). Walsh (1965) proposed the pressure and volumetric strain relation under hydrostatic loading condition (see Figure 2.4). At pressure P_c, which is the pressure that all pores and microcracks are completely closed, the responding volumetric strain $\varepsilon_v(P_c)$ can be divided into two parts: 1) the volumetric strain caused by microcrack porosity (η_0), and 2) the volumetric strain representing the linear elastic compressibility of the intact rock (βP_c). Thus, microcrack volumetric strain can be calculated using following equation:
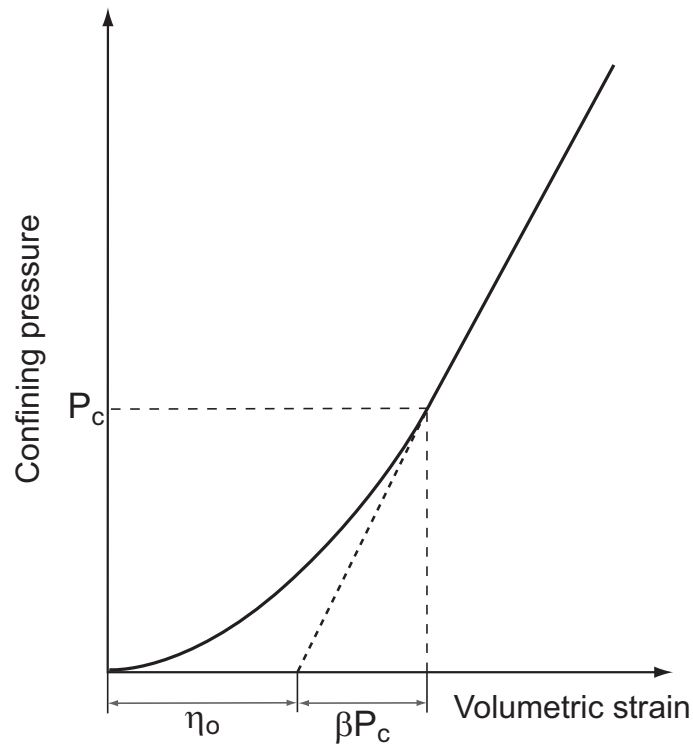
Figure 2.4: Confining pressure versus volumetric strain curve for a low porosity rock sample. P_c: confining pressure when all pores and microcracks are completely closed. η_0: microcrack porosity, βP_c: linear elastic compressibility (modified from Walsh (1965)).

$$\eta_0(P_c) = \varepsilon_v(P_c) - \beta P_c, \quad \beta = \frac{3(1 - 2\nu)}{E} \tag{2.1}$$

Brace (1965) applied the concept to cylindrical rock core samples and found the linear compressibility for the low porosity rocks can be reached within 100 MPa. Simmons and Siegfried (1974) and Siegfried and Simmons (1978) developed the differential strain analysis (DSA) method to measure microcrack porosity based on the work of Walsh (1965). Later Strickland and Ren (1980) proposed the differential strain curve analysis (DSCA) method to trace the history of *in situ* stress based on the degree of microcracking.

From measuring microcrack porosity using the DSA technique, Carlson and Wang (1986) established a correlation between volumetric crack porosity and mean *in situ* stress for the granite cores taken from 0.7 to 1.6 km depth from Illinois Deep Hole UPH 3. Carlson and Wang (1986) found the increasing trend of microcrack porosity
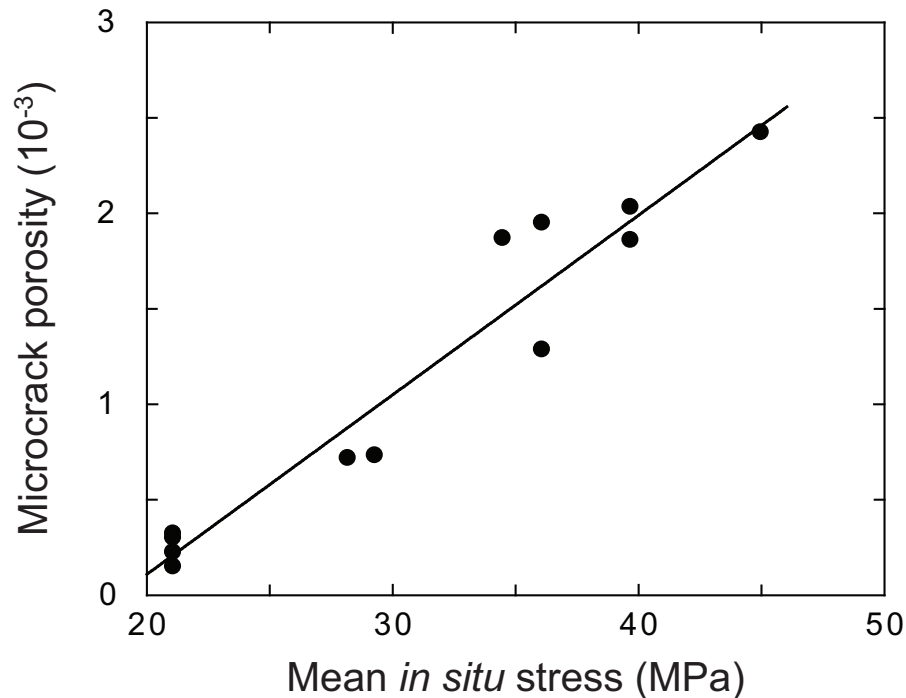
Figure 2.5: Microcrack porosity versus mean *in situ* stress (data from Carlson and Wang (1986)).

with core sampling depth, and measured *in situ* stress using the hydraulic fracturing test of Haimson and Doe (1983), and demonstrated a linear correlation between mean *in situ* stress and microcrack porosity with depth (see Figure 2.5).

2.2 Core disking

Core disking is a phenomenon in which the drilled core disks with uniform spacing and shape due to the transient stress changes, and stress release during drilling. Solid core disking occurs during normal coring; ring-core disking occurs during overcoring. Figure 2.6 shows typical (a) solid core disking and (b) ring-core disking samples obtained from the Underground Research Laboratory (URL), Canada and Forsmark, Sweden respectively.

The investigation of the core disking mechanism and its application to estimating *in situ* stress state began in the early 1960s. The literature review summarizes the main issues for investigating core disking (see Table 2.1):

(a)

(b)

Figure 2.6: Typical core disking: (a) Solid core disking and (b) Ring-core disking.

1. Failure mechanism and criteria - tension/shear/extension strain

2. Disking fracture initiation and propagation - core axis/core surface/ throughout the entire core, above the drill bit bottom/same level with drill bit bottom/ below the drill bit bottom

3. Influence factors

   - *In situ* stress magnitude and orientation

   - Properties of rock (UCS, tensile strength, Poisson′s ratio, grain size, texture, etc.)

   - Geometry of borehole bottom

   - Drill bit pressure and pore pressure

   - Scale of drill bit

4. The relationship between *in situ* stress magnitude and core disk thickness

5. The relationship between *in situ* stress orientation and core disk shape

Table 2.1: Literature review for core disking studies.

Author/Year	Investigation method	Failure Mechanism	Failure criterion	Fracture initiation points	Disk thickness	Disk shape
Jaeger and Cook (1963)	Laboratory test (Biaxial test)	Tension	The load stress at failure is of the order of the unconfined compressive strength (60 % of UCS)	Axis of the core (Core center)	Disks thickness decreases as the stress increases	Slightly cup-shape
Obert and Stephenson (1965)	Laboratory test (Conventional triaxial test)	Shear	$\sigma_r = K_1 + K_2\sigma_a$, $K_1 = -3400(Psi) - 2.0\ S_0$, σ_r: applied radial stress, σ_a: applied axial stress, K_1: σ_r axis intercept, K_2: slope of the least square line, S_0: shear strength	Exterior surface of the core	The disks produced at higher stress values are thinner	–

Author/Year	Investigation method	Failure Mechanism	Failure criterion	Fracture initiation points	Disk thickness	Disk shape
Durelli et al. (1968)	Laboratory test (Photoelastic model)	Shear	$\sigma_r = \sigma_t/5 + 0.3\sigma_a$, σ_r: applied radial stress, σ_a: applied axial stress, σ_t: tangential stress acting in a cut boundary	Lowest point in the borehole bottom area (at the point of maximum shear stress)	–	–
Sugawara et al. (1978)	Numerical modeling (FEM 3D) & Laboratory test (Triaxial test)	Tension	$1/2(Px + Py) \geq -4\sigma_t + Pz$, $2.5 \geq Px/Py \geq 0.4$, Pz: axial stress, Px, Py: radial stresses, σ_t: Brazilian tensile strength	Root of the core stub	Required radial stress should be increased to get thinner disks	–
Stacey (1982)	Numerical modeling (FEM 2D)	Extension strain	$e \geq e_c$, e_c: critical extension strain, e: $1/E[\sigma_3 - \nu(\sigma_1 + \sigma_2)]$, σ_1, σ_2, σ_3: principal stresses, E: modulus of elasticity, ν: Poisson's ratio	External core boundary, core axis, or ahead of the borehole bottom	–	Concave
Dyke (1989)	Numerical modeling (BEM 3D)	Tension		Surface of core/ Interior of core simultaneously	–	Concave/ Saddle
Haimson and Lee (1995)	Laboratory test (Triaxial test)	Tension	$T_d = 238.03\sigma_H^{-0.88} + 0.008\sigma_h + 0.003\sigma_v - 0.023$, T_d: disk thickness, σ_H, σ_h, σ_v: maximum horizontal, minimum horizontal and vertical far-field stress respectively	At the exterior of core stub in the minumum horizontal far-field stress side	The thickness decreases with increasing maximum horizontal stress	Saddle
Li and Schmitt (1997)	Numerical modeling (FEM 3D)	Tension	When generated tensile stress exceeds the tensile strength of rock	Cup-shape: at the root of the core away from the cut. Saddle/ Petal shape: at the inner corner of the borehole bottom	Disk thickness is always less than 25% of core diameter. The higher stresses produce thinner core disks.	Cup/ Saddle/ Petal

Continued on next page

24

Author/Year	Investigation method	Failure Mechanism	Failure criterion	Fracture initiation points	Disk thickness	Disk shape
Hakala (1999a)	Numerical modeling (FDM-FLAC 3D)	Combined yield/ Tension	When generated tensile stress exceeds the tensile strength of rock	Normal coring: core side (in the root/on the top), Overcoring: pilot hole wall/ at the top edge of pilot hole wall	$(0.12-1) \times D$, D: core diameter	Flat/ Cup/ Saddle/ Petal/ Ring
Kaga et al. (2003)	Numerical modeling (FEM 3D)	Tension	$\sigma_t = -A\sigma_m + B\sigma_z - C\sigma_x^2/\sigma_m - D(\sigma_x - \sigma_y)$, A, B, C, D: coefficients that depend on the core length	Throughout the core stub	Any length of disk thickness	–
Corthesy and Leite (2008)	Numerical modeling (FDM - FLAC 2D)	Tension	When generated tensile stress exceeds the tensile strength of rock	Center of the core	–	Flat

2.2.1 Core disking failure mechanism

Extensive research explores the failure mechanism of core disking, suggesting three major failure mechanisms: tensile failure, shear failure, and extension strain failure; and combinations of them.

Tensile failure mechanism

Jaeger and Cook (1963) initially suggested the tensile failure mechanism. During a lateral loading test with rock specimens, they found that core disking occurred when applied lateral stress reached nearly double the tensile strength of the rock. Later Sugawara et al. (1978), Dyke (1988), Li and Schmitt (1997), Hakala (1999b) and most recently Kaga et al. (2003) also suggested the tensile failure mechanism.

Kaga et al. (2003) suggested the principal tensile stress failure mechanism based on the 3D numerical analysis using a finite element method (FEM). Figure 2.7 shows the schematic cross-sectional view explaining the failure mechanism. According to Kaga et al. (2003), the generated tensile stress on the core stub increases because of

drill bit advancement, and the contour of principal tensile stress changes from (a) to (c). Core disking occurs when the principal tensile stress contour distributes like (b), and the magnitude of tensile principal stress reaches the tensile strength of the rock. Kaga et al. (2003) suggested a single formulation as a core disking criterion, described in Equation (2.2).

$$S_t = -A\sigma_m + B\sigma_x - C\sigma_x^2 - D(\sigma_x - \sigma_y) \qquad (2.2)$$

S_t: critical tensile stress

A, B, C, D: coefficients as a function of core length

$\sigma_m = \sigma_x + \sigma_y + \sigma_z$

$\sigma_x, \sigma_y, \sigma_z$: applied stresses

Principal tensile stress zone

(a)   (b)   (C)
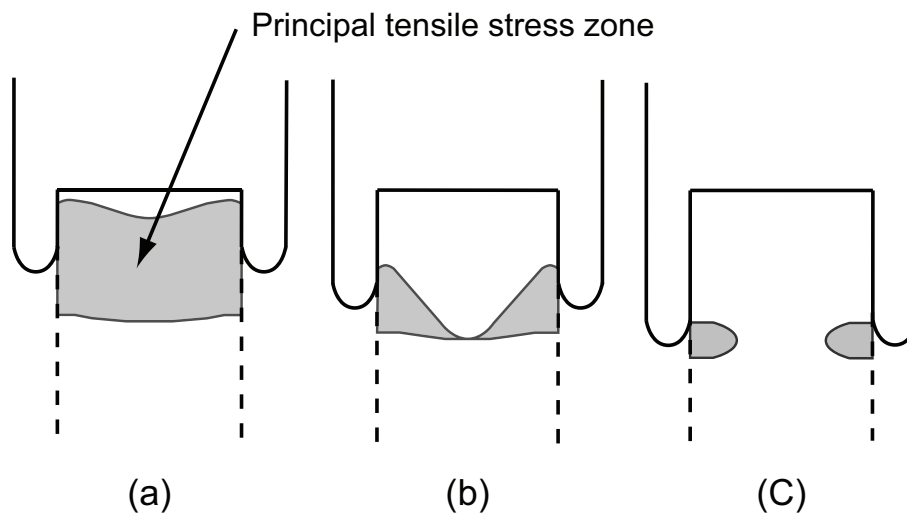
Figure 2.7: Schematic cross-sectional views of contour planes of tensile principal stress (modified from Kaga et al. (2003)).

Shear failure mechanism

Obert and Stephenson (1965) conducted an extensive laboratory traditional triaxial compression test to explore the core disking mechanism and disking initiation stress criterion. Based on their results, Obert and Stephenson (1965) insisted that

shear stress generates core disks. They found that rupture lines on the surface of Maryland marble were highly similar to shear lines appearing on the surface of triaxially loaded specimens. Obert and Stephenson (1965) also noted that neither purely tensile stress nor compression stress has ever produced rupture lines. Obert and Stephenson (1965) suggested the following equation as a core disking criterion.

$$\sigma_r = K_1 + K_2 \, \sigma_a, \quad K_1 = 23.44 + 2S_o \tag{2.3}$$

σ_r: applied radial stress

σ_a: applied axial stress

K_1: σ_r axis intercept

K_2: slope of the least square line

S_o: shear strength (cohesion)

Figure 2.8 shows the linear function of K_1 versus the shear strength for five different rock types. Durelli et al. (1968) also suggested the shear failure mechanism. According to Durelli et al. (1968), core disking begins at the point of maximum shear stress, and the required magnitude of the shear stress is much larger than the shear strength of the rock.

Extension strain failure mechanism

Stacey (1981) introduced the extension strain criterion for initiation of a fracture in brittle rock. According to the theory, fractures begin when the total extension strain in the rock exceeds a critical value. Stacey (1981) suggested that core disking fracture also follows the role of extension strain failure criterion, expressed as Equation (2.4).

$$\varepsilon > \varepsilon_c \tag{2.4}$$

where ε_c is the critical value of extension strain for the rock. Fractures form in the
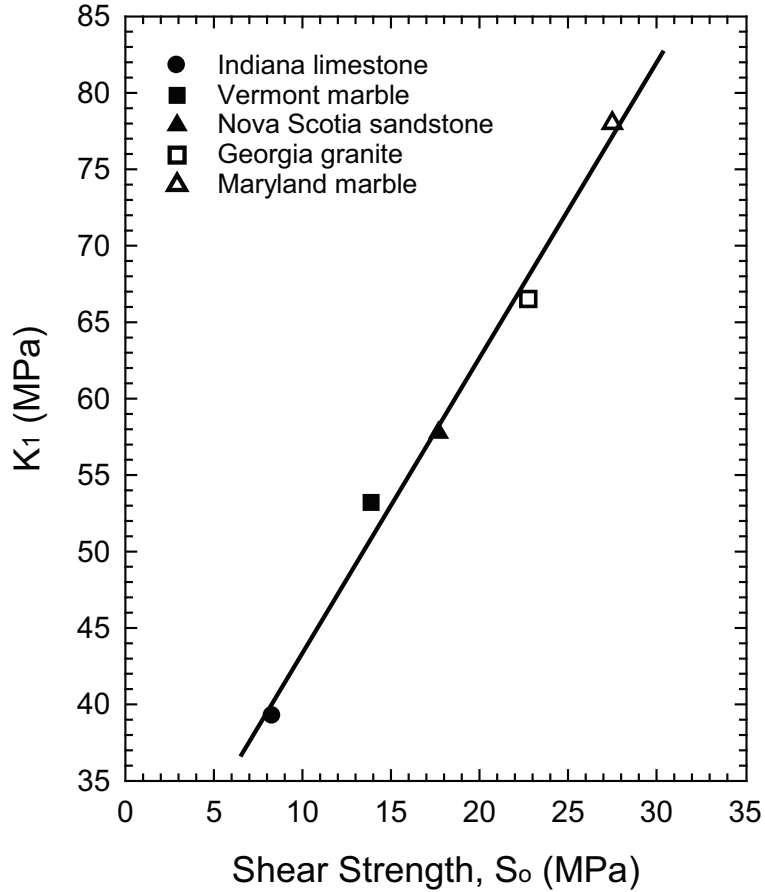
Figure 2.8: K_1 increases linearly with the shear strength, S_o (modified from Obert and Stephenson (1965)).

plane normal to the direction of extension strain, corresponding to the direction of the minimum principal stress. For a material which shows ideal linear elastic behavior, the strain in this direction is related to the three principal stresses according to the following equation:

$$\varepsilon_3 = 1/E[\sigma_3 - \nu(\sigma_1 + \sigma_2)] \tag{2.5}$$

where σ_1, σ_2 and σ_3 are the principal stresses, E is the modulus of elasticity, and ν is Poisson's ratio. Figure 2.9 shows an example of extension strain distribution around the core stub.

28
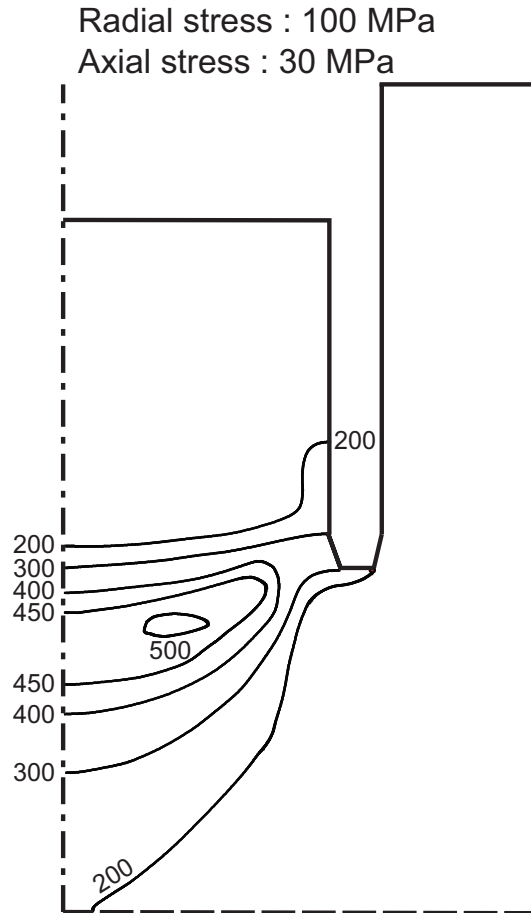
Figure 2.9: The distribution of extension strain around borehole bottom (modified from Stacey (1982)).

Combination failure mechanism

Dyke (1989) suggested the combination failure mechanism of tensile and shear-based stress on the 3D numerical analysis using Boundary Element Method (BEM). Dyke (1989) concluded that tensile stress plays the major role in initiating core disking fractures because the shear stress magnitudes are insufficient to cause failure.

2.2.2 Disking fracture initiation and propagation

Identifying disking fracture initiation and propagation is critical to understanding the core disking mechanism. Jaeger and Cook (1963) found that disking fracture began in the interior of the core, whereas Obert and Stephenson (1965) noted that

core disking fractures began on the core exterior.

Dyke (1989), however, suggested that disking fracture begins simultaneously on the core's interior and surface. Li and Schmitt (1998) also proposed that disking fracture can begin at different locations depending on *in situ* stress conditions and disk shape. Li and Schmitt (1998) insisted that cup-shape disking fractures can begin away from the cut at the root of the core, but that saddle-shaped core disk fracture begins at the inner corner of the borehole bottom, or at the root of the core stub. Maury et al. (1988) suggested three possible fracture initiation zones: the core axis, the area near the drill bit bottom, and the core surface in the middle of the core stub. Figure 2.10 shows the potential fracture initiation zones suggested by Maury et al. (1988).
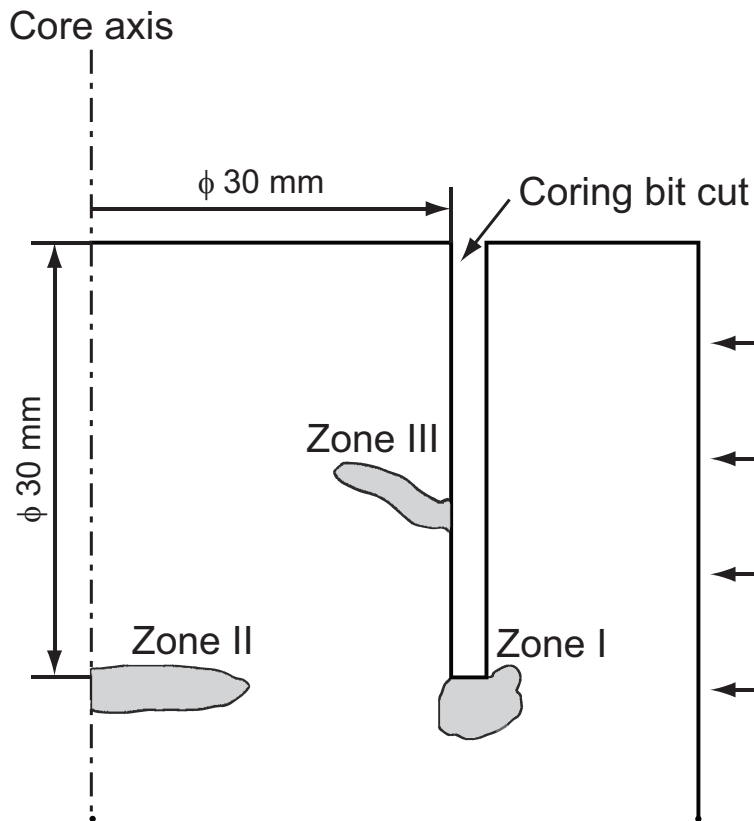
Figure 2.10: Core disking fracture initiation zone. Modified from Maury et al. (1988).

2.2.3 Influence factors on core disking

To obtain a proper simulation of core disking by numerical analysis, and to control the core disking in the field, analysts should carefully consider the major influence factors listed below.

In situ stress

The magnitude of *in situ* principal stresses and their mutual relationship are the most critical cause of core disking. Obert and Stephenson (1965) found that lateral applied stress (horizontal *in situ* stress) acting perpendicular to the core axis is the key component, and the axial stress (vertical *in situ* stress) also highly encouraged the formation of core disking. Li and Schmitt (1997) reported that axial stress decreases the magnitude of tensile stress generated through the core stub. Moreover, Song and Haimson (1999) observed from a laboratory core disking test that the core disk thickness is influenced not only by maximum radial and axial stress, but also by minimum radial stress. Song and Haimson (1999) found that if applied minimum radial stress increases under constant maximum radial and axial stress, the core disk thickness increases linearly. Kaga et al. (2003) also suggested a core disking criterion based on the mutual relationship among the three principal stress components.

Rock properties

Material properties are a key factor behind core disking. Based on the results of a laboratory core disking test, Obert and Stephenson (1965) suggested that shear strength (cohesion) of rock decides the disking initiation stress. Most of the previous numerical modeling based on tensile stress mechanism assumed that if a generating tensile stress is higher than the tensile strength of the rock, core disking will occur (Sugawara et al., 1978; Dyke, 1989; Li and Schmitt, 1997; Kaga et al., 2003). In this assumption, the tensile strength of the rock acts as one of the major factors in the core disking phenomenon. Moreover, Li and Schmitt (1997) proved through numerical analysis that increasing Poisson′s ratio decreases the possibility of core

disking. Everitt (2001) and Martin et al. (1997) reported that grain size and rock texture affected the degree of core damage as well.

Bottom hole geometry

The geometry at the bottom of the borehole corresponds to the geometry of the drill bit. Li and Schmitt (1997) found that rounded bottom hole geometry, instead of flat shape geometry, can decrease stress concentration around the bottom of the bit.

Drill bit pressure and pore pressure

Hakala (1999b) considered the drill bit pressure for numerical stress analysis and insisted that if fluid pressure in the borehole is smaller than the pore pressure, then tensile stress will be induced near the bottom of the hole. On the other hand, if the fluid pressure is higher than the pore pressure, a hydrostatic compression will manifest at the relieved part of the core stub.

Scale of drill bit

Lim et al. (2006) reported core disks with different diameters (from 76 mm–1000 mm). Lim et al. (2006) suggested that drill bit size influences core disk thickness. In personal communication, Stacey (2006) shared speculation that drilling speed could affect disk thickness as well.

2.2.4   Core disk thickness and *in situ* stress magnitude

Once the failure mechanism is chosen and material properties are determined, the final step is to create the relationship between core disk thickness and *in situ* stress magnitude, as well as core disk shape and *in situ* stress direction using core disking as a stress indicator.

Li and Schmitt (1997) conducted extensive numerical analysis and suggested the relationship between core disk thickness and *in situ* stress magnitude for the different Poisson′s ratios (see Figure 2.11). The applied radial stress decreases sharply with

the increase of core disk thickness where the normalized disk thickness is less than 0.15. However, the required radial *in situ* stress is almost constant when normalized core disk thickness is greater than 0.15.
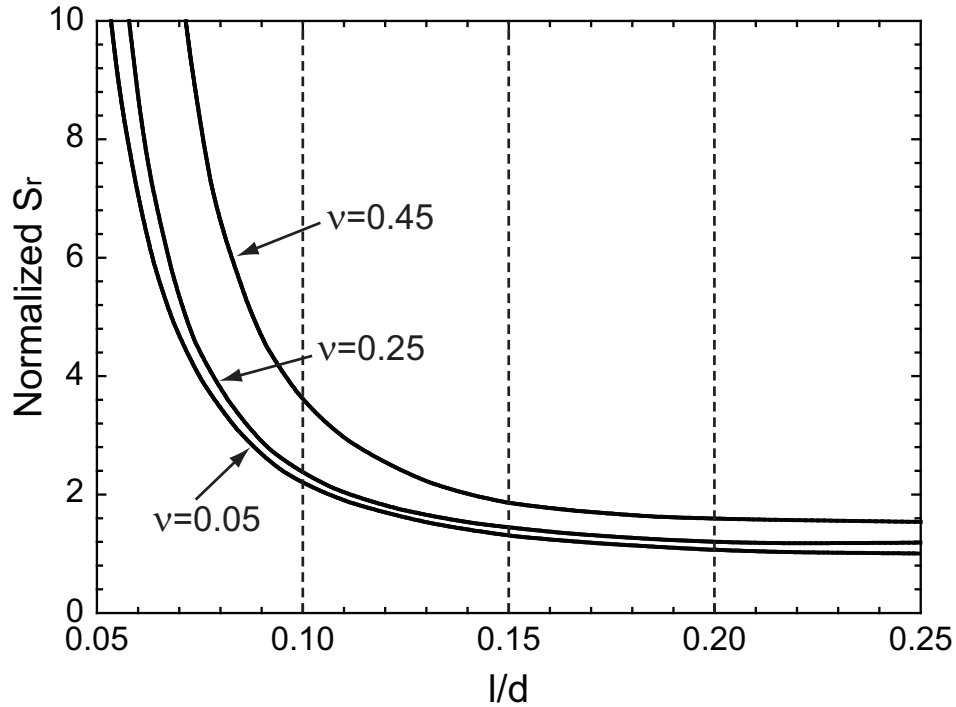
Figure 2.11: The relation of core disk thickness and *in situ* radial stress S_r under *in situ* axial stress $S_a = 0$. Modified from Li and Schmitt (1997).

2.2.5 Core disk shape and orientation of the *in situ* stress

Hakala (1999b) summarized the observed core disk shapes. The core disking fracture shapes could be flat, concave, convex, petal, ring, saddle and petal center line (see Figure 2.12). Also, it is well known that the saddle shape, or petal center line shape core disks can tell the direction of maximum, or minimum horizontal *in situ* stress.

2.3 Summary

There is ample evidence from the literature that the development of stress-induced microcracking suggested in Figure 2.2 is a a function of *in situ* stress magnitudes.

When the *in situ* stress magnitudes reach a critical value the stress-induced microcracking are expressed as core disking. In following chapters the *in situ* stress magnitudes associated with stress-induced microcraking and core disking are explored.
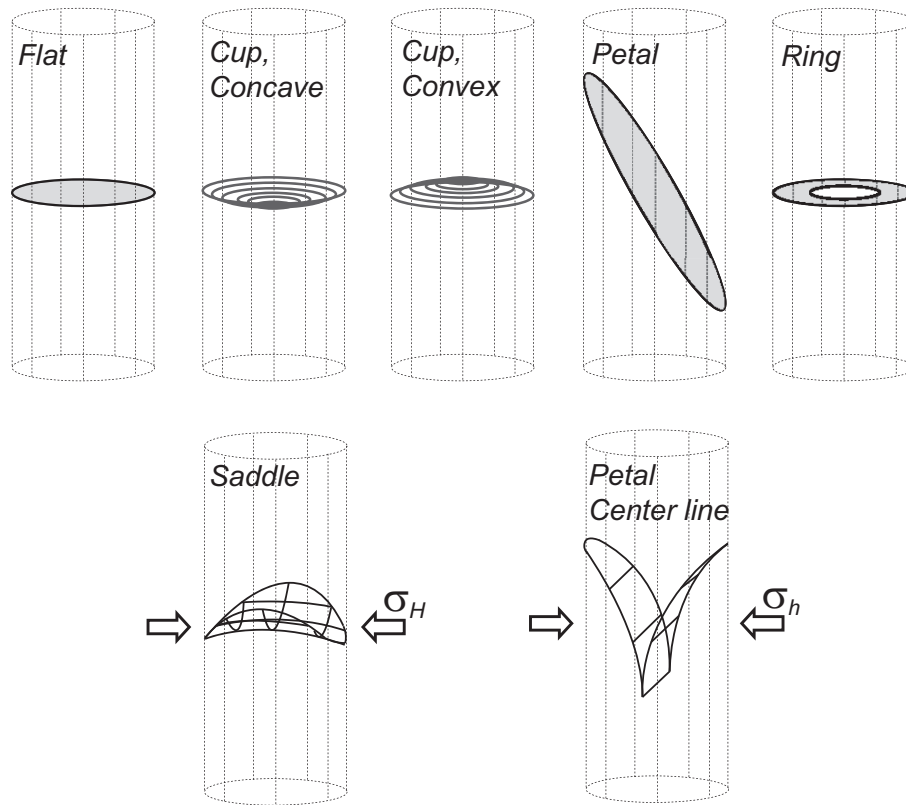
Figure 2.12: Observed disk fracture types and their orientation with respect to the *in situ* state of stress. Modified from Hakala (1999b).

Bibliography

Amadei, B., Stephansson, O. 1997. *Rock Stress and Its Measurement*. first ed. Chapman & Hall, London.

Brace, W.F. 1965. Some new measurements of linear compressibility of rocks. *J. Geophys. Res.* 70(2): 391–398.

Brace, W.F., Silver, E., Hadley, K., Goetze, C. 1972. Cracks and pores: A closer look. *Science* 178: 162–164.

Carlson, S.R., Wang, H.F. 1986. Microcrack porosity and in-situ stress in Illinois borehole UPH 3. *J. Geophys. Res.* 91: 10421–10428.

Chernis, P.J. 1984. Comparison of the pore-microstructure of shallow and deep samples of the Lac du Bonnet granite. *Technical Record 223*, Atomic Energy of Canada Limited, Onterio.

Corthesy, R., Leite, M.H. 2008. A strain-softening numerical model of core discing and damage. *Int. J. Rock Mech. Min. Sci.* 45(3): 329–350.

Durelli, A.J., Obert, L., Parks, V. 1968. Stresss required to initiate core discing. *Transactions Sociaty of Mining Engineers*. 1065–1073.

Dyke, C.G. 1988. *In situ stress indicators for rock at great depth*. Ph.D. thesis, University of London (Imperial College of Science, Technology & Medicine), London, United Kingdom.

Dyke C.G. 1989. Core discing: Its potential as an indicator of principal *in situ* stress directions. In: *Proceedings of ISRM–SPE International Symposium Rock*

at Great Depth, *Pau*. Maury, V., Fourmaintraux, D. *editors*. A.A. Balkema, Rotterdam, vol. II, pp. 1057–1064.

Everitt R.A. 2001. *The influence of rock fabric on excavation damage in the Lac du Bonnet granite.* Ph.D. thesis, Department of Civil & Geological Engineering, University of Manitoba, Winnipeg, Manitoba, Canada

Haimson, B.C., Doe, T.W.J. 1983. State of stress, permeability, and fractures in the Precambrian granite of Northern Illinois. *J. Geophys. Res.* 88(9): 7355–7371.

Haimson B.C., Lee M.Y. 1995. Estimating deep in istu stresses from borehole breakouts and core disking – experimental results in granite. In: *Proceedings of the International Workshop on Rock Stress Measurement at Great Depth, The 8th International Congress on Rock Mechanics*, *Tokyo*, pp. 19–24.

Hakala, M. 1999a. Numerical study of the core disk fracturing and interpretation of the in-situ state of stress. In: *Proceedings Ninth Congress of International Society for Rock Mechanics*, *Paris*, Vouille, G., Berest, P. *editors*. A.A. Balkema, Rotterdam, vol. 2. pp. 1149–1153.

Hakala, M. 1999b. Numerical study on core damage and interpretation of in-situ state of stress. *Technical Report POSIVA-99-25*, Posiva Oy, Helsinki, Finland.

Ishida, T., Saito, T. 1995. Observation of core discing and in situ stress measurements; stress criteria causing core discing. *Rock Mechanics and Rock Engineering*. 41(3): 167–181.

Jacobsson, L., Flansbjer, M., Christiansson, R., Jansson, T. 2007. Measurement of micro crack volume in low porosity crystalline rock. In: *11th Congress of the International Society for Rock Mechanics*, *Rolla*. Ribeiro e Sousa, Olalla, Grossmann, *editors*. University of Missouri, Rolla, pp. 523–532.

Jaeger, J.C., Cook, N.G.W. 1963. Pinching-off and disking of rocks. *J. Geophys. Res.* 888(6): 1759–1765.

Kaga, N., Matsuki, K., Sakaguchi, K. 2003. The in situ stress states associated with

core discing estimated by analysis of principal tensile stress. *Int. J. Rock Mech. Min. Sci.* 40: 653–665.

Kowallis, B.J., Wang, H.F. 1983. Microcrack study of granitic cores from Illinois deep borehole UPS 3. *J. Geophys. Res.* 88(B9): 7373–7380.

Kranz, R.L. 1983. Microcracks in rocks: A review. *Tectonophysics* 100: 449–480.

Kutter, H.K. 1991. Influence of drilling method on borehole breakout and core disking. In: *Proc. 7th International Congress on Rock Mechanics*, pp. 1659–1663.

Li, Y., Schmitt, D. 1997. Effects of poisson′s ratio and core stub length on bottom-hole stress concentrations. *Int. J. Rock Mech. Min. Sci.* 34(5): 761-773.

Li, Y., Schmitt, D. 1998. Drilling-induced core fractures and in situ stress. *J. Geophys. Res.* 103: 5225–5239.

Lim, S.S., Martin, C.D. 2010. Core disking and its relationship with stress magnitude for Lac du Bonnet granite. *Int. J. Rock Mech. Min. Sci.* 47(2): 254–264.

Lim, S.S., Martin, C.D., Christiansson, R. 2006. Estimating in-situ stress magnitudes from core disking. In: *Proceedings of International Symposium on In-situ Rock Stress, Trondheim*. Lu, M., Li, C.C., Kjorholt, H., Dahle, H. *editors*. A.A. Balkema, Rotterdam, pp. 159–166.

Martin, C.D., Christiansson, R. 1991. Overcoring in highly stressed granite – The influence of microcracking. *Int. J. Rock Mech. Min. Sci.* 28(1): 53-70.

Martin, C.D., Read, R.S., Martino, J.B. 1997. Observations of brittle failure around a circular test tunnel. *Int. J. Rock Mech. Min. Sci.* 34(7): 1065-1073.

Martin, C.D., Stimpson, B. 1994. The effect of sample disturbance on laboratory properties of Lac du Bonnet granite. *Can. Geotech. J.* 31(5): 692–702.

Maury, V.M., Santarelli, F.J., Henry, J.P. 1988. Core discing: a review In: *Proc. 1st Regional ISRM Symposium for Africa: Rock Mechanics in Africa*. Maury, V., Fourmaintraux, D. *editors*. South African National Group on Rock Mechanics, Swaziland, pp. 221–231.

Nadan, B., Engelder, T. 2009. Microcracks in New England granitoides: A record of thermoelastic relaxation during exhumation of intracontinental crust. *Geol. Soc. Am. Bull.* 121: 80–99.

Nur, A., Simmons, G. 1970. The origin of small cracks in igneous rocks. *Int. J. Rock Mech. Min. Sci.* 7(3): 307–314.

Obert, L., Stephenson, D.E. 1965. Stress conditions under which core discing occurs. *Transactions Sociaty of Mining Engineers*. 232(3): 227–235.

Ren, N.K., Roegiers, J.C. 1983. Differential strain curve analysis - a new method for determining the pre-existing in-situ stress state from rock core measurements. In: *Proc. 5the Cong. Int. Soc. Rock Mech. (ISRM)*, *Melbourne*. A.A. Balkema, Rotterdam, pp. F117–127.

Siegfried, R., Simmons, G. 1978. Characterization of oriented cracks with differential strain analysis. *J. Geophys. Res.* 83(B3): 1269-1278.

Simmons, G., Richter, D. 1976. Microcracks in rock. In: *The Physics and Chemistry of Minerals and Rocks*. Strens, R. *editor*. Willey, New York, pp. 105–137.

Simmons, G., Siegfried, R. 1974. Differential strain analysis: A new method for examining cracks in rocks. *J. Geophys. Res.* 79(29): 4383-4385.

Song, I., Haimson, B.C. 1999. Core disking in Westerly granite and its potential use for in situ stress estimation In: *Proc. 31st U.S. Rock Mechanics Symposium*, *Rotterdam*. Amadei, Kranz, Scoot, *editors*. A.A. Balkema, Rotterdam, pp. 1173-1180.

Stacey, T.R. 1981. A simple extension strain criterion for fracture of brittle rock. *Int. J. Rock Mech. Min. Sci.* 18: 469-474.

Stacey, T.R. 1982. Contribution to the mechanism of core discing. *Journal South African Institute of Mining and Metallurgy* 99: 269-274.

Stacey, T.R. 2006. In personal cummunication.

Stephens, D.R. 1964. The hydrostatic compression eight rocks. *J. Geophys. Res.* 69(14): 2967–2978.

Strickland F.G. Ren, N.K. 1980. Use of differential strain curve analysis in predicting the in-situ stress state for deep wells. In: *Proc. 11the Cong. Int. Soc. Rock Mech. (ISRM)*. Ribeiro e Sousa, Olalla, Grossmann, *editors*. Taylor & Francis Group, London, pp. 55–58.

Sugawara, K., Kameoka, Y., Saito, T., Oka, Y., Hiramatsu, Y. 1978. A study on core disking of rock. *Journal of Japanese Association of Mining* 94: 19-25.

Vollbrecht, A., Rust, S., Weber, K. 1991. Development of microcracks in granites during cooling and uplift: examples from the Variscan basement in NE Bavaria, Germany. *J. Struct. Geol.* 13(7): 787–799.

Walsh, J.R. 1965. The effect of cracks on the compressibility of rock. *J. Geophys. Res.* 70(2): 381–389.

Wang, H.F., Simmons, G. 1978. Microcracks in crystalline rock from 5.3-km depth in the Michigan basin. *J. Geophys. Res.* 83(B12): 5849–5856.

Chapter 3

In situ stress and microcracking in gran-
ite cores with depth [1]

3.1 Introduction

It is well known that extracting core from deep boreholes can lead to a signifi-
cant increase in microcrack porosity commonly referred to as sample disturbance
or stress-induced damage (Chernis, 1984; Martin and Stimpson, 1994). These mi-
crocracks affect the physical properties of intact rock such as strength, compress-
ibility, elastic wave velocities, permeability and electrical conductivity (Chernis,
1984; Kranz, 1983; Martin and Stimpson, 1994; Simmons and Richter, 1976; Wang
and Simmons, 1978). Chernis (1984) examined samples of Lac du Bonnet (LdB)
granite using a Scanning Electron Microscope (SEM) to determine the types of mi-
crocracks, i.e., grain-boundary, intragranular and transgranular, and concluded that
the origin and types of microcracks, strongly impact the physical properties of the
rock samples. The stress-induced transgranular microcracks increased the porosity
and permeability and reduced the rock strength while the natural grain boundary
microcracks had little effect on these properties.

---

[1] This chapter has been published to the Engineering Geology Journal 147: 1–13.

Martin and Stimpson (1994) investigated the sample disturbance caused by the stress-induced microcracks using the laboratory mechanical properties for LdB granite cores extracted from depths ranging from the ground surface to 1000 m. They found that the strength, P-wave velocity and tangent Young′s modulus of the granite samples decrease as the magnitude of *in situ* stresses increase. Martin and Stimpson (1994) suggested that the stress-induced microcracking that affects the laboratory properties initiates when the maximum stress reaches a critical threshold.

Microcracks can also influence *in situ* stress results from overcore measurements. Martin and christiansson (1991) found that microcracks induced during overcore drilling created modulus-anisotropy in the overcore samples that influenced both the orientations and magnitudes of the *in situ* principal stresses. On the other hand, techniques such as anelastic strain recovery and differential strain curve analysis have used microcracks and the rate of microcracking to estimate *in situ* stress magnitudes (Amadei and Stephansson, 1997). Hence, the characteristics and quantity of microcracks measured in core samples may provide indirect evidence on the *in situ* stress magnitudes. In this paper we examine granite core samples obtained from Pinawa, Canada and Forsmark, Sweden. Sample depths ranged from the ground surface to approximately 1000 m. The microcrack patterns including crack type, length, density and orientation were investigated. The microcrack volume was quantified in the rock core samples and correlated with the *in situ* stress magnitudes measured using traditional overcoring and hydraulic fracturing techniques.

3.2   Origin and types of microcracks

The terms used to describe the types of microcracks are usually based on their petrographic characteristics (Kranz, 1983; Simmons and Richter, 1976). In this study the following terminology is used:

- Grain boundary cracks: microcracks associated with grain boundaries,

- Intragranular cracks: microcracks which are totally lying within mineral grains, and

- Transgranular cracks: microcracks that run across several mineral grains and grain boundaries.

Microcracks in crystalline rocks nucleate when the local stresses exceed the local strength and can be classed as: 1) natural microcracks, which form by natural processes and exist over geological time, and 2) drilling-induced microcracks produced by stress changes associated with the coring process (Nur and Simmons, 1970). The drilling-induced microcracks have been defined as stress-induced microcracks in this study.

3.2.1 Natural microcracks

Cracks nucleate when the internal local stresses exceed the internal local strength of the material. These local internal stresses are primarily created by thermal cooling and decompression as the rock mass evolves over geological time (Nadan and Engelder, 2009; Nur and Simmons, 1970; Vollbrecht et al., 1991). Nadan and Engelder (2009) examined microcracking mechanisms in New England granites and suggested that during the solidification process the rock mass experienced initial isobaric cooling under laterally constrained boundaries, creating a deviatoric stress condition. This lateral unloading and high vertical compressive stress produces vertically aligned microcracks. After isobaric cooling, the rock mass will be exhumed, removing the overburden stress. Nadan and Engelder (2009) suggest that this latter process will cause additional cooling and decompression of the rock generating high horizontal stresses and horizontally aligned microcracks. Figure 3.1a illustrates both processes that can lead to the formation of natural microcracks. As noted by Brace et al. (1972) natural microcracks seldom form sharp fracture surfaces. The contact surfaces of such fractures are serrated with rounded contact points, likely reflecting their formation over geological time (Figure 3.1b).

Nadan and Engelder (2009) identified three general types of natural microcracks: (1) healed microcracks often associated with fluid inclusion planes that formed during isobaric cooling, (2) filled microcracks, containing foreign minerals and (3) open microcracks produced during the isothermal decompression process and tec-

42

(a)

(b)
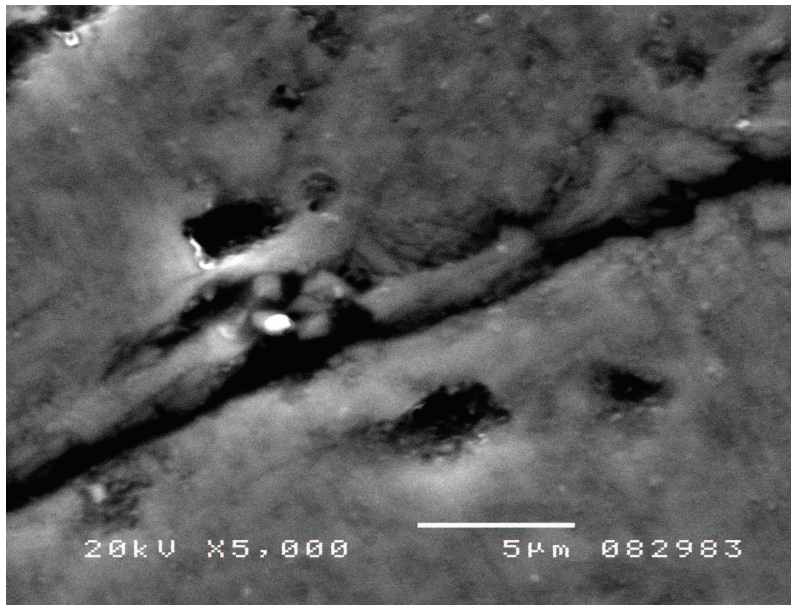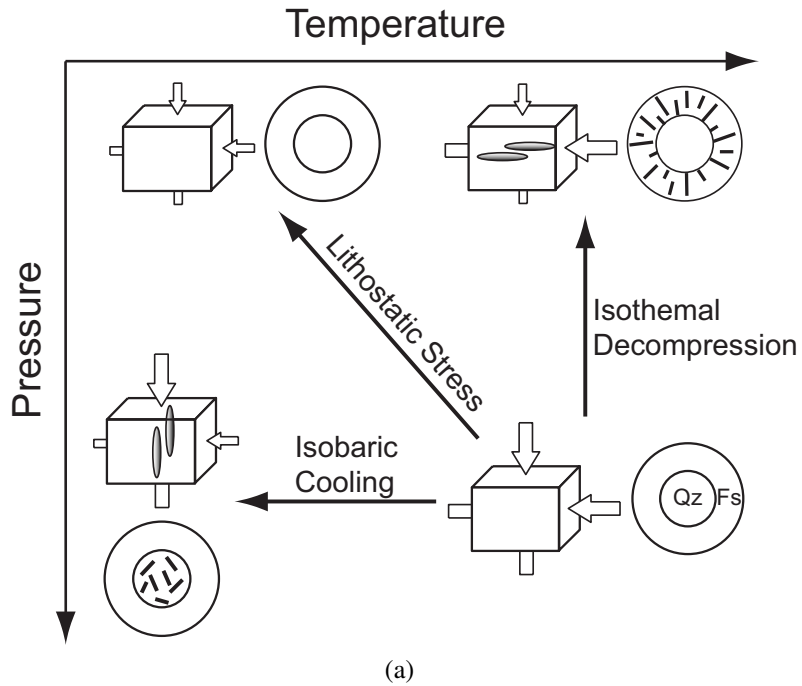
Figure 3.1: Illustration of the origin of natural microcracks: (a) geological processes involved in the formation of natural microcrack (modified from (Nadan and Engelder, 2009; Vollbrecht et al., 1991)) and (b) an example of a natural microcrack, taken with a Scanning Electron Microscope (SEM).

tonic stress activities. Vollbrecht et al. (1991) found that the dominant healed microcracks in granite developed in quartz and the majority of these were intragranular microcracks, whereas the open microcracks were transgranular type cracks. Vollbrecht et al. (1991) and Kowallis and Wang (1983) suggested that the healed microcracks in quartz were produced mainly by cooling-induced thermal stresses and tectonic stresses at higher crustal levels might be the main stress source for open microcracks. Most of the natural microcracks were observed as grain boundary and intragranular type cracks.

3.2.2 Stress-induced microcracks

Various researchers have examined the origin and characteristics of stress-induced microcracks. Intact rocks at depth may be crack free or contain closed pre-existing cracks and the microcracks open during the stress-relief coring process (Wang and Simmons, 1978; Lei at al, 2000). Wang and Simmons (1978) showed from their laboratory and *in situ* studies that *in situ*, the seismic velocities were nearly constant, while the measured laboratory velocities decrease with sampling depth. From the optical and scanning electron microscope observations and elastic properties measurement of Illinois granite, Kowallis and Wang (1983) found that the stress-induced microcracks are long, narrow shaped and absent of alteration and secondary mineralization, and that such cracks are closed under 20 MPa of confinement. In their study the stress-induced microcracks are developed primarily along the pre-existing healed cracks and cleavage planes in feldspar. Kowallis and Wang (1983) concluded that the core removal process causes such microcracks. Chernis (1984) also observed that granite core samples extracted from about 800 m contained a high proportion of stress-induced microcracks developed during the drilling process. Chernis (1984) noted that while the natural microcracks have irregular walls, rounded edges and small infillings, stress-induced microcracks show sharp-ended, parallel-walled and echelon features.

It is well known that the thin slot produced during the drilling process concentrates and redistributes the *in situ* stresses. When the magnitude of concentrated stresses
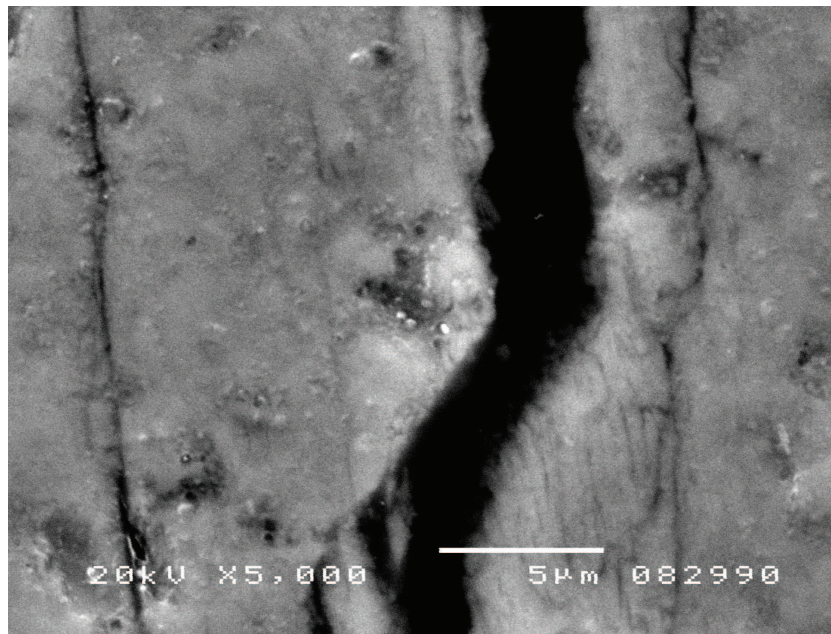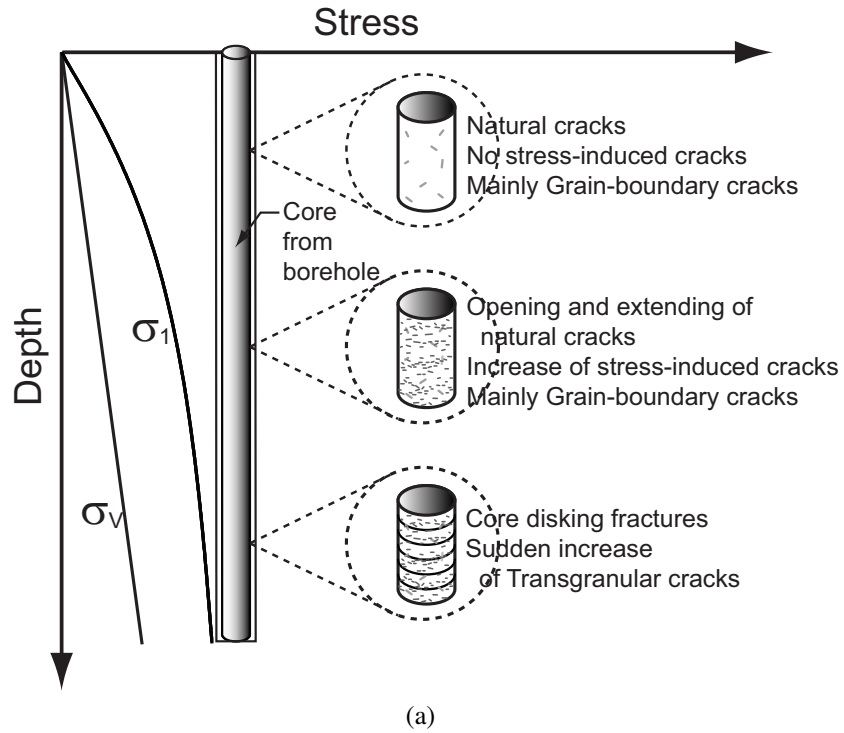
Figure 3.2: Illustration of the origin of stress-induced microcracks in high horizontal stress regime: (a) formation of stress-induced microcracking during drilling and (b) an example of stress-induced microcrack taken with a SEM.

is higher than the stress required initiating the formation of a microcrack, stress-induced fractures may initiate and propagate (Obert and Stephenson, 1965; Stacey, 1982; Dyke, 1988; Lim and Martin, 2010). Stacey (1982) proposed that these concentrated stresses produce an extensional strain near the bottom of the drill bit that can lead to stress-induced microcracking and ultimately core disking. As shown in Figure 3.2a gradually increasing stress magnitudes could lead to a gradual increase in microcrack porosity for samples cored at increasing depth, assuming that there is a correlation between stress magnitudes and crack porosity. Carlson and Wang (1986) examined the core from a borehole in granite between 0.7 and 1.6 km depth and found a linear correlation between mean *in situ* stress and microcrack porosity with depth. In Figure 3.2a the horizontal stress is the maximum stress reflecting the *in situ* stress conditions found in the Canadian and Scandinavian Shields and hence the mean stress would increase more rapidly for this geological stress regime. In addition the stress ratios are much greater at shallow depths in this stress regime and hence it is not obvious if the linear trend between mean *in situ* stress and microcrack porosity observed by Carlson and Wang (1986) could be expected in such geological conditions.

3.3   Sample collection and investigation

3.3.1   Geology

Cores from two sites (Forsmark, Sweden and Pinawa, Canada) were examined for this study. Forsmark is located in the Scandinavian Shield approximately 150 km north of Stockholm, Sweden. Core was collected from surface drilled 76-mm-diameter boreholes that were part of the Forsmark site investigation for the purposes of selecting a site for a geological repository for nuclear waste (SKB, 2005). At Pinawa, the cores were taken from both surface drilled boreholes and boreholes drilled from the 420 m Level of AECL′s Underground Research Laboratory (URL) (Martin and Stimpson, 1994). The geology at both sites has been extensively investigated. The main rock type at both sites is relatively uniform Precambrian granite (Forsmark granite, and Lac du Bonnet granite) with similar mechanical and strength

properties. In addition to the geological investigations to depths of 1000 m, extensive *in situ* stress investigations were also carried out at both sites to depths of 1000 m (Martin, 1990; Read, 1994; Thompson and Chandler, 2004). Hence, the site data provide a unique opportunity to examine possible correlations between microcrack porosity in cored samples and *in situ* stress magnitudes.

Cores were examined for the entire depth of the study and samples were selected for laboratory testing and imaging. In addition to the laboratory testing carried out for this study, existing laboratory test results were also used to examine trends. A total of nine (9) granite specimens were prepared for image analysis (Table 3.1). The specimens labelled F-G1, F-G2, F-G3 and F-G4 were selected from the Forsmark granite and LdB-G1, LdB-G2, LdB-G3, LdB-G4 and LdB-G5 are samples from Lac du Bonnet granite. The sample locations were chosen to examine the effect of *in situ* stress on the microcrack patterns.

3.3.2   Sample preparation and image analysis

The samples in Table 3.1 were prepared for microcrack analysis. Each core sample was cut in half through the core axis and the cutting plane was polished, and then vacuum impregnated with an epoxy resin containing fluorescent dye. A total of 15

Table 3.1: List for samples used for image analysis. LdB-G: Lac du Bonnet granite, F-G: Forsmark granite, Ring-disking: the disking occurs when a sample is cored over an existing hole.

Sample No.	Borehole ID	Vertical depth (m)	Sample description
LdB-G1	URL-6, Pinawa	13.20–13.42	Solid core
LdB-G2	URL-5, Pinawa	440.41–440.10	Solid core
LdB-G3	421-012-MVP4, Pinawa	420m Level URL	Solid core
LdB-G4	423-009-MVP1, Pinawa	420m Level URL	Solid disking
LdB-G5	421-012-MVP5, Pinawa	420m Level URL	Solid disking
F-G1	KFM01A, Forsmark	308.55–308.76	Solid core
F-G2	KFM01A, Forsmark	514.58–514.79	Solid core
F-G3	KFM01B, Forsmark	236.96–237.22	Ring disking
F-G4	KFM01B, Forsmark	475.54–475.74	Ring disking

thin sections were prepared for image analysis and the size of each thin section was 35 x 42 mm. Figure 3.3a and Figure 3.3b shows the examples of plane polished slabs impregnated with epoxy containing fluorescent dye for LdB and Forsmark granite respectively.

Two images taken with optical microscopy were used for the microcrack analysis, one using fluorescent light and one using polarized light. The area for each image is 2.78 x 2.10 mm and the image resolution is 680 x 512 pixels. The thin section was fixed on a motorized stage, which was programmed such that the images can be photographed edge to edge, thus creating a 12-image mosaic in order to evaluate a larger area in high resolution. Both the fluorescent and polarized images were considered to evaluate where the microcracks are formed (see Figure 3.4), and Figure 3.5 shows the microcrack pattern in detail for solid core, solid disking and ring disking.

(a)

(b)
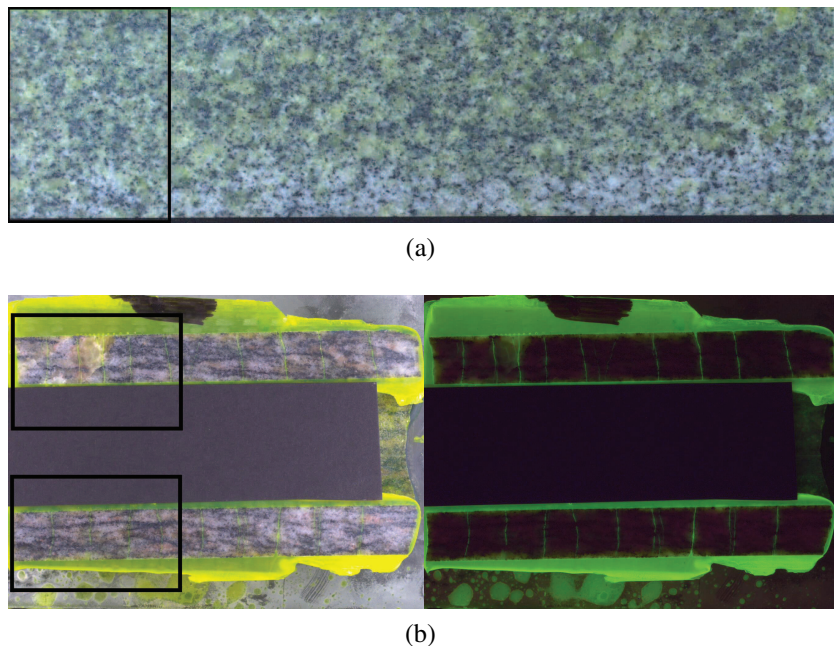
Figure 3.3: Sample preparation for image analysis: (a) LdB granite–solid core specimen and (b) Forsmark granite–ring core specimen. The polished core specimen is impregnated with epoxy containing fluorescent dye. The black rectangular boxes in the left side of each specimen indicate the location for the thin sections.
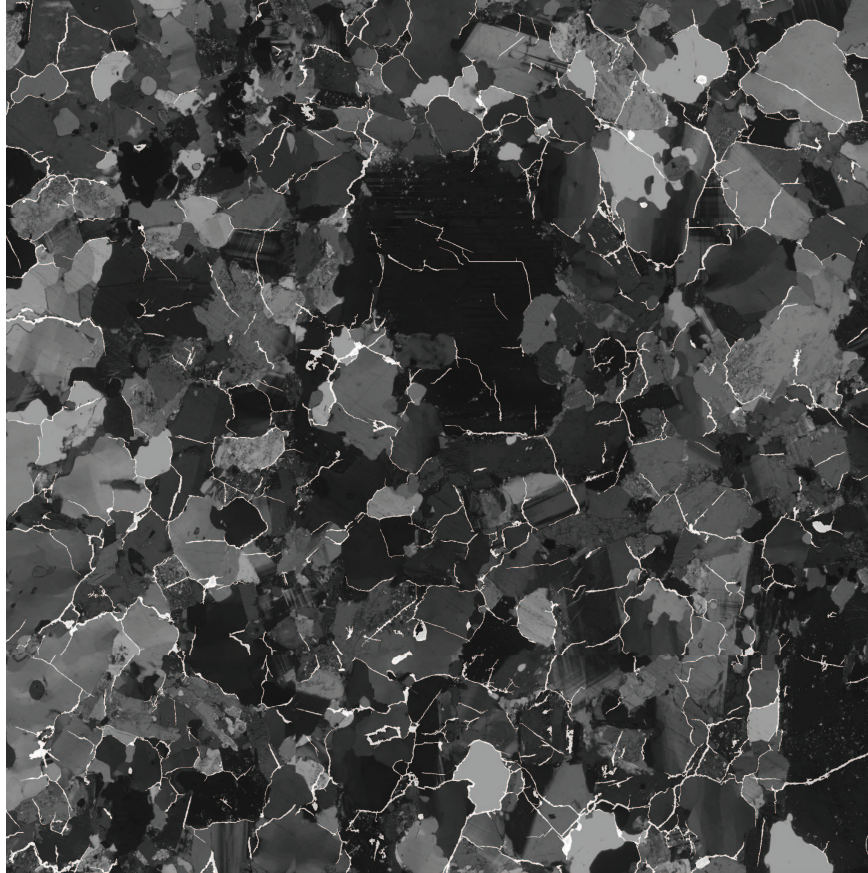
Figure 3.4: A 12 image mosaic in combined polarized and fluorescent light. Image size is 8.3 x 8.3 mm.

The image analysis was used to establish the grain size distribution, and the microcrack type, pattern, density, length and orientation. The grain size distribution and the density of the different microcrack types were determined using linear-traverse measurements. The line transects were oriented parallel and perpendicular to the core axis. For the grain size distribution, the maximum ferret diameter was measured on each mineral intersected by the traverse. For the microcrack analysis, each microcrack that cuts a traverse line was counted, and each crack type was counted separately (see Figure 3.6). The density of microcracks was expressed as cracks/mm.

In order to measure the length and orientation of intragranular and transgranular microcracks, the combined images were printed with a size of 272 x 269 mm and then

by using transparent paper, each crack-type was traced and colored. The line draw-ings were scanned into the computer, and by using RGB-thresholding technique, the length and orientation were measured separately (Åkesson, 2004).
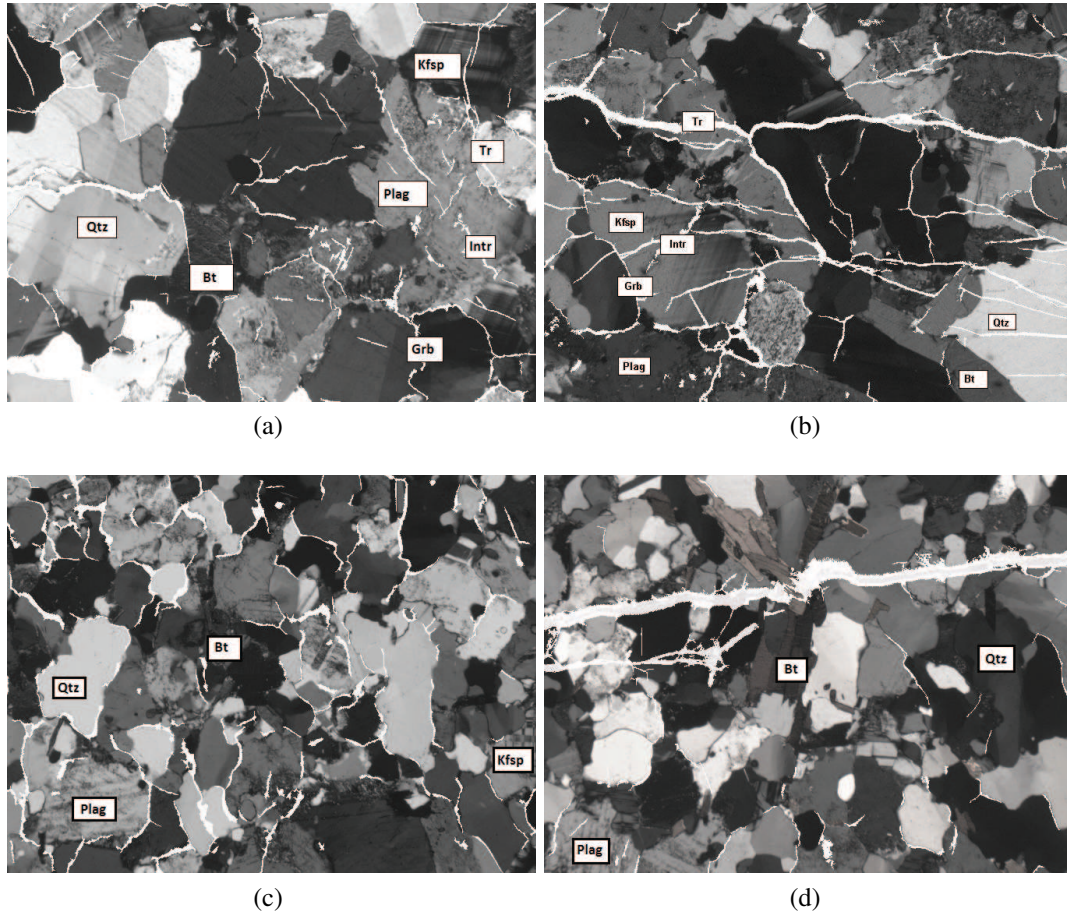
Figure 3.5: Microphotographs by combination of the binary fluorescent and po-larized light: (a) LdB granite – solid core, (b) LdB granite – solid disking, (c) Forsmark granite – solid core and (d) Forsmark granite – ring disking. Minerals and microcrack types are indicated: quartz (Qtz), plagioclase (Plag), potassium feldspar (Kfsp), biotite (Bt), gain boundary (Grb), intragranular (Intr) and transgranular (Tr). Image sizes are 2.78 x 2.10 mm.
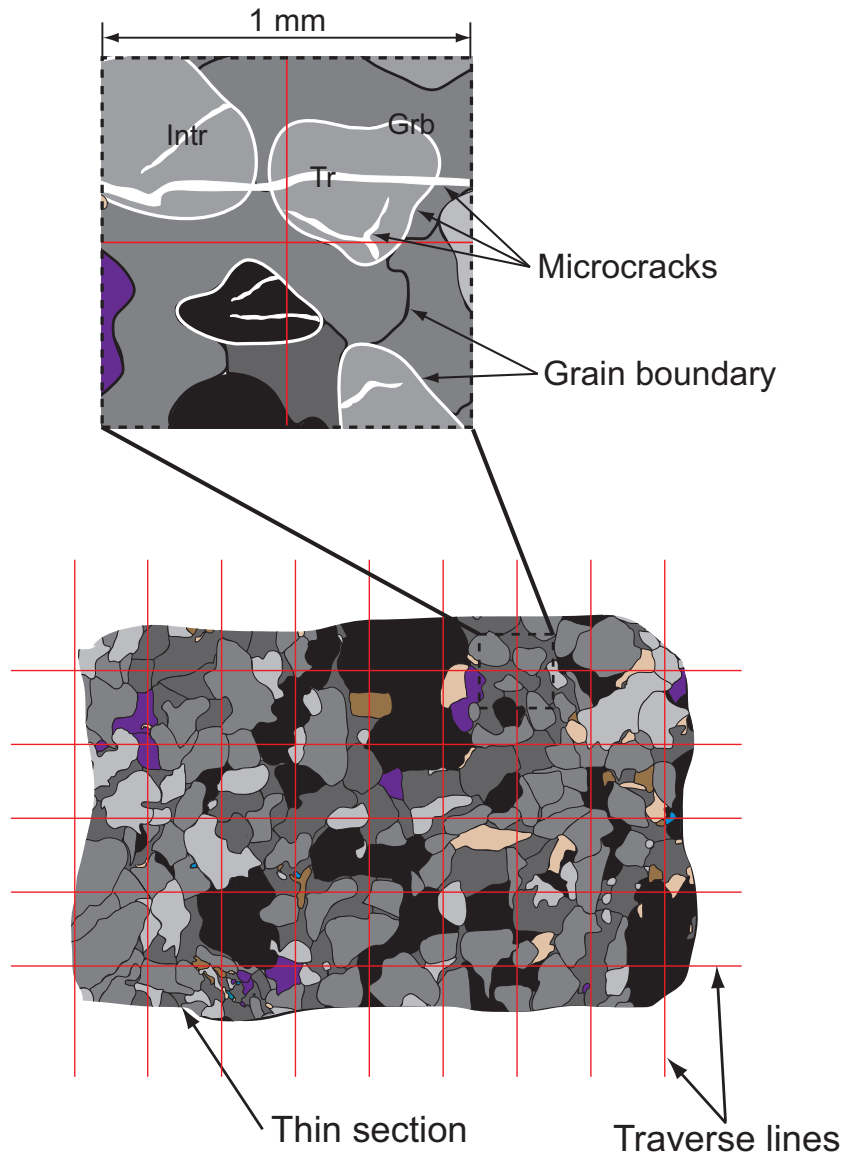
Figure 3.6: The bases for the linear-traverse measurements.

3.4 Findings from image analysis

3.4.1 Rock type

While both rock types are named granite there are subtle differences in the mineral composition, as shown by the Quartz–Alkali feldspar–Plagioclase feldspar modal classification in Figure 3.7. The Forsmark granite contains a higher average quartz

content; 38 % versus 23 % for LdB granite, while the LdB granite contains higher
alkali feldspar content. According to Figure 3.7, LdB granite belongs to both
syeno-granite and monzo-granite, while the Forsmark granite plots near the granite–
granodiorite boundary.
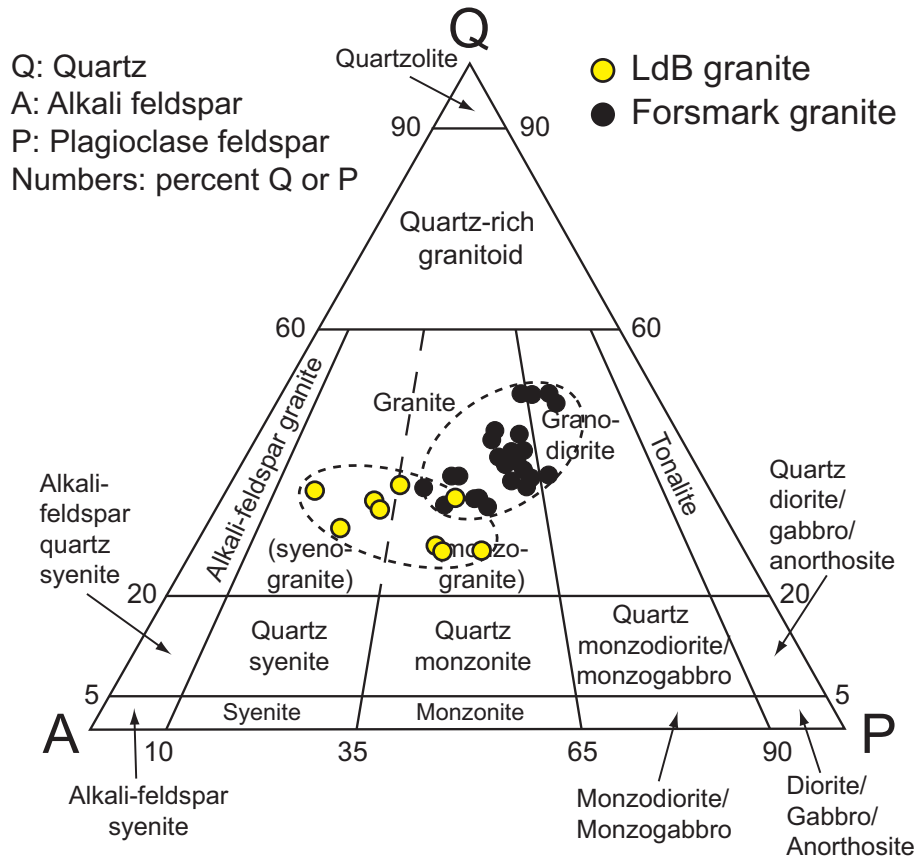
Figure 3.7: The comparison of mineralogical composition between LdB granite and
Forsmark granite on QAP diagram. Data from Read (1994); SKB (2008)

3.4.2 Grain size distribution

The grain size distribution was determined using linear-traverse measurement tech-
nique. The average grain size for LdB granite and Forsmark granite was 1.0 mm
and 0.2 mm respectively (Figure 3.8). Researchers have suggested a relationship
between grain size and the strength of rock. For example, Olsson (1974) suggested
the yield stress of marble increases linearly with the inverse square root of the
mean grain size. A comparison of average laboratory geotechnical properties for
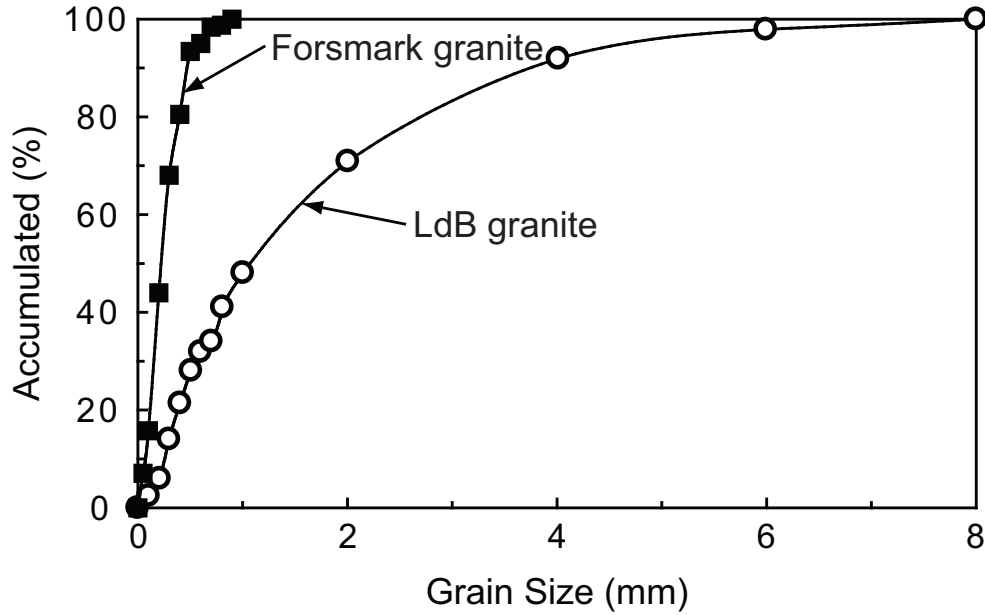
Figure 3.8: Grain size distribution for typical LdB granite and Forsmark granite. Generally the grain size of LdB granite is about 5 times bigger than that of Forsmark granite.

LdB granite and Forsmark granite is provided in Table 3.2. Inspection of Table 3.2 shows that finer grained Forsmark granite is stronger and stiffer than LdB granite. However, it is clear that this difference may not be totally related to grain size because Forsmark granite also contains a higher percentage of quartz which is both stiffer and stronger than feldspar (SKB, 2008). Regardless of the reasons for the strength difference between the two rock types, the mean grain size of Forsmark granite is 5 times smaller than the mean grain size of LdB granite.

Table 3.2: Comparison of laboratory geotechnical properties of LdB granite and Forsmark granite (σ_c = uniaxial compressive strength, BT= Brazilian tensile strength, γ = density, E = Young's modulus, ν = Poisson's ratio).

Rock Type	σ_c (MPa)	BT (MPa)	γ (kg/m^3)	E (GPa)	ν
LdB Granite	213 ± 2	9.3 ± 1.3	2630 ± 10	65 ± 5	0.25 ± 0.05
Forsmark Granite	226 ± 2	13 ± 2.0	2660 ± 10	76 ± 3	0.23 ± 0.03

3.4.3 Microcrack characteristics

Using the methodology previously described, three types of microcracks were identified: (1) grain-boundary, (2) intragranular and (3) transgranular. Table 3.3 provides a summary of the types of microcracks measured in the samples expressed in microcracks per millimeter (cracks/mm) and as a percentage of microcrack types. The types of microcracks were examined from the perspective if the sample was oriented parallel and perpendicular to the core axis. The data in Table 3.3 will be discussed in the following sections.

Table 3.3: Density of microcracks of different types for the investigated samples, based on linear traverse measurements.

Sample		Grain-boundary		Intragranular		Transgranular	
No.	Direction	cracks/mm	%	cracks/mm	%	cracks/mm	%
LdB-G1	Parallel to drill core	0.53	47	0.49	44	0.10	9
	Perpendicular to drill core	0.51	58	0.28	32	0.09	10
	Ratio Parallel/Perpendicular	1.04		1.75		1.11	
	Total	1.04	52	0.77	38	0.19	10
LdB-G2	Parallel to drill core	1.48	64	0.71	31	0.12	5
	Perpendicular to drill core	1.27	61	0.64	31	0.18	9
	Ratio Parallel/Perpendicular	1.17		1.11		0.67	
	Total	2.75	62	1.35	31	0.30	7
LdB-G3	Parallel to drill core	0.93	58	0.64	40	0.03	2
	Perpendicular to drill core	0.64	45	0.60	42	0.18	13
	Ratio Parallel/Perpendicular	1.45		1.07		0.17	
	Total	1.57	52	1.24	41	0.21	7
LdB-G4	Parallel to drill core	0.60	39	0.78	51	0.15	10
	Perpendicular to drill core	0.65	31	0.72	35	0.71	34
	Ratio Parallel/Perpendicular	0.92		1.08		0.25	
	Total	1.25	35	1.50	41	0.86	24
LdB-G5	Parallel to drill core	1.57	72	0.52	24	0.10	4
	Perpendicular to drill core	1.39	60	0.48	21	0.46	20
	Ratio Parallel/Perpendicular	1.13		1.08		0.22	
	Total	2.96	66	1.00	22	0.56	12
F-G1	Parallel to drill core	0.99	78	0.22	17	0.06	5

| Sample | | Grain-boundry | | Intragranular | | Transgranular | |
No.	Direction	cracks/mm	%	cracks/mm	%	cracks/mm	%
	Perpendicular to drill core	1.31	82	0.21	13	0.07	4
	Ratio Parallel/Perpendicular	0.76		1.05		0.86	
	Total	2.30	80	0.43	15	0.13	5
F-G2	Parallel to drill core	1.64	92	0.11	6	0.04	2
	Perpendicular to drill core	1.48	89	0.19	11	-	-
	Ratio Parallel/Perpendicular	1.11		0.58		-	
	Total	3.12	90	0.30	9	0.04	1
F-G3(0)$_{ave}$	Parallel to drill core	2.26	87	0.22	9	0.10	4
	Perpendicular to drill core	1.94	82	0.21	9	0.20	9
	Ratio Parallel/Perpendicular	1.17		1.08		0.53	
	Total	4.19	85	0.43	9	0.30	6
F-G3(90)$_{ave}$	Parallel to drill core	2.30	87	0.26	10	0.08	3
	Perpendicular to drill core	1.87	74	0.29	11	0.39	15
	Ratio Parallel/Perpendicular	1.24		1.03		0.21	
	Total	4.16	81	0.55	10	0.47	9
F-G4(0)$_{ave}$	Parallel to drill core	2.85	85	0.42	13	0.06	2
	Perpendicular to drill core	2.34	80	0.35	12	0.25	8
	Ratio Parallel/Perpendicular	1.21		1.20		0.24	
	Total	5.19	83	0.76	12	0.31	5
F-G4(90)$_{ave}$	Parallel to drill core	1.97	80	0.39	16	0.11	4
	Perpendicular to drill core	2.56	80	0.33	10	0.33	10
	Ratio Parallel/Perpendicular	0.77		1.14		0.37	
	Total	4.52	79	0.72	13	0.43	8

Rock type

Figure 3.9a shows a comparison of the microcrack types for LdB and Forsmark granite for samples taken at an approximate depth of 500 m. It is clear that the grain boundary cracks are dominant for the Forsmark granite, while LdB granite has higher distributions for intragranular and transgranular microcrack types. The transgranular microcracks were found to be 7 % in the LdB granite but only 1 % in

the Forsmark granite. Transgranular microcracks have been used by Chernis (1984) to be an indicator for stress-induced microcracks. This notion will be discussed later.

Sampling depth and stress environment

Figure 3.9b shows a comparison of the density of each microcrack type for LdB granite samples from different depths and stress conditions. The grain boundary, intragranular and transgranular cracks increase about 150 %, 100 % and 50 % respectively for the 450-m-deep sample, compared to the 13-m-deep sample. It is clearly observed that the density of microcracks for all types is higher for the 450-m sample, than for the 13-m sample, with the total density of microcracking increasing to more than 100 % for the 450-m sample. The large increase of total microcrack density is consistent with the observation by Chernis (1984) and Martin and Stimpson (1994). Chernis (1984) found that the microcrack porosity for deep samples (800 m) was twice as high as the microcrack porosity of samples taken from 480 m depth. Martin and Stimpson (1994) also found that the laboratory P-wave velocity of LdB granite samples decreases continuously from ground surface to 1000 m. They suggested that this velocity decrease was related to an increase in microcrack density.

In the same figure, the microcrack density for the solid core sample taken from 450 m depth is compared to microcrack density measured in disked core sample taken from the wall of an underground opening at 420 Level of URL. It was shown in Figure 3.2 that core disking is an extreme form of microcracking in high stress environments. Figure 3.9b shows that the amount of grain boundary and intragranular type microcracks, and the total microcracks for two samples are similar. However, the disked core contained an 85 % increase in the density of transgranular microcracks.

Figure 3.9c shows the comparison of microcrack densities for each microcrack type for two different depths and stress conditions for Forsmark granite. The microcrack density and the types of microcracks are similar for the samples obtained from about
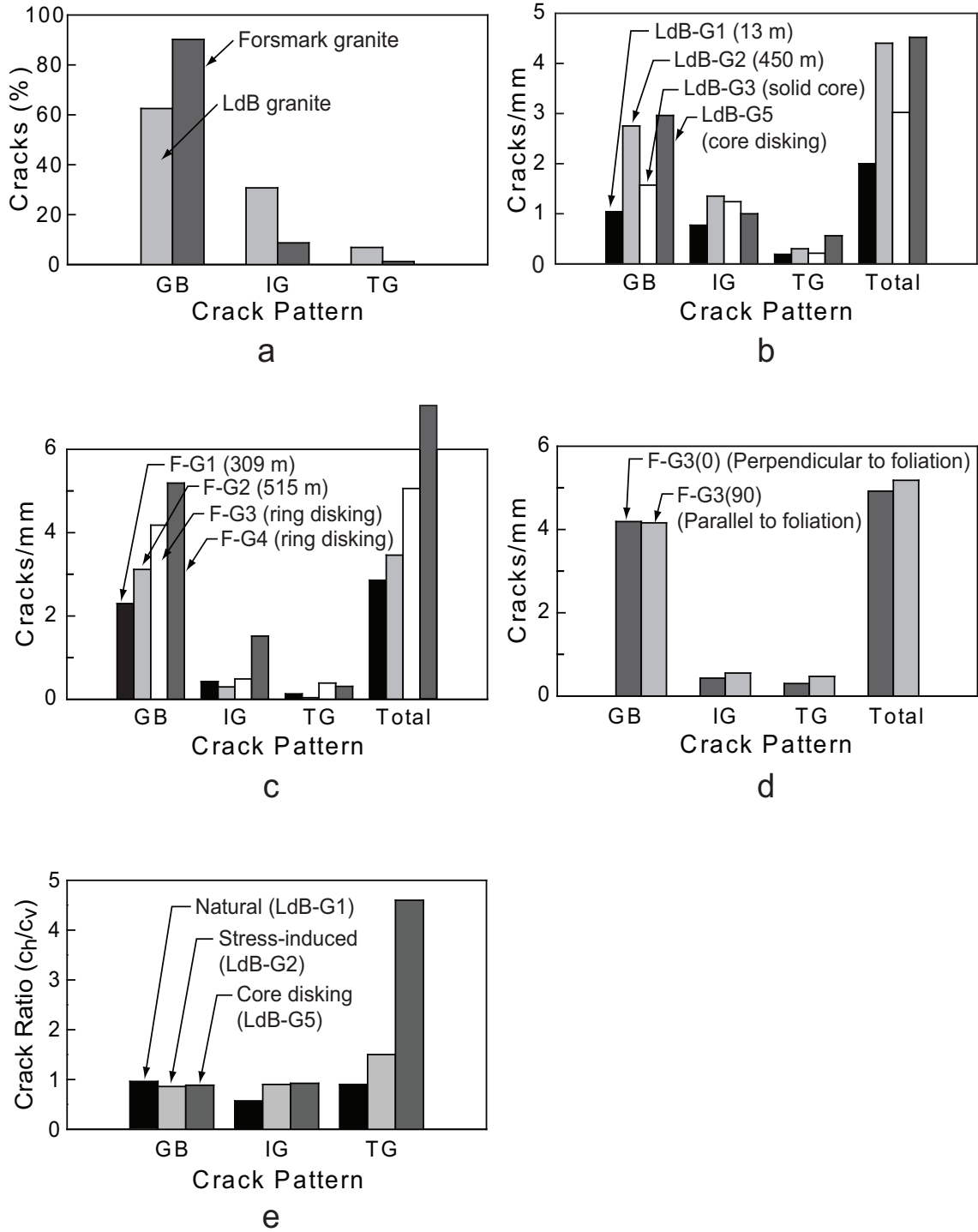
Figure 3.9: Comparison of microcrack patterns, for (a) rock type, (b) and (c) sampling depth and stress environment, (d) foliation direction and (e) stress condition.

300 and 500 m depth. Unfortunately there is no microcrack pattern analysis data for near-ground samples of Forsmark granite, however, as will be shown later, there is no evidence to suggest it is very different than the 300 m sample. Ring-disking is another indicator of sampling in a high stress environment. The microcrack density in Figure 3.9c, for the ring-disk sample shows a large increase in the densities for all types of microcracks.

Foliation

The Forsmark granite has a weak foliation that can be observed with the naked eye. Jacobsson (2004a) concluded that the Brazilian tensile strength of Forsmark granite was 18 % higher when tested perpendicular to the foliation. To investigate the influence of foliation on microcracking pattern, a total of 8 thin sections from samples F-G3 and F-G4 were analyzed. Two thin sections were perpendicular to the foliation labeled as (0) and two thin sections were sampled parallel to the foliation labeled as (90). The averaged microcrack frequencies for samples F-G3 and F-G4 are shown in Table 3.3, and F-G3(0) and F-G3(90) are compared for each microcrack type in Figure 3.9d. Figure 3.9d shows that the foliation has little impact on the total microcrack density for each type.

Orientation and length of microcracks

As illustrated in Figure 3.1a the orientation of natural microcracks depends on the rock mass stress history. During the initial isobaric cooling vertical cracks may form and isothermal decompression can induce horizontally aligned microcracks. Martin and christiansson (1991) mapped the stress-induced microcracks in the overcore granite samples from 240 Level of URL and found that the orientation of the microcracks aligned with major sub-vertical discontinuous fractures. Everitt (2001) observed the low-dipping horizontal natural microcracks in the granite cores extracted from 420 Level of URL. These microcracks in the massive granite tended to be aligned with the foliation. In high stress environments the stress-induced microcracks are aligned in the plane perpendicular to the direction of drilling (Lim and

Martin, 2010; Stacey, 1982).

Figure 3.9e shows the comparison of the ratio of the number of horizontally aligned microcracks (c_h) to the vertically aligned microcracks (c_v) relative to the core axis, for three samples cored from different stress conditions. The samples LdB-G1, LdB-G2 and LdB-G5 were cored from near ground surface, 450 m and 420 Level of URL respectively. Only natural microcracks were observed in the sample LdB-G1, while LdB-G2 sample contained extensive stress-induced microcracks which could be seen with naked eyes. The sample LdB-G5 was taken from a hole drilled from an underground opening on the 420 Level of the URL. The elevated stress magnitudes around the underground opening resulted in solid core disking fractures aligned perpendicular to the core axis (Lim and Martin, 2010). Figure 3.9e shows that with an increase in stress-induced damage in the cores, the ratio of horizontal to vertically aligned microcracks is much higher for the transgranular cracks. Consequently the preferred direction of transgranular type microcracks could indicate the presence of damage in the rock core.

As a part of microcrack analysis the length and orientation of microcracks for both intragranular and transgranular types were measured. Figure 3.10 shows the percentage of each microcrack length for: (a) solid core and (b) disked core. It appears that the predominant microcrack length is very similar for each microcrack type regardless of the amount of stress-induced damage in the core, showing 0.2–0.4 mm for intragranular cracks and 1.0–2.0 mm for transgranular cracks.

Figure 3.11 compares the orientation of intragranular and transgranular microcracks, in a plane parallel to core axis, for the solid cores and disked cores. The LdB-G1 sample (Figure 3.11a) primarily contains only natural microcracks. The dominating orientation of both intragranular and transgranular type microcracks for LdB-G1 is similar to that of existing sub-vertical joint sets observed near ground surface at URL (Martin, 1990). In contrast, transgranular microcracks in the LdB-G4 (Figure 3.11c) are aligned perpendicular to the core axis, suggesting stress-induced core damage.
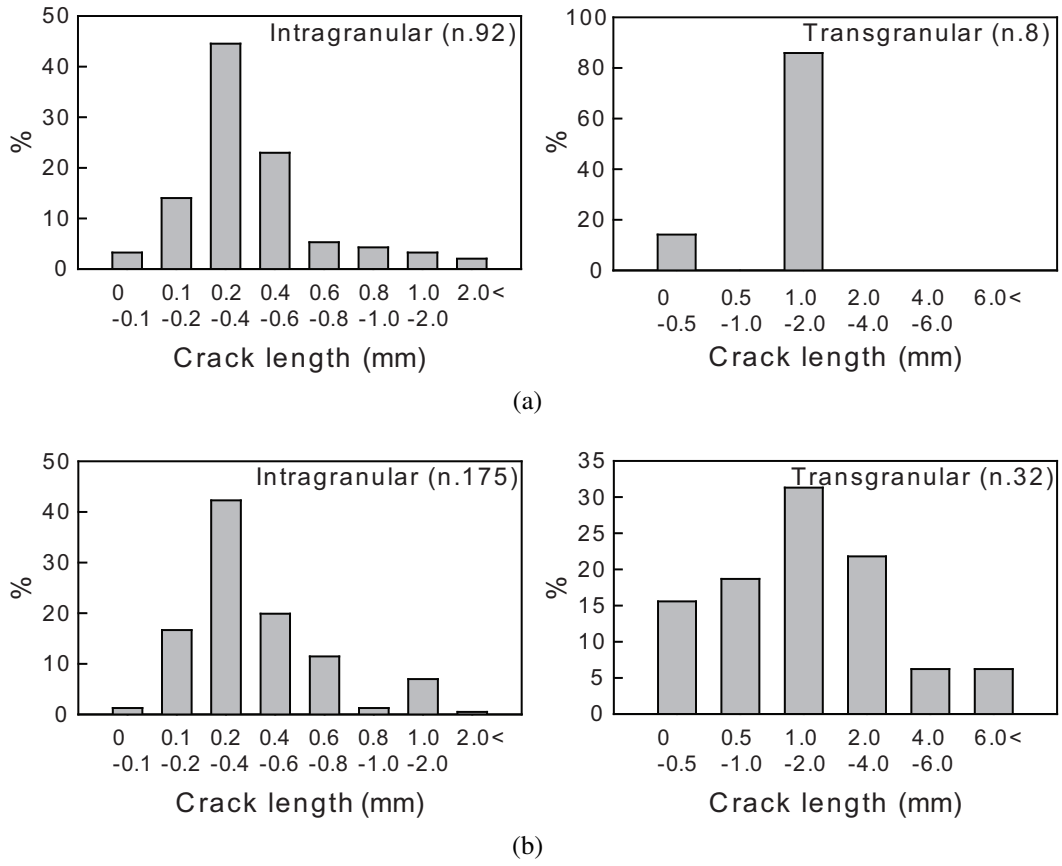
Figure 3.10: Crack length distribution diagram for intragranular and transgranular microcracks, with (a) LdB-G1 (solid core, depth 13 m) and (2) LdB-G4 (disking induced in solid core by drilling from the underground openings on the 420 Level) specimen. The microcrack type and the number of analyzed microcracks are shown in the top- right side of each figure.

The predominating orientation of transgranular microcracks for Forsmark granite shows the same trend as that of LdB granite. While a few transgranular microcracks were observed in F-G2 sample (Figure 3.11b), a large number of transgranular microcracks were observed in F-G4 sample aligned perpendicular to core axis, (Figure 3.11d). Both F-G2 (solid core) and F-G4 (ring-disking core) were taken from similar depth at Forsmark area.
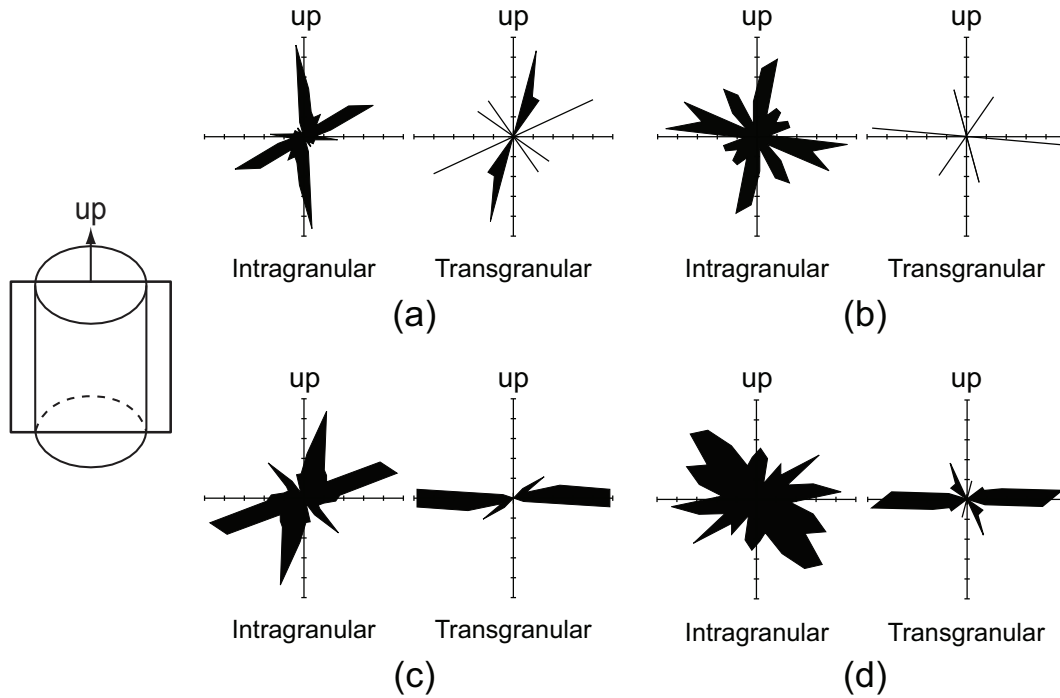
Figure 3.11: Rose diagrams showing the orientation of intragranular and transgranular microcracks in a plane parallel to core axis, for (a) LdB-G1–solid core, (b) F-G2–solid core, (c) LdB-G4–solid core disking and (d) F-G4–ring disking.

3.4.4 Summary

Microcrack pattern and grain size distribution analysis were conducted using image analysis and linear-traverse measurement for LdB granite and Forsmark granite. The average grain size of Forsmark granite is 1/5 the average grain size of LdB granite. From the analysis it appears that natural microcracks are dominated by grainboundary and intragranular type cracks. However, an increase in the density of transgranular cracks appears to be an indicator for stress-induced microcracking and these cracks tend to be aligned perpendicular to the direction of drilling.

The samples of LdB granite showed a significant increase in crack density at depth while the samples from Forsmark granite did not show a significant increase. However, when compared to the crack density in disked samples, only a minor increase in crack density was observed in the LdB samples while a significant increase was observed in the Forsmark samples. It appears that samples of Forsmark granite do

61

not contain a significant amount of stress-induced cracking compared to samples of LdB granite taken from similar depths. In the next section, we will explore the volume of microcracks and its correlation with *in situ* stress magnitude.

3.5 Microcrack volumetric strain with depth

From the microcrack analysis it was found that the amount and pattern of the microcracks are dependent on the rock type and depth. However, the microcrack image analysis while suitable for establishing qualitative trends and classifying the types of cracks, is not practical for establishing quantifiable trends. The image analysis clearly showed the crack density increases with depth and hence a method that quantifies the microcrack volume should be a suitable indicator of microcrack density.

An increase in stress-induced crack volume will lead to significant increase in nonlinear stress-strain behavior during the early stages of loading for both unconfined and confined compression tests (Martin and Stimpson, 1994). This initial nonlinear behavior for low porosity crystalline rock is associated with microcrack closure (Martin and Stimpson, 1994; Lei at al, 2000).

Lim et al. (2007) quantified the amount of this initial nonlinearity (area obc in Figure 3.12) in the axial stress-strain response using crack closure energy. The crack closure energy was defined as the energy required to close the microcracks and was calculated by subtracting the elastic potential strain energy from the total measured strain energy.

The concept used by Lim et al. (2007) can be extended to the volumetric response of the cylindrical samples using microcrack volumetric strain. The laboratory testing program measures both the axial and lateral strains. Figure 3.12 shows the volumetric stress-strain diagram obtained from a single uniaxial compression test. Figure 3.12 illustrates the regions of crack closure and growth, volumetric strain response, and the changes of crack volumetric strain. The volumetric strain (ε_v) is determined by summing the elastic volumetric strain (ε_v^e) and the volumetric strain
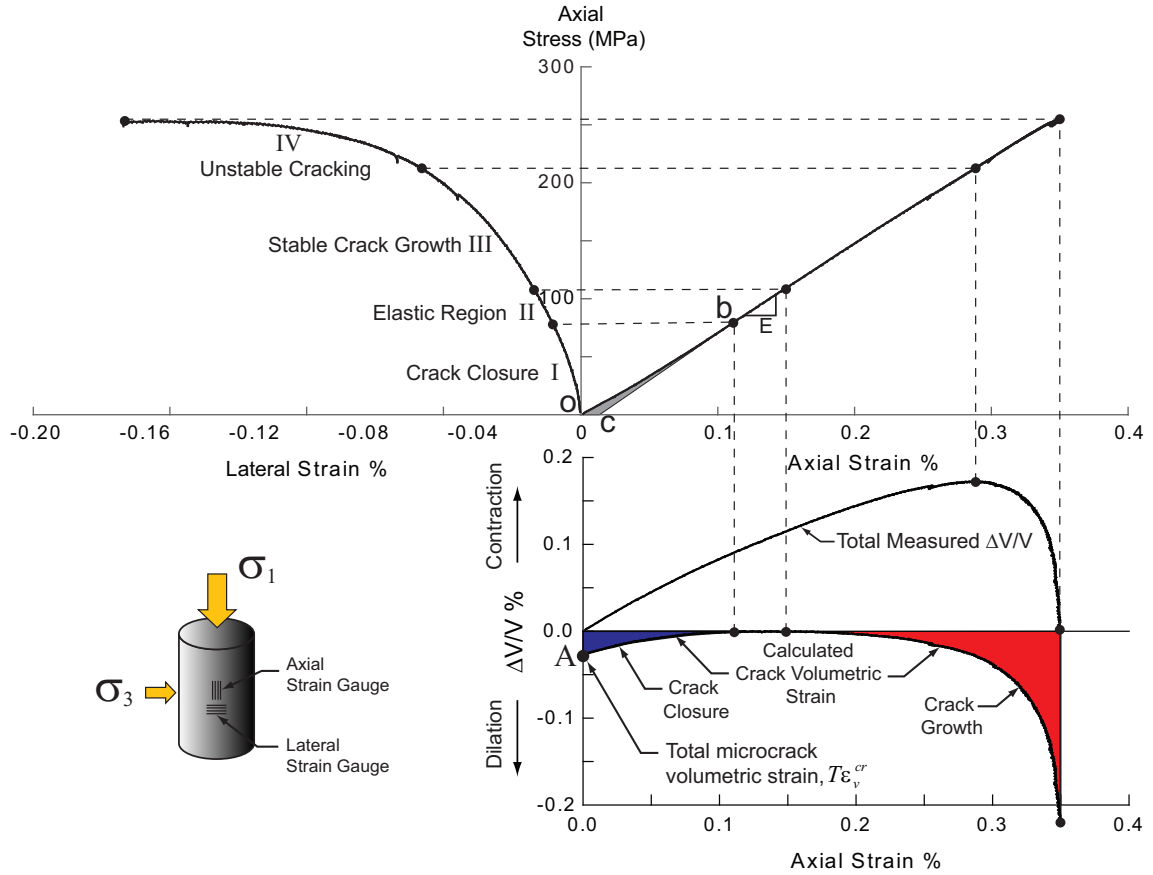
Figure 3.12: Volumetric strain diagram obtained from a single uniaxial compression test showing the definition of total microcrack volumetric strain ($T\varepsilon_v^{cr}$). The regions of crack closure and growth, volumetric strain response, and the change of crack volumetric strain are illustrated.

associated with microcrack closure (ε_v^{cr}). If the elastic properties of the sample are determined once the cracks are closed, the microcrack volumetric strain can be calculated from Equation (3.1).

$$\varepsilon_v^{cr} = \varepsilon_v - \varepsilon_v^e \tag{3.1}$$

The volumetric strain (ε_v) for cylindrical samples, under small strains, can be calculated by using Equation (3.2) (Brown, 1981):

$$\varepsilon_v = \frac{\Delta V}{V} \cong \varepsilon_{axial} + 2\varepsilon_{lateral} \tag{3.2}$$

For a cylindrical sample subjected to uniaxial loading, without a confining stress, the elastic volumetric strains can be estimated using:

$$\varepsilon_v^e = \frac{(1 - 2\nu)}{E}\sigma_1 \tag{3.3}$$

The elastic constants (E,ν) can be obtained from the linear portion of stress-strain curves in Region II. The total microcrack volumetric strain, $T\varepsilon_v^{cr}$, in this study is defined as the accumulated microcrack volumetric strain given by Point A in Figure 3.12.

A total of 87 rock core samples were analyzed to quantify the total microcrack volumetric strain. The standard Uniaxial Compression Strength (UCS) test was conducted for 42 LdB granite specimen extracted from 2 boreholes at 7 different depths. The UCS tests were carried out according to the ISRM Suggested Methods (Brown, 1981). Stress-strain data from 45 UCS tests of Forsmark granite (Jacobsson, 2004b,c, 2005), were also analyzed to measure the total microcrack volumetric strain. Table 3.4 provides a summary of the tested samples including borehole ID, coring depth and the number of specimens.

In our approach, and based on the findings from Chernis (1984), Martin and Stimpson (1994), stress-induced fractures will close in the early stage of axial loading. Two facts are supporting this assumption. First, the stress-induced microcracks, particularly transgranular type, generally occur perpendicular to the core axis. Second, when stress magnitudes are sufficient to cause stress-induced cracking the significant crack volume increase depends mostly on the transgranular type cracks due to their shape and characteristics (Chernis, 1984; Martin and Stimpson, 1994).

Figure 3.13a shows the plot of mean total microcrack volumetric strain as well as the minimum and maximum values with depth for Forsmark granite. An increasing trend of total microcrack volumetric strain with depth is observed. In Figure 3.13a,

Table 3.4: A list of samples for measuring total microcrack volumetric strain.

Rock type	Borehole ID	Sampling depth (m)	Number of test sample
LdB Granite	URL-6	13	6
		147	6
		242	6
		303	6
	URL-5	441	6
		592	6
		961	6
Forsmark Granite	KFM01A	226	5
		495	6
		688	6
	KFM04A	141	5
		508	6
		704	6
	KFM05A	284	5
		486	6

the microcrack volumetric strain, obtained from the mean pressure (hydrostatic) approach introduced by Brace (1965), is also plotted. The approach of Brace (1965) was used by Jacobsson et al. (2007) for the testing of Forsmark granite to determine the linear region when most of the microcracks are closed. The tested samples were obtained from the borehole KFM01A, which is one of the boreholes investigated in this study. Jacobsson et al. (2007) concluded that a mean stress of 50 MPa is needed to achieve the linear compressibility. The trend of the crack volumetric strain obtained by Jacobsson (2007) and Jacobsson et al. (2007), is compared to the trend using the uniaxial pressure approach in Figure 3.13a. As shown in Figure 3.13a, the same trend is obtained with both methods, but as expected the total crack volumetric strain is less than that obtained using the mean pressure approach. The difference between the two approaches may be caused by the axially oriented natural pores and microcracks that will not be closed by the axial loading. However, it should be noted that a mean stress of 50 MPa is not achieved *in situ* and hence *in situ* some of these cracks would be open.

Figure 3.13b shows the plot of mean total microcrack volumetric strain for LdB

granite at URL. The trends in Figure 3.13a and Figure 3.13b appear similar. However, the amount of total microcrack volumetric strain for LdB granite at depths <200 m is one order of magnitude larger than that for Forsmark granite. In order to compare both data sets, the total microcrack volumetric strains are normalized to the initial mean total microcrack volumetric strain. Because the image analysis showed that at shallow depths the majority of the microcracks are grain boundary cracks, this initial microcrack volumetric strain is referred to as "Natural", implying there is no evidence for volumetric strain caused by stress-induced microcracks. Figure 3.14 shows the normalized trends for both LdB granite and Forsmark granite and it is clear that both rocks display very similar trends with depth. The *in situ*
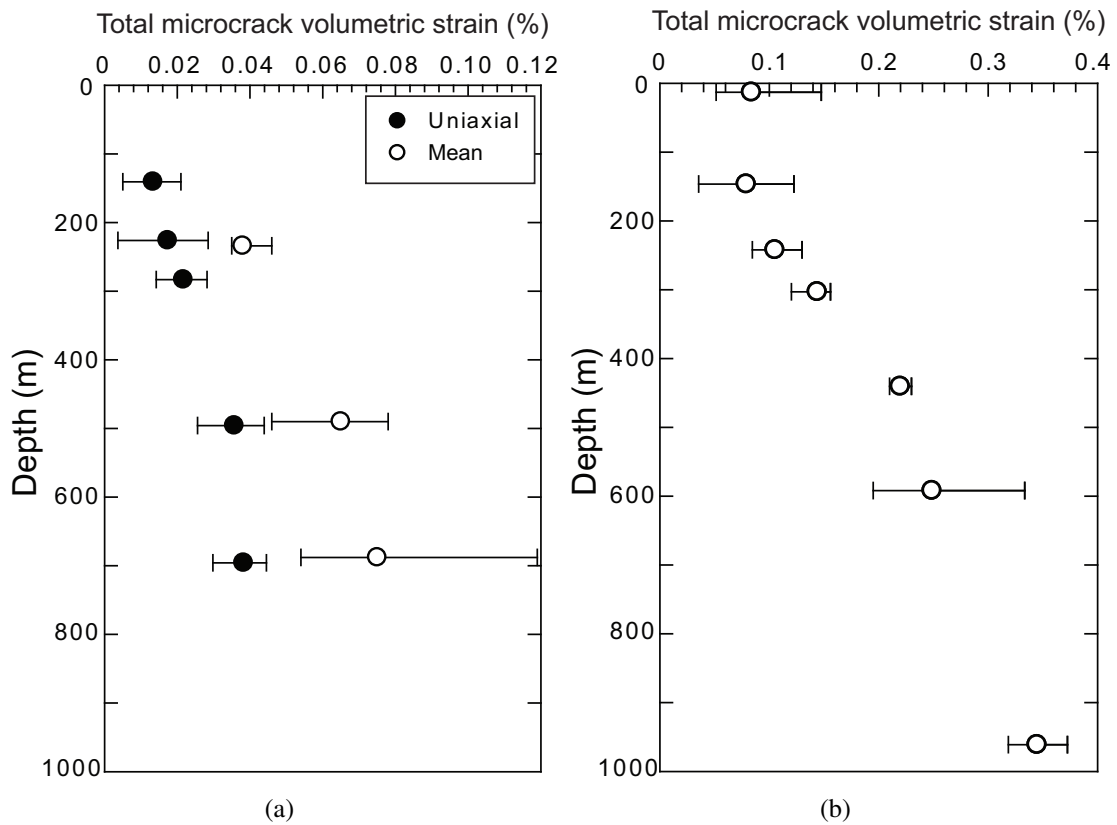
Figure 3.13: Total microcrack volumetric strain versus depth, for (a) Forsmark granite at Forsmark and (b) LdB granite at the URL. The microcrack volumetric strain obtained by mean pressure loading approach is compared to that by uniaxial loading approach for Forsmark granite.

66
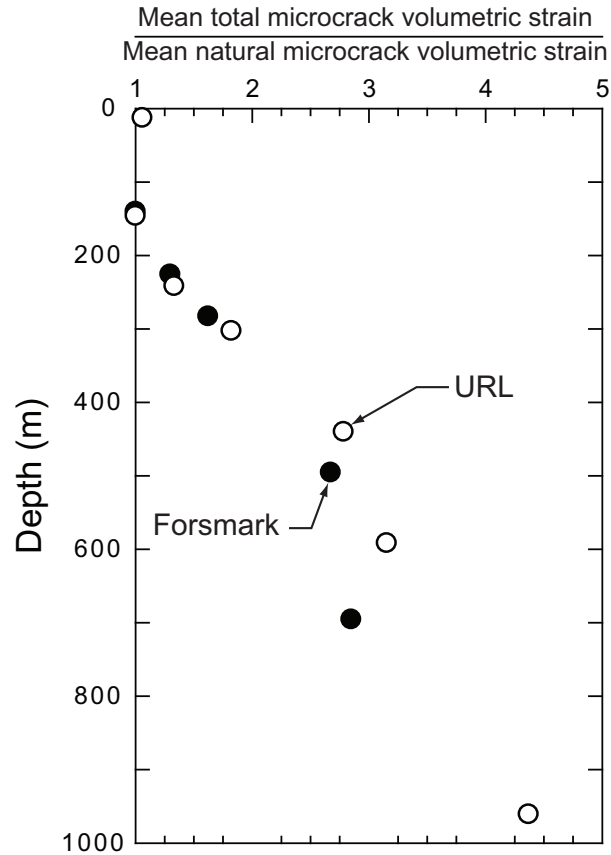
Figure 3.14: The plot of mean total microcrack volumetric strain normalized by initial microcrack volumetric strain for both LdB and Forsmark granite.

stress condition for the investigated sites and its correlation with the measured total mirocrack volumetric strain will be discussed in the following section.

3.6 Comparison of *in situ* stress magnitudes and microc-rack volume

It was shown using image analysis that the microcrack density increases significantly when the stress magnitudes are sufficient to cause core disking, suggesting a relationship between stress magnitudes and microcrack density. In the previous section it was also shown that the total microcrack volume increases with depth. In this section we explore the notion that the increase in stress-induced microcrack volume is related to the increase in *in situ* stress magnitudes with depth.

3.6.1 *In situ* stress profiles

URL

The *in situ* stress trends with depth at AECL′s URL were initially characterized using traditional triaxial overcoring, hydraulic fracturing and back analysis of convergence measurements (Thompson and Chandler, 2004). Large scale *in situ* experiments were used to confirm and refine the variability in the *in situ* stress magnitudes to a depth of 420 m (Martin et al., 1997). More recently, using a modified door stopper technique (DDGS), Thompson and Chandler (2004) reported the stress magnitudes at the URL to a depth of approximately 1000 m. Based on the extensive *in situ* stress characterization program, three distinctive stress domains were defined and these are shown in Figure 3.15a. Also shown in Figure 3.15a are the locations of the fracture zones (e.g., FZ 2.5, 2) and change from fractured rock to massive rock.

Stress domain I extends from surface to fracture zone (FZ) 2.5 which is the boundary between fractured pink granite and massive gray granite. In this domain there is a gradual increase in the magnitude of the mean *in situ* stress, $\sigma_m = (\sigma_1 + \sigma_2 + \sigma_3)/3$), to 15 MPa. Stress domain II is transitional zone between domains I and III. The stress domain III resides entirely in the massive, fracture-free granite. The mean *in situ* stress in this domain reaches about 50 MPa near 900 m depth.

Forsmark

In the Forsmark area, extensive stress measurements were conducted in the 1970s′ and 1980s′ to a maximum depth of 500 m for the construction of the nuclear power plants and the final repository for the low and intermediate nuclear waste repository (SFR) (Sjöberg et al., 2005). The current stress measurement campaign began in 2003 and consisted of hydraulic fracturing in boreholes to depth of 1000 m and overcoring using the Borre Probe (Sjöberg and Klasson, 2003) to the target depth of a repository for spent fuel (approximately 400 to 600 m). Those campaigns have established the stress magnitudes and orientation to a depth of approximately
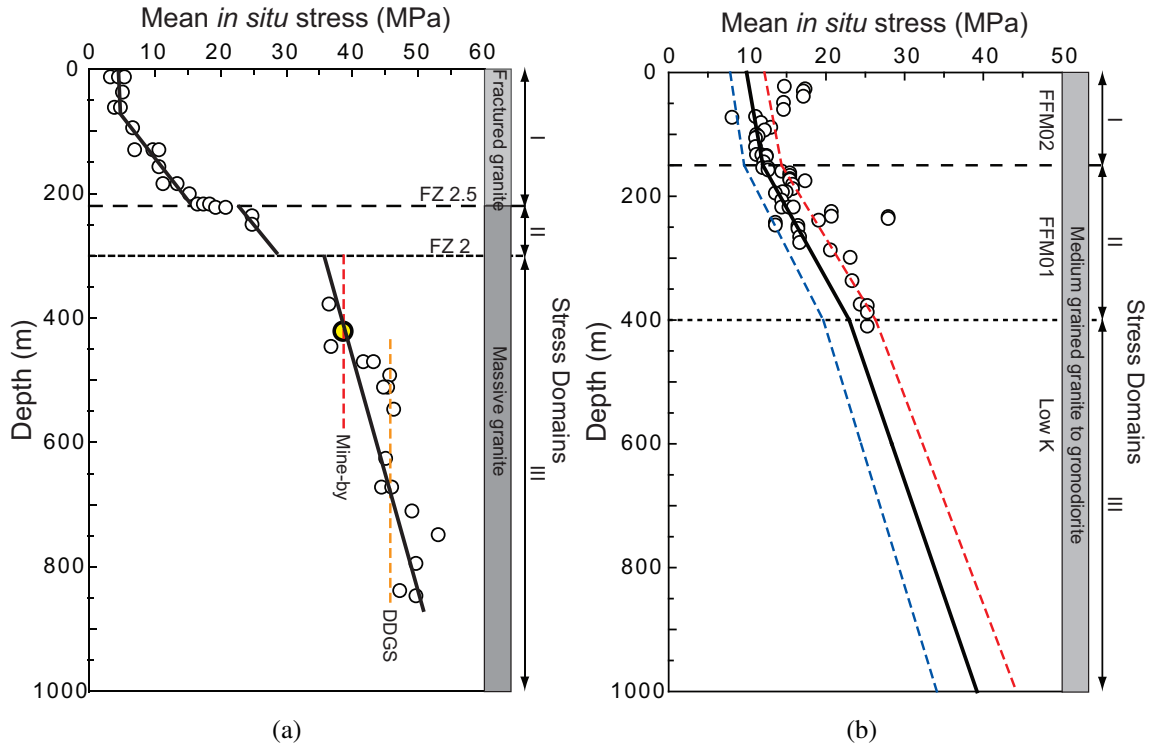
Figure 3.15: Mean *in situ* stress ($\sigma_m = (\sigma_1 + \sigma_2 + \sigma_3)/3$) magnitude and stress domains, for (a) URL and (b) Forsmark. Stress data from (Martin, 2007; SKB, 2008).

1000 m. Below 400 m the confidence of the *in situ* stress magnitudes is significantly reduced because the *in situ* stress measurement program during site investigation phase was limited to hydraulic fracturing in the 76-mm-diameter surface-drilled boreholes. Most recently, Martin (2007) established the stress gradient model using borehole breakout analysis utilizing principle stress ratio, mean principal stress and spalling ratio, and suggested the horizontal and vertical *in situ* stress gradients to the depth of 1000 m given in Figure 3.15b. The mean stress reaches approximately 40 MPa at 1000 m depth.

3.6.2 *In situ* stress magnitudes and microcracking

The trend lines in Figure 3.15 were used to establish the relationship between mean stress magnitude and normalized total microcrack volumetric strain shown in Figure 3.14. Figure 3.16 shows the trend established from those data sets. The

mean stress magnitudes have been normalized to the tensile strength provided in Table 3.2. Figure 3.16 shows a linear increase in total microcrack volumetric strain with mean stress magnitude. Similar findings were reported by Carlson and Wang (1986) who measured the microcrack volume porosity using polyaxial cubes. It would appear that regardless of the reason the volumetric strain due to microcracks in core samples can be expected to increase with depth and, hence, stress magnitude.
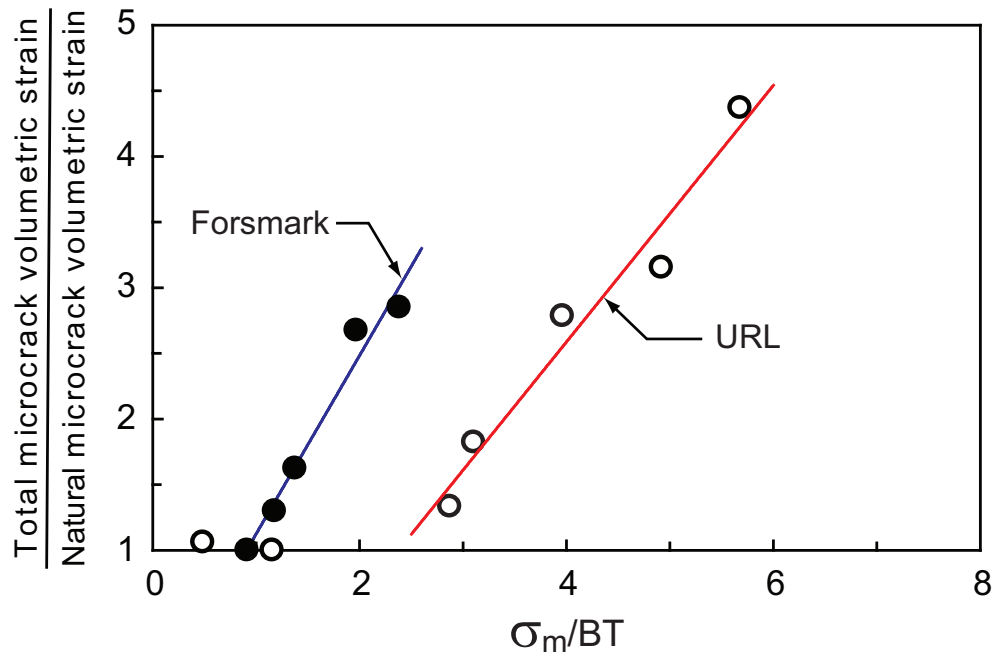
Figure 3.16: Relationship between normalized microcrack volumetric strain and mean *in situ* stress, $\sigma_m = (\sigma_1 + \sigma_2 + \sigma_3)/3$, normalized to the Brazilian tensile strength, BT, given in Table 3.2 for LdB granite at URL and Forsmark granite at Forsmark.

3.7   Conclusion

The image analysis combining both fluorescent and polarized microscopy techniques was conducted to quantify the microcracking in two different granites. Microcrack type, density, length and orientation as well as the grain size for each granite sample were measured and analyzed. The results indicated that natural microcracks were primarily observed in the samples at shallow depth ($<$200 m) and

that the majority of these microcracks were grain boundary cracks. The density of microcracking increased with depth. While the density of all three types of microcracks (grain boundary, intragranular and transgranular) increased with depth, a significant increase in density of transgranular microcracks signalled an association with elevated stress magnitudes.

Analysis of the increase in the density of transgranular microcracks showed that these cracks were perpendicular to the core axis. It was found that the ratio of horizontal to vertical transgranular microcracks could be an indicator of the extensive stress-induced microcracking. The microcrack volume in laboratory samples can be estimated using the total microcrack volumetric strain. This was measured for 87 granite samples from the study sites. It was found that the volume of microcracks for LdB granite was approximately one order of magnitude greater than the volume found in Forsmark granite, even though the total number of microcracks is similar for both granites. Because the crack volumes tend to be dominated by grain boundary cracks it appears that the difference in the microcrack volumetric strain is related to the larger grain size in LdB granite (approximately 5 times larger than the Forsmark granite). Linear trends were established between the normalized mean *in situ* stress and total microcrack volumetric strain for both LdB granite and Forsmark granite. Carlson and Wang (1986) reported a similar linear trend for Illinois granite. It appears that granite samples taken at depth show a linear increase in microcrack volume with mean *in situ* stress.

Bibliography

Åkesson, U. 2004. Characterisation of microcracks in the Bohus granite, western Sweden, caused by uniaxial cyclic loading. *Engineering Geology* 72: 131–142.

Amadei, B., Stephansson, O. 1997. *Rock Stress and Its Measurement*, first ed. Chapman & Hall, London.

Brace, W.F. 1965. Some new measurements of linear compressibility of rocks. *J. Geophys. Res.* 70(2): 391–398.

Brace, W.F., Silver, E., Hadley, K., Goetze, C. 1972. Cracks and pores: A closer look. *Science* 178: 162–164.

Brown, E.T. 1981. *Rock characterization testing and monitoring*. International Society for Rock Mechanics–the Commission on Testing Methods, Pergamon.

Carlson, S.R., Wang, H.F. 1986. Microcrack porosity and in-situ stress in Illinois borehole UPH 3. *J. Geophys. Res.* 91: 10421–10428.

Chernis, P.J. 1984. Comparison of the pore-microstructure of shallow and deep samples of the Lac du Bonnet granite. *Technical Record 223*, Atomic Energy of Canada Limited, Onterio.

Dyke, C.G. 1994. *In situ stress indicators for rock at great depth*. Ph.D. thesis, University of London (Imperial College of Science, Technology & Medicine), London, United Kingdom.

Everitt, R.A. 2001. *The influence of rock fabric on excavation damage in the Lac*

du Bonnet granite. Ph.D. thesis, Department of Civil & Geological Engineering, University of Manitoba, Winnipeg, Manitoba, Canada.

Jacobsson, L. 2004a. Drill hole KFM01A–indirect tensile strength test. *SKB P-04-170*, Swedish Nuclear Fuel and Waste Management Co., Stockholm.

Jacobsson, L. 2004b. Forsmark site investigation: Borehole KFM01A–uniaxial compression test of intact rock. *SKB P-04-223*, Swedish Nuclear Fuel and Waste Management Co., Stockholm.

Jacobsson, L. 2004c. Forsmark site investigation: Borehole KFM04A–uniaxial compression test of intact rock. *SKB P-04-226*, Swedish Nuclear Fuel and Waste Management Co., Stockholm.

Jacobsson, L. 2005. Forsmark site investigation: Borehole KFM05A–uniaxial compression test of intact rock. *SKB P-05-97*, Swedish Nuclear Fuel and Waste Management Co., Stockholm.

Jacobsson, L. 2007. Forsmark site investigation: Borehole KFM01A and KFM02B–Microcrack volume measurements and triaxial compression tests on intact rock. *SKB P-07-93*, Swedish Nuclear Fuel and Waste Management Co., Stockholm.

Jacobsson, L., Flansbjer, M.,Christiansson, R.,Jansson, T. 2007. *Measurement of micro crack volume in low porosity crystalline rock.* In: *11th Congress of the International Society for Rock Mechanics*. Ribeiro e Sousa, Olalla, Grossmann, *editors*, Taylor & Francis Group, London, pp. 55–58.

Kowallis, B.J., Wang, H.F. 1983. Microcrack study of granitic cores from Illinois deep borehole UPH 3. *J. Geophys. Res.* 88(B9): 7373–7380.

Kranz, R.L. 1983. Microcracks in rocks: A review. *Tectonophysics*. 100: 449–480.

Lei, X.-L., Kusunose, K., Nishizawa, O., Cho A., Satoh, T. 2000. On the spatio-temporal distribution of acoustic emissions in two granitic rocks under triaxial compression: the role of pre-existing cracks. *Geophysical Research Letters* 27(13): 1997–2000.

Lim, S.S., Martin, C.D. 2010. Core disking and its relationship with stress magnitude for Lac du Bonnet granite. *Int. J. Rock Mech. Min. Sci.* 47(2), 254–264.

Lim, S.S., Martin, C.D., Christiansson, R. 2007. In-situ stress estimation using crack closure energy in crystalline rock. In: *Proceedings 1st Canada–U.S. Rock Mechanics Symposium*, *Vancouber*. Eberhardt, E., Stead, D., Morrison, T. *editors*. Taylor & Francis Group, London, pp. 683–689.

Martin, C.D. 1990. Characterizing *in situ* stress domains at the AECL Underground Research Laboratory. *Can. Geotech. J.* 27:631–46.

Martin, C.D. 2007. Quantifying in-situ stress magnitudes and orientations for Forsmark–Forsmark stage 2.2. *SKB P-07-26*, Swedish Nuclear Fuel and Waste Management Co., Stockholm.

Martin, C.D., Christiansson, R. 1991. Overcoring in highly stressed granite–The influence of microcracking. *Int. J. Rock Mech. Min. Sci.* 28(1): 53-70.

Martin, C.D., Read, R.S., Martino, J.B. 1997. Observations of brittle failure around a circular test tunnel. *Int. J. Rock Mech. Min. Sci.* 34(7):1065–1073.

Martin, C.D., Stimpson, B. 1994. The effect of sample disturbance on laboratory properties of Lac du Bonnet granite. *Can. Geotech. J.* 31(5): 692–702.

Nadan, B., Engelder, T. 2009. Microcracks in New England granitoides: A record of thermoelastic relaxation during exhumation of intracontinental crust. *Geol. Soc. Am. Bull.* 121: 80–99.

Nur, A., Simmons, G. 1970. The origin of small cracks in igneous rocks. *Int. J. Rock Mech. Min. Sci.* 7(3): 307–314.

Obert, L., Stephenson, D.E. 1965. Stress conditions under which core discing occurs. *Transactions Sociaty of Mining Engineers* 232(3): 227–235.

Olsson, W.A. 1974. Grain size dependence of yield stress in marble. *J. Geophys. Res.* 79: 4859–4862.

Read, R.S. 1994. *Interpreting excavation-induced displacements around a tunnel*

in highly stressed granite. Ph.D. thesis, Department of Civil & Geological Engineering, University of Manitoba, Winnipeg, Manitoba, Canada.

Simmons, G., Richter, D. 1976. Microcracks in rock, In: *The Physics and Chemistry of Minerals and Rocks*. Strens, R. *editor*. Willey, New Youk, pp. 105–137.

Sjöberg, J., Klasson, H. 2003. Stress measurements in deep boreholes using the Borre (SSPB) probe. *Int. J. Rock Mech. Min. Sci.* 40(8): 1205–1223.

Sjöberg, J., Lindfors, U., Perman, F., Ask, D. 2005. Forsmark site investigation: Borehole KFM05A–uniaxial compression test of intact rock. *SKB R-05-35*, Swedish Nuclear Fuel and Waste Management Co., Stockholm.

SKB, 2005. Preliminary site description Forsmark area–version 1.2. *SKB R-05-18*, Swedish Nuclear Fuel and Waste Management Co., Stockholm.

SKB, 2008. Site description of Forsmark at completion of the site investigation phase. SDM-Site Forsmark. *SKB TR-08-05*, Swedish Nuclear Fuel and Waste Management Co., Stockholm.

Stacey, T.R. 1982. Contribution to the mechanism of core discing. *Journal South African Institute of Mining and Metallurgy* 99: 269-274.

Thompson, P.M., Chandler, N.A. 2004. In situ rock stress determinations in deep boreholes at the Underground Research Laboratory. *Int. J. Rock Mech. Min. Sci.* 41(8): 1305–1316.

Vollbrecht, A., Rust, S., Weber, K. 1991. Development of microcracks in granites during cooling and uplift: examples from the Variscan basement in NE Bavaria, Germany. *J. Struct. Geol.* 13(7): 787–799.

Wang, H.F., Simmons, G. 1978. Microcracks in crystalline rock from 5.3-km depth in the Michigan basin. *J. Geophys. Res.* 83(B12): 5849–5856.

Chapter 4

Core disking and its relationship with stress magnitude for Lac du Bonnet granite [2]

4.1 Introduction

There is no question that *in situ* stress magnitudes and directions are required for the design of deep underground excavations. Yet, *in situ* stress measurements are particularly difficult in deep small diameter (<100 mm) boreholes and high-stress environments with horizontal stresses greater than the vertical stress (Doe et al., 2006). In such situations core disking and borehole breakouts may occur. Observations of these phenomena indicate that the *in situ* stress magnitudes are high relative to the rock strength. However, as noted by Doe et al. (2006) core disking like borehole breakouts is generally viewed as a qualitative method for estimating stress magnitudes. Nonetheless in the early stages of site investigation such observations are important and may play a critical role when evaluating the *in situ* stress magnitudes for a site.

Core disking has been investigated since the 1960′s using either laboratory testing and/or numerical analyses (Jaeger and Cook, 1963; Obert and Stephenson, 1965; Sugawara et al., 1978; Stacey, 1982; Dyke, 1989; Haimson and Lee, 1995; Li and

---

[2] This chapter has been published to the Int. J. of Rock mech. and Min. Sci. 47(2): 254–264.

Schmitt, 1998; Song and Haimson, 1999; Hakala, 1999a; Kaga et al., 2003). While these studies have provided insight into the core disking mechanism there is still uncertainty as to the relationship between core disking and the stress magnitudes required to cause disking. This uncertainty arises because of the lack of core-disking field data where the *in situ* stress magnitudes are known with confidence. Relationships relating disking and stress magnitudes based on laboratory data are often questioned because the core diameter used in laboratory studies is usually less than 25 mm diameter, and it is well known that intact rock properties are affected by scale effects when samples are relatively small (Hoek and Brown, 1980; Martin, 1997).

Disked cores from boreholes drilled from underground excavations in massive unfractured rock Lac du Bonnet granite are characterized for disk thickness, surface geometry and fracture persistence. The *in situ* stress magnitudes were characterized in previous studies and hence provided a unique opportunity to establish relationships between core disking in core from 75-mm-diameter boreholes and stress magnitudes. In this study we focus primarily on the relationship between the maximum stress and disk thickness, as tunnel stability is often related to the maximum stress, e.g., see Hoek and Brown (1980), and when disking is encountered an obvious question is will the maximum stress magnitude be sufficient to impact tunnel stability.

4.2   Background

AECL′s Underground Research Laboratory (URL) was constructed between 1983 and 1990 and operational experiments have been ongoing since then (Read, 2004). The majority of the geomechanics experiments were carried out on the 420 Level in a massive unfractured rock mass (Figure 4.1). The characteristics of the rock mass and the properties of the intact rock are given in Martin et al. (1997). The *in situ* stress state at AECL′s URL was described by Martin (1990) and Read (1994) used deformations ahead of a tunnel advance to develop a statistically rigorous technique to establish the *in situ* stress state at the 420 Level of the URL. Table 4.1 gives the

(a)

Room 418-U3

Borehole & stress calculation lines

15.11 m

Room 418-U2

14.79 m

3.23 m
D
1m
2m
T A 1m
T

Room 418-U1

σ_3 σ_1

15.88 m
D
σ_2

D : Designed geometry
T : Transient zone
A : As-built geometry

<Far field stress>

(b)
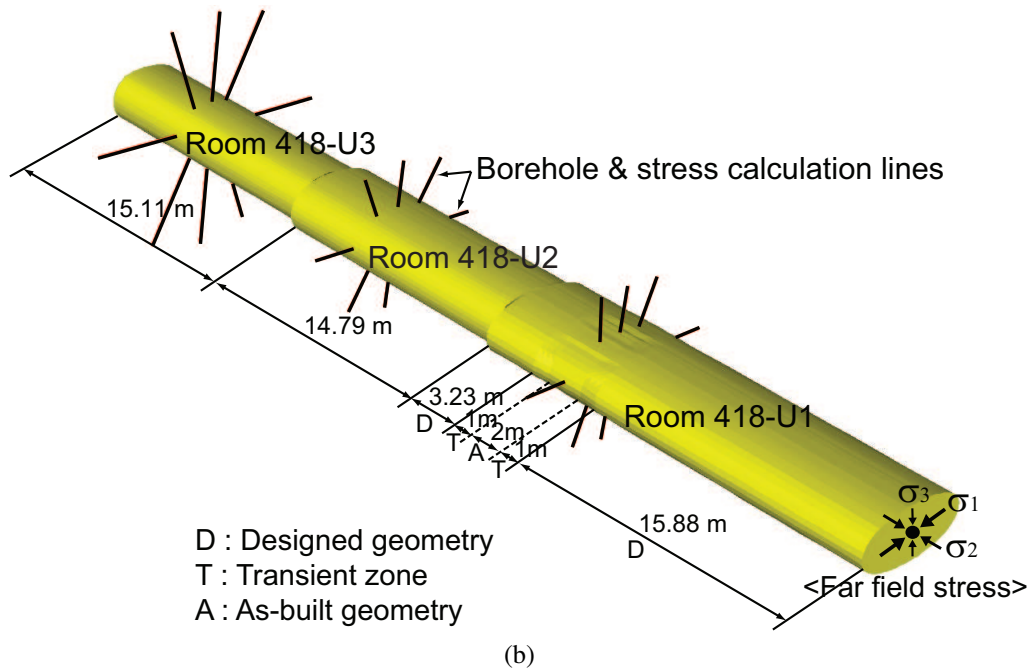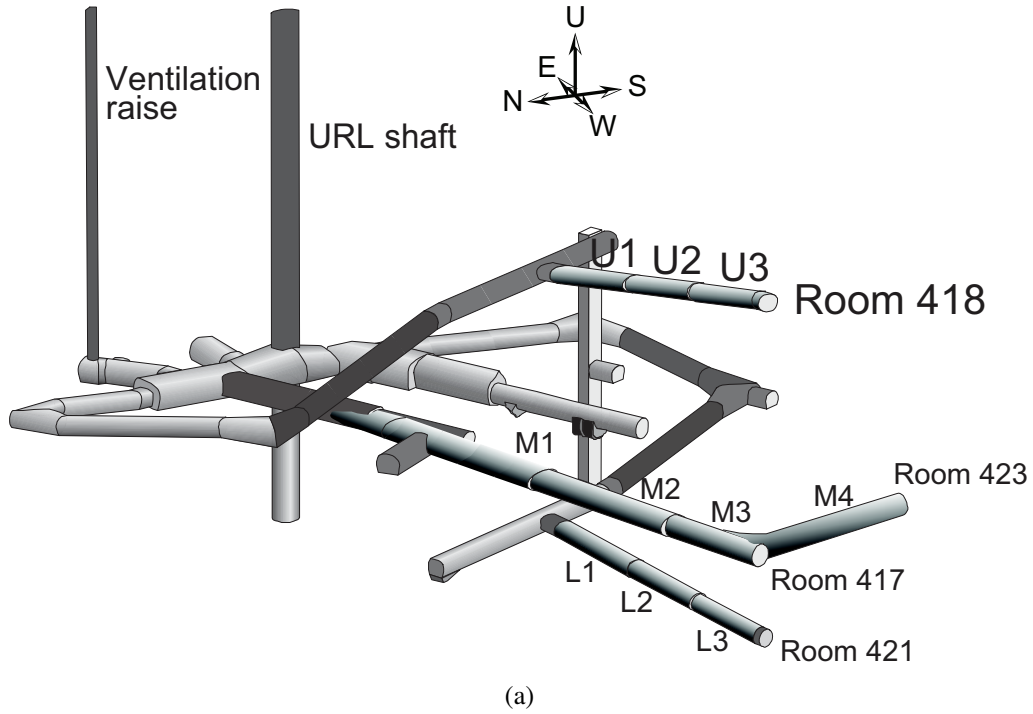
Figure 4.1: General layout of the 420 Level of AECL′s Underground Research Laboratory and location of MVP boreholes used in Array 418-U1, -U2 and -U3: (a) URL 420 Level and (b) Boreholes in Room 418 used in the core disking study.

stress magnitudes on the 420 Level where the excavations and experiments were conducted (Martin and Read, 1996).

Table 4.1: *In situ* principal stress magnitudes and orientations for the 420 Level, after Martin and Read (1996).

Stress	σ_1	σ_2	σ_3
Magnitude (MPa)	60 ± 3	45 ± 4	11 ± 4
Trend/Plunge ($^\circ$)	145/11	054/08	290/77

Between 1995 and 1997 a series of openings with different geometries were excavated on the 420 level as part of the Excavation Stability Study (ESS) (Read, 2004). According to Read (2004), the excavation geometries were optimized to reduce the stress concentrations on the boundaries of the openings. By creating ovaloid shaped openings and varying orientation of the long axis of the room cross section relative to the maximum in-plane stress, the maximum tangential stress on the boundary, and hence the damage around the opening, could be controlled. To characterize the excavation damaged zone around these openings a series of radially oriented 75-mm-diameter (NQ3-size) boreholes (labelled MVP) were drilled from each opening to a nominal depth of 2.50-5.30 m (Martino and Chandler, 2004). The boreholes were drilled using standard triple-tube diamond-drilling coring technology typically used in underground excavation in Canada, with a nominal hole diameter of 75-mm, which produced a nominal core diameter of 45-mm. The cores from these boreholes were used for this study.

The ESS study produced two types of tunnels, those with no obvious signs of an excavation damaged zone (EDZ) and those with a visible v-shaped notch, clearly indicating the creation of an EDZ. The boreholes and core used in this study were chosen from both types of tunnels. Figure 4.2 illustrates the quality and shape of the excavations and Figure 4.3 shows the typical 45-mm-diameter core retrieved from the MVP boreholes. Normally the core from the 420 level is fracture free, i.e., there are no joints or discontinuities related to the geological history. Hence all the fractures observed in Figure 4.3 are stress-induced fractures related to the core-

Figure 4.2: Photo of Room 418 showing the room geometry at U1, -U2 and -U3. See Figure 4.1 for the locations of the rooms.

drilling and retrieval process. In this paper, the regularly spaced stress-induced fractures, such as those shown in Figure 4.3, are termed core disking.

Extensive core disking was observed in the core from 39 out of the 54 MVP boreholes drilled in Room 417, Room 418, Room 421 and Room 423 (see Figure 4.1 for room locations). In this paper, all disked and solid cores from the 54 MVP boreholes were analyzed. The core from each borehole was logged for rock type, disk thickness (t) and fracture orientation. These characteristics varied spatially around the excavation and with distance from the excavation boundary. Whether or not an EDZ was present in the form of a v-shaped notch also affected the stress-induced fracturing near the boundary of the opening. The effect of geology and EDZ on the stress-induced fractures is discussed in the following sections.
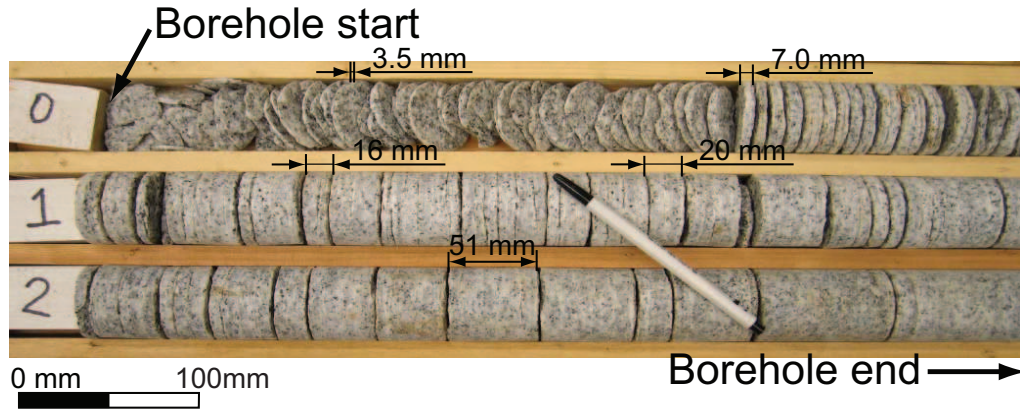
Figure 4.3: Typical core disking from a MVP borehole, 420 Level of URL, Canada. The diameter of cores is 45 mm and the total length of the MVP borehole is 2.54 m.

4.2.1 Local geology of the test tunnel

The AECL's URL is located within the Lac du Bonnet granite batholith near the western edge of the Canadian Shield and is considered to be representative of many granitic intrusions of the Precambrian Canadian Shield (Brown, 1989). The batholith, dated as Late Kenoran age (2680 ± 81 Ma), trends east-northeast and its elongated body is about 75 by 25 km in surface area and extends to a depth of at least 10 km. The URL geology is given by Everitt and Lajtai (2004) and in summary consists of an undifferentiated pink and grey massive porphyritic granite-granodiorite with relatively uniform texture and composition and local sub-horizontal gneissic banding. Colour is not a distinguishing characteristic of the rock units but the pink colouring indicates where the rock has been exposed to long-term groundwater circulation. The pink colouring occurs mainly from the ground surface to a depth of approximately 300 m

Everitt and Lajtai (2004) note three distinct textural varieties of the Lac du Bonnet granite: (1) fine grained granite dykes with subvertical flow banding (mapped as granodiorite), (2) medium grained and weakly to moderately layered granite forming the main mass of the batholith (mapped as granite), and (3) a generally coarse grained and leucocratic unit that occurs as sills and recrystallized zones in the main

unit. The major rock types encountered on the 420-Level are medium grained gray granite and fine grained granodiorite, with minor amounts of pegmatite and leucocratic granite (Everitt, 2001). The general geology of Room 418 is shown in Figure 4.4 and is considered typical of the geology on the 420 Level.
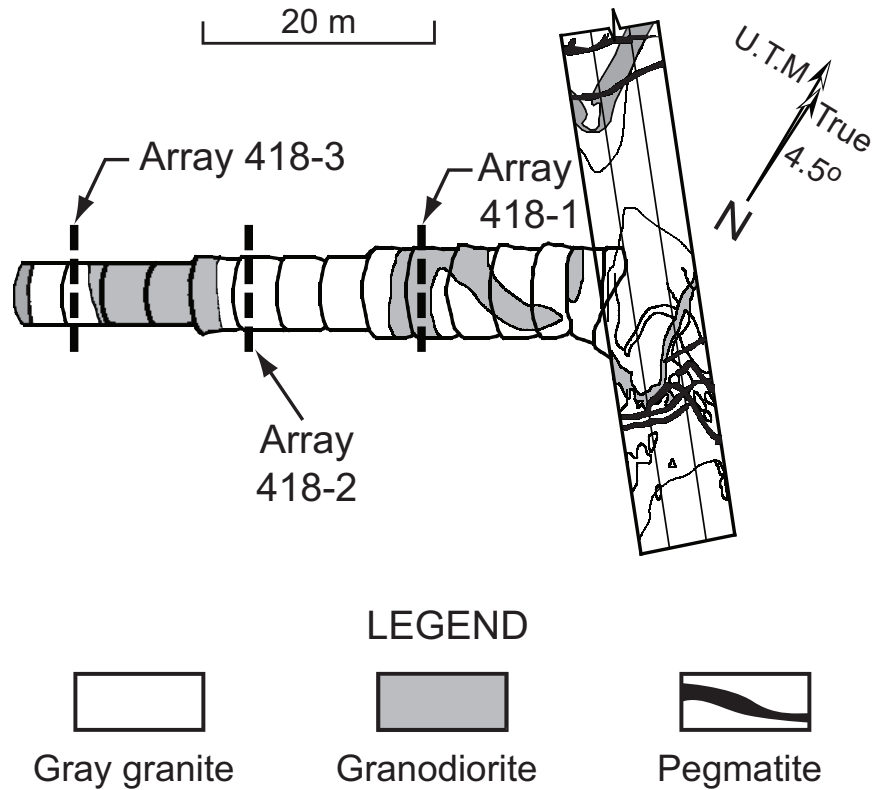
Figure 4.4: Geology of Room 418. Modified from Everitt (2001).

4.3 Core disking and fracturing in granite and granodiorite

Granite and granodiorite at URL fall within the same granite classification according to International Union of Geological Sciences (Martin et al., 1997). As noted by Everitt and Lajtai (2004) the main difference between the two rock types is the grain size and the texture. Figure 4.5 shows the comparison of average grain size distribution for main minerals found in the granite and granodiorite. While both rock types are composed of the same minerals, Read (2004) observed that the granodiorite
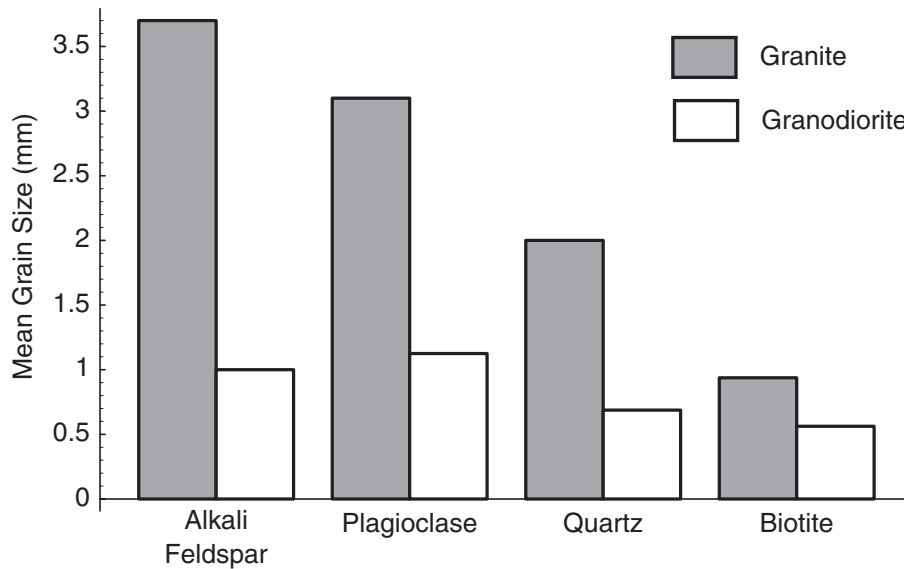
Figure 4.5: Grain size distribution of granite and granodiorite (after Martin et al. (1997)).

was less prone to stress-induced damage than the granite. Everitt and Lajtai (2004) also found from the laboratory uniaxial compressive and Brazilian tensile testing that the granodiorite was 17 percent stronger than the medium grained granite in both compression and tension. Figure 4.6 shows the disked cores from a 180 mm long section of core from MVP1 borehole in Room 418-U1 and clearly shows a distinct difference in disk thickness for the granite (4 to 8 mm) and granodiorite (15 to 25 mm). The varying disk thickness in Figure 4.6 suggests disking thickness is sensitive to the subtle differences between the granodiorite and granite. Obert and Stephenson (1965) also found that core disking thickness varied significantly in different rock types, e.g., granite and limestone. However, the observations in Figure 4.6 suggests that a 17 percent strength increase in this crystalline rock was sufficient to cause a 300 percent increase in the disk thickness.

4.3.1 Characteristics of core disking fracture

The thickness of the core disks were usually thin (several millimetres) at the collar of the MVP boreholes and gradually increased in thickness to several centimetres or completely disappeared towards the end of the boreholes. Most of the core disk

83
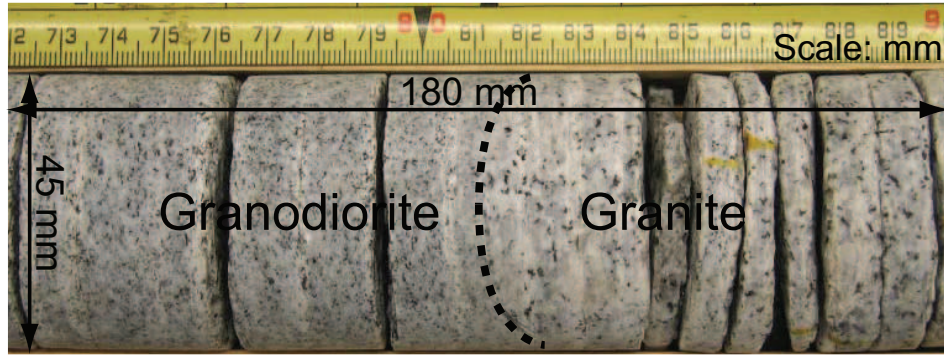
Figure 4.6: Observed core disks in coarse grained granite (gray granite) and fine grained granite (granodiorite). The average core disk thickness for granodiorite is thicker than that of gray granite under similar stress condition.

fractures had propagated across the cores resulting in thin disks completely separated from each other. In other cases, usually towards the end of the borehole, fractures were clearly visible but these fractures were not sufficiently developed to completely separate the disks. These are referred to as partial disks and is defined as the occurrence of a disking fracture that does not separate the core into two pieces. Figure 4.7 shows the partial core disks in the granodiorite core section from MVP5 borehole. Partial disks often are expressed as relatively thin white lines on the core, spaced at regular intervals.

To observe the detailed characteristics of the disking fractures, partial disks were examined by cutting a core and using a microscope and a digital camera. The

Figure 4.7: The partial core disking fractures.
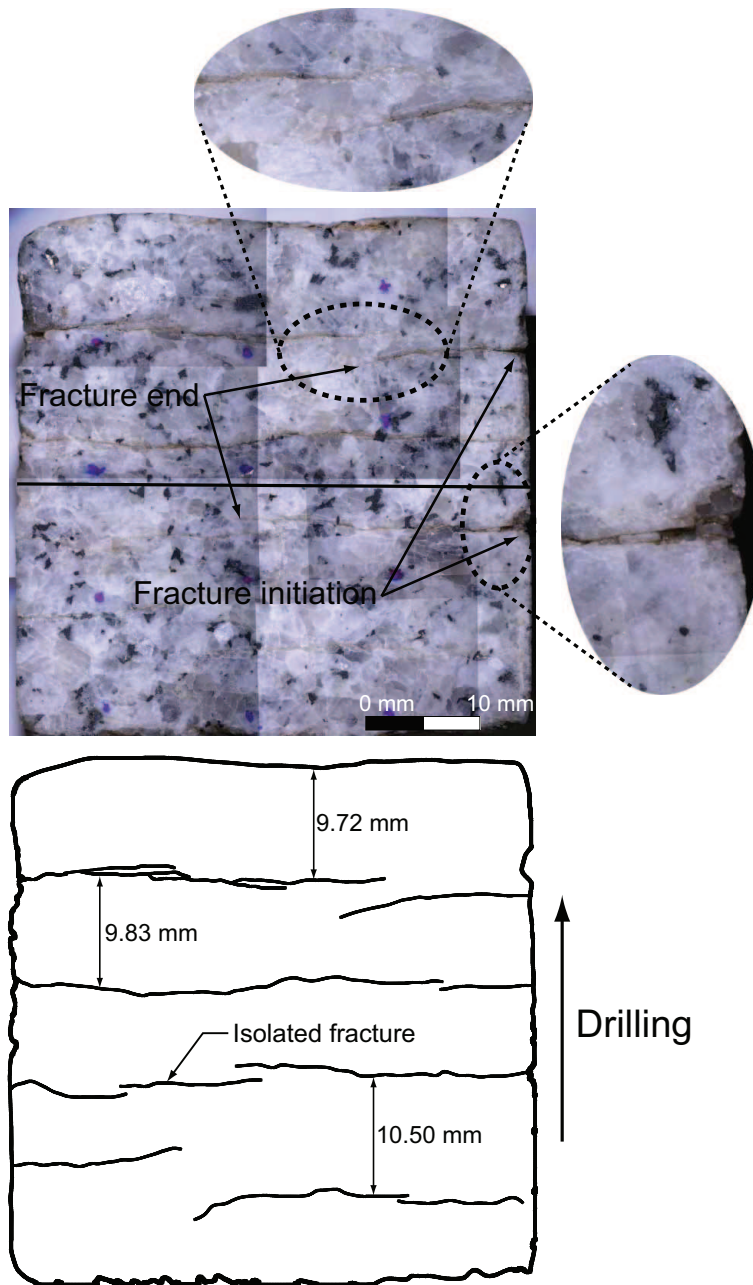
Figure 4.8: Initiation and propagation of core disking fractures. A partially fractured core was cut through the core axis.

cores were cut parallel to the core axis and polished using a No. 80 to No. 360 grit. Figure 4.8 shows there are clear indications that some fractures appear to have initiated at the core surface and propagated into the interior of the core, while other fractures are isolated inside of the core indicating that those fractures initiated at the

interior of the core and did not propagate to the outer surface of the core. Obert and Stephenson (1965) noted that core disking fractures initiated at the exterior surface of the core while Maury et al. (1988) reported, based on scanning observations of a rock core from a deep well, that the fracture can initiate in the interior of the core. Regardless of the initiation of the fracture, the overall disk shape is relatively flat, with fractures relatively uniformly spaced even when only partial disking is observed.

4.3.2   Core fracturing in the EDZ

The excavation damage zone (EDZ) can be defined as an irreversible damage zone in the rock mass due to the tunnel excavation (Tsang et al., 2005). The EDZ is a function of the *in situ* stress state, the rock mass strength and the excavation method. Two distinctly different EDZ regions can be observed around tunnels where the stress anisotropy is large, such as the URL. In the regions of the maximum compressive stress, slabbing and microcracking, i.e., spalling, is commonly observed. In contrast, in the tensile regions of the tunnel, discrete fractures are seldom observed. However, according to Martino and Chandler (2004), low seismic velocities in the tensile region of the tunnel wall suggest that the rock has been damaged by tensile microcracking. Hence, near the boundary of the opening, two stress-induced processes are noted; one resulting in compressive-stress-induced discrete fractures, while the other results in tensile-stress-induced microcracking.

In all 8 MVP arrays on the 420 Level of URL core disking was found in boreholes that were drilled in the high compressive stress region, i.e, roof and floor. No core disking was observed in the core from the boreholes drilled in the side wall, i.e., the tensile stress region. However, the cores obtained from the tensile region did show evidence of blast-induced fractures (see Figure 4.9). As shown in Figure 4.9 the shape and direction, relative to the core axis, of blast-induced fractures was irregular while the core disking fractures were just opposite. The blast-induced fractures are not considered in the core-disking analyses that follow.
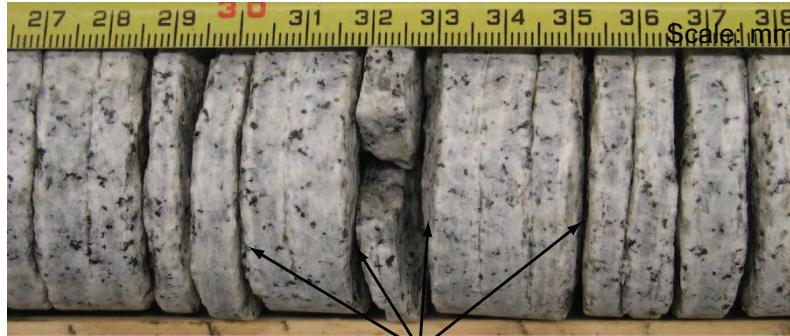
Core disking fracture

(a)
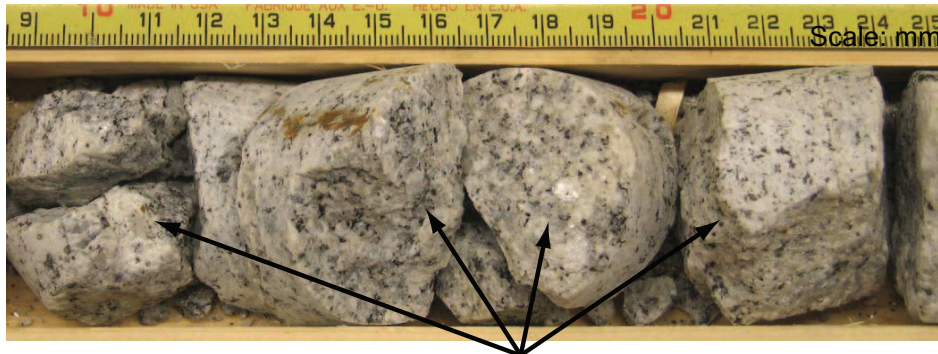
Blast-induced excavation damage cracks

(b)

Figure 4.9: Comparison between (a) core disking fractures obtained from MVP2 borehole located in the tunnel roof and (b) blast-induced excavation damage cracks obtained from MVP3 borehole located in the side wall of the MVP array in Room 418-U1. Core disking fractures are very uniform in their shape and space but the blast-induced excavation damage cracks have irregular shape and the direction of fractures vary.

4.4 Stress analyses

Room 418 was excavated using a full-face drill and blast technique (Read, 2004). Figure 4.2 shows Room 418 after completing the excavation. The direction of Room 418 tunnel was aligned parallel to the azimuth of the *in situ* intermediate principal stress. The tunnel perimeter was designed as an ovaloid with the major axis as 6.6, 5.3, 4.4 m for Room 418-U1, -U2 and -U3 respectively. The minor axis was 3.0 m for all three sections. The major cross sectional axes of Room 418-U1,
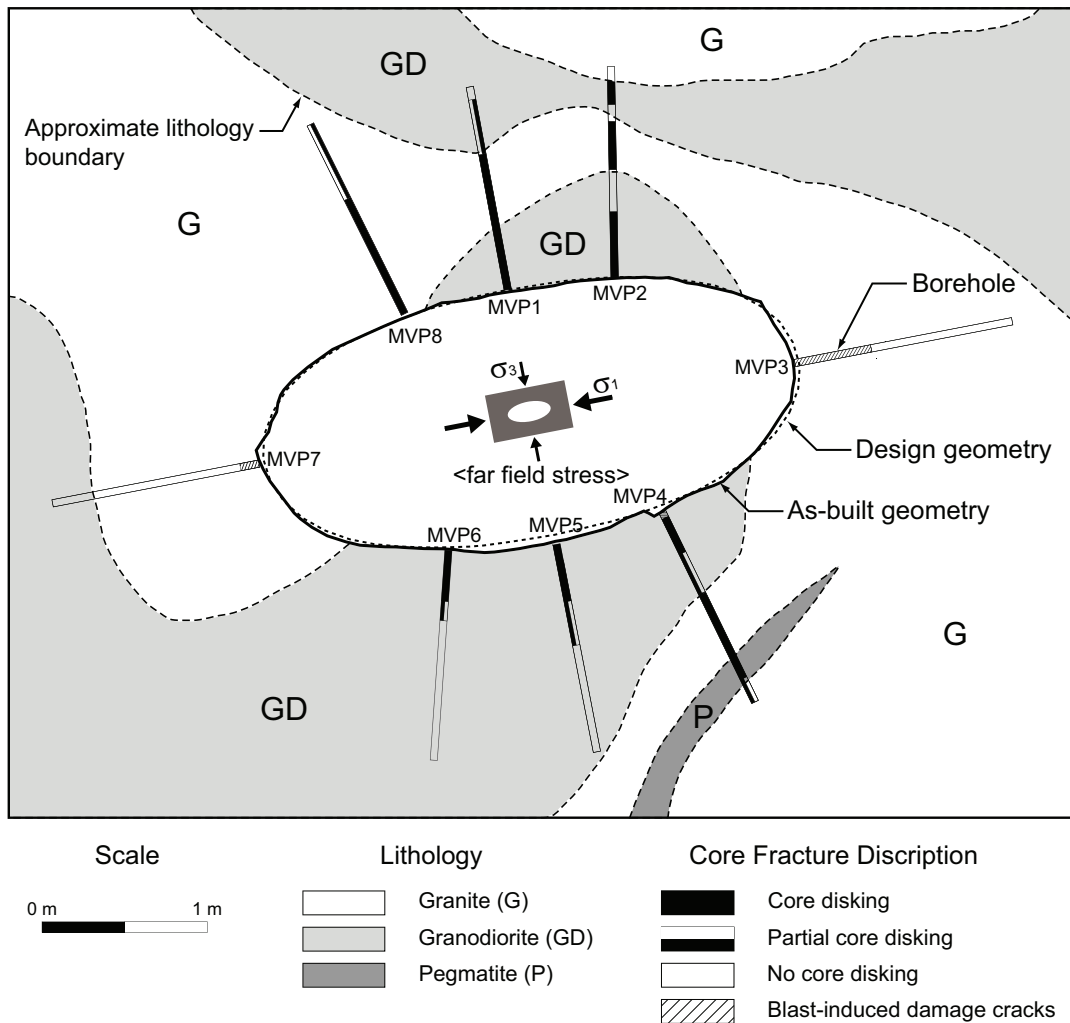
Figure 4.10: The cross section of Room 418-U1 array. The tunnel geometry and each MVP borehole location are described. The fracture characteristics and the lithology of the cores are illustrated as well.

-U2 and U3 were aligned in the direction of maximum principal *in situ* stress, i.e., the major axis was inclined 11 degree from the horizontal plane (see Figure 4.10).

The three dimensional numerical stress analyses were carried out using Examine3D[*], a three dimensional elastic boundary element code. The overall view of the model used in the numerical analyses is shown in Figure 4.1b. Figure 4.10 shows the geological detail encountered in Room 418. As seen in Figure 4.10 there are two major

---

[*]available from www.rocscience.com

rock types: granite and granodiorite. While these rocks have different grain size (see Figure 4.5), which results in the slightly different rock color and texture, the mechanical properties are very similar (Table 4.2). Because the Young's Modulus of the granite (65 GPa) and granodiorite (66 GPa) are so similar there is no significant impact of the geology on the stress analyses. To increase the accuracy of the stress calculation near the tunnel periphery in the areas of the region of the boreholes, the exact surveyed cross sectional geometry was used to build the numerical model.

Table 4.2: Summary of laboratory geotechnical properties for Lac du Bonnet granite and granodiorite (data from Read and Martin (1992) and Everitt (2001)).

Rock Type	Granite	Granodiorite
Uniaxial Compressive Strength (MPa)	213 ± 20	228 ± 20
Brazilian Tensile Strength (MPa)	9.3 ± 1.30	10.9 ± 1.52
Density (kg/m^3)	2630 ± 10	2660 ± 20
Tangent Young's Modulus (GPa)	65 ± 5	66 ± 5
Poisson's Ratio	0.25 ± 0.05	0.25 ± 0.05

Figure 4.10 shows the cross section of designed and as-built geometry of Room 418-U1 and the location of 8 MVP boreholes. The three dimensional elastic analyses were used to establish the stress distribution along the MVP boreholes. The maximum principal stress distribution for Figure 4.10 is shown in Figure 4.11. The maximum compressive stresses were concentrated in the crown and invert around boreholes (MVP1, MVP2, MVP4, MVP5, MVP6, MVP8), while relatively low compressive stresses were generated in the sidewall of the tunnel along boreholes MVP3 and MVP7. The stress magnitudes along the location of the MVP boreholes were determined using the three dimensional tunnel geometry and the maximum principal stress is summarized in Figure 4.12. The stresses in Figure 4.12 were extended beyond the borehole length to check convergence to the maximum far-field stress. As shown in Figure 4.12, 5 m from the tunnel the stresses were approaching the 60 MPa far-field maximum *in situ* stress.

Figure 4.12 shows that the boreholes in the roof and floor were drilled in regions
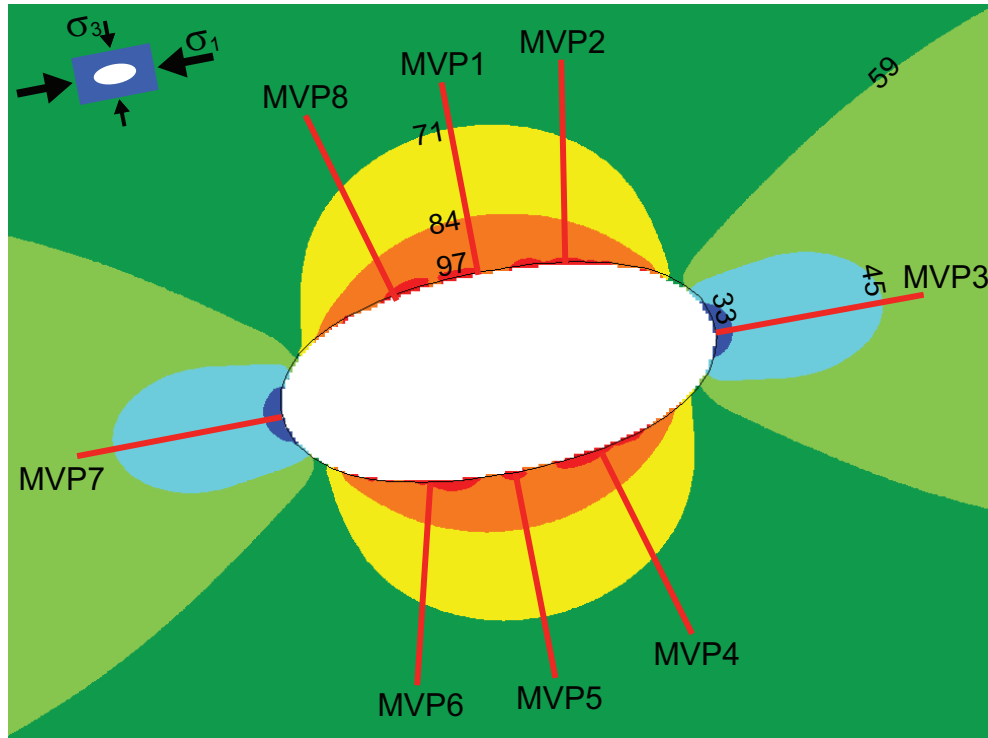
Figure 4.11: Maximum principal stress distribution in the plane of the MVP borehole array in Room 418-U1 tunnel. The contour values are in MPa.

where the maximum compressive stresses reached approximately 100 MPa near the collar of the boreholes with this stress rapidly decreasing to approximately 70 MPa near the end of the boreholes (≈ 2.5 m). In the sidewall of the tunnel the maximum compressive stress decreased from the far-field maximum stress of 60 MPa to approximately 30 MPa near the collar of the borehole. Hence around the excavation the MVP boreholes were drilled into widely different stress conditions. These varying stress conditions are correlated with disk thickness in the next section.

4.5 Stress magnitudes and disk thickness

The cores from the MVP boreholes were logged for rock types (granite and granodiorite) and MVP8 revealed uniform medium grained granite. Figure 4.13 shows the distribution of the core disking fractures measured in MVP8. The top illustration in Figure 4.13 shows the distribution of σ_1, σ_2 (intermediate principal stress),
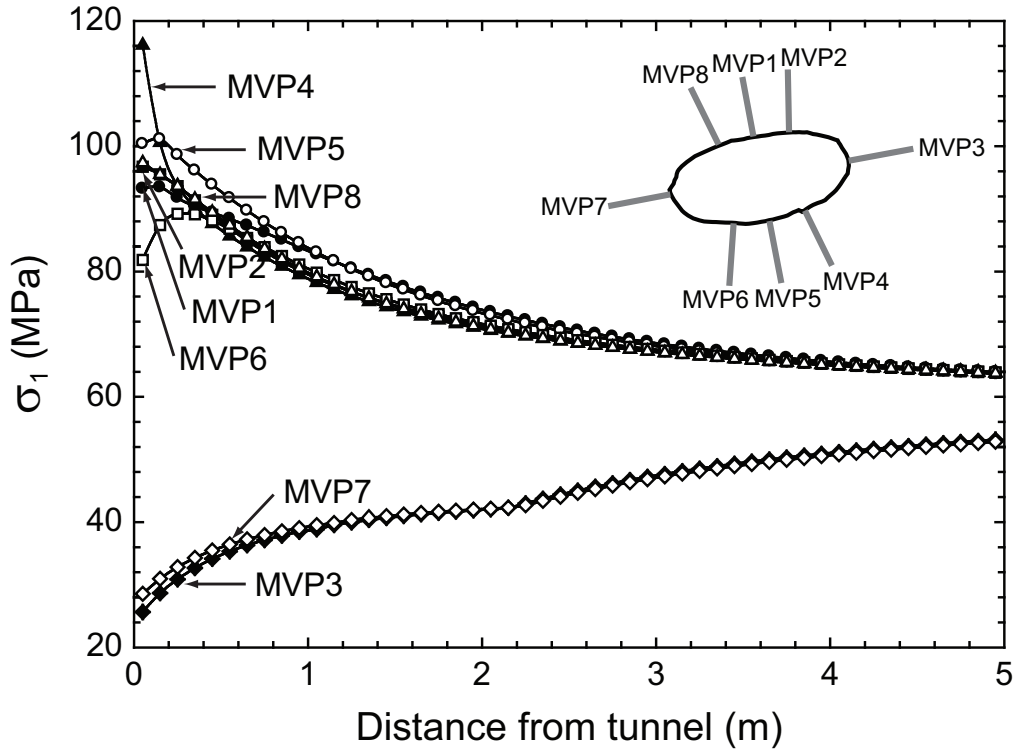
Figure 4.12: The magnitude of maximum principal stress (σ_1) generated along the MVP borehole lines.

σ_3 (minimum principal stress) and $\sigma_1 - \sigma_3$ (maximum deviatoric stress) along a fictitious line that represents the MVP8 borehole. The maximum value of σ_1 was approximately 98 MPa near the tunnel wall decreasing to approximately 66 MPa at the end of borehole. As shown in Figure 4.13 the thickness of the core disks increases and the frequency of the disk decreases with distance from the borehole collar. The average disk thickness for each 100 mm along the borehole is plotted in the bottom illustration in Figure 4.13. The average disk thickness increases from a few millimeters near the borehole collar to several centimetres near the end of the borehole.

While σ_1 decreased through the entire borehole, σ_3 increased from 0 MPa near the collar of the borehole to 10 MPa at the end of the borehole (see Figure 4.13). Although Obert and Stephenson (1965) and Haimson and Lee (1995) found from the laboratory core disking tests that the maximum principal stress, σ_1, is the main
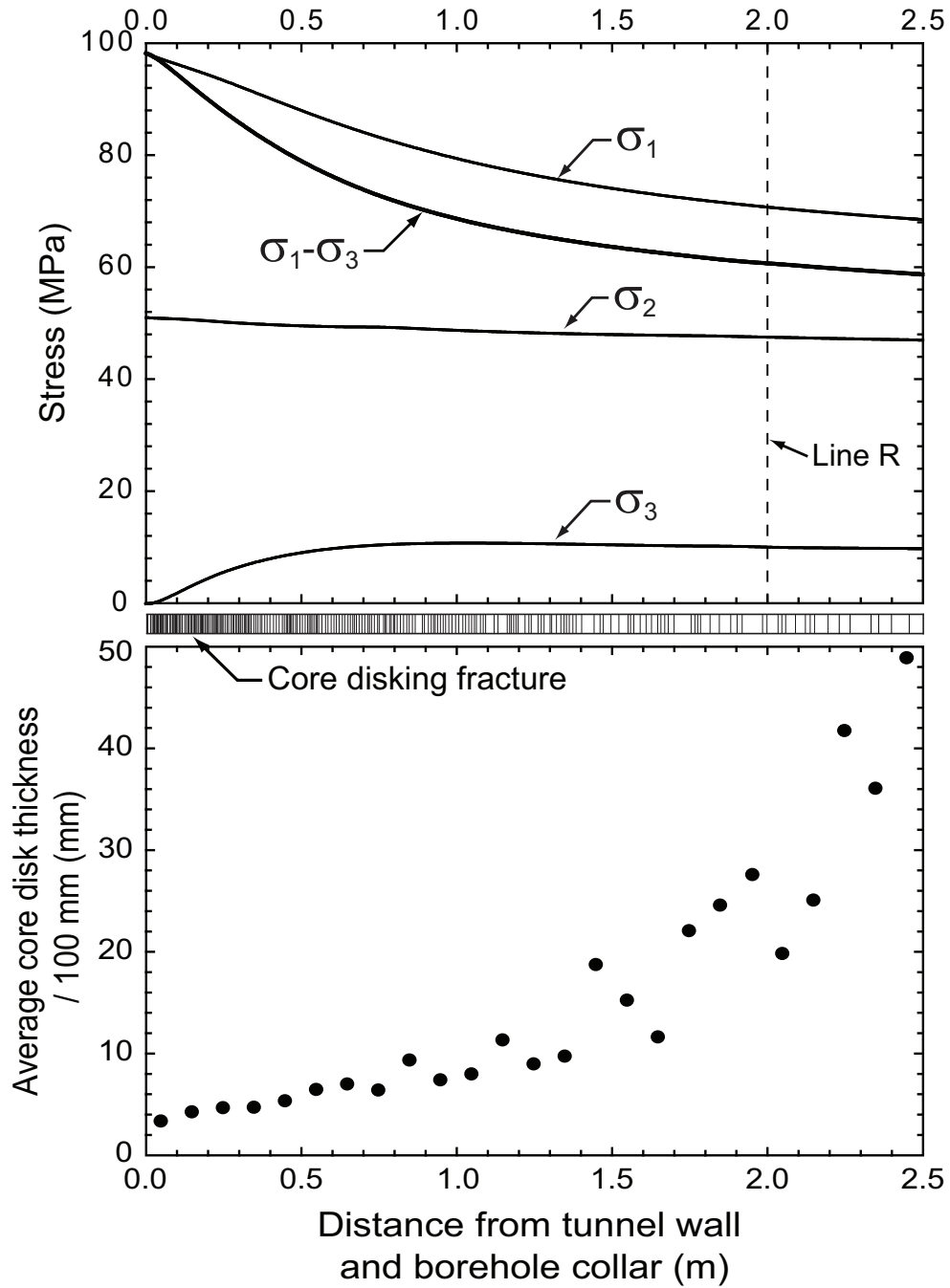
Figure 4.13: Depiction of core disk fractures for the core from MVP8 borehole in Room 418-U1 (middle). Distribution of the magnitude of maximum principal stress, (σ_1) along the borehole (Top figure) and the measured average core disk thickness for every 100 mm along the borehole (Bottom figure).

stress component for initiation of core disking, Obert and Stephenson (1965) observed that the magnitude of σ_1 causing core disking is affected by the magnitude of axial stress, σ_3. For σ_3 in Figure 4.13, however, most of the stress increase occurred near the collar of the borehole within 0.5 m depth, making it difficult to evaluate the effect of σ_3 on the core disking initiation and its thickness. The magnitude of σ_2 is essentially constant along the entire borehole. The effects of σ_2 and σ_3 have not been considered in this study but are not expected to make a significant contribution to the relationship between stress magnitude and core disk thickness.

The data in Figure 4.13 was re-plotted in Figure 4.14 and clearly shows that the disk thickness is a function of the magnitude of the maximum principal stress σ_1. Each point in Figure 4.14 represents an average core disk thickness versus an average σ_1 for 100 mm long sections. Figure 4.14 indicates that a maximum principal stress greater than 100 MPa is needed to cause disks that are thinner than the approximate average grain size (less than 3 mm). As the magnitude of the maximum princi-
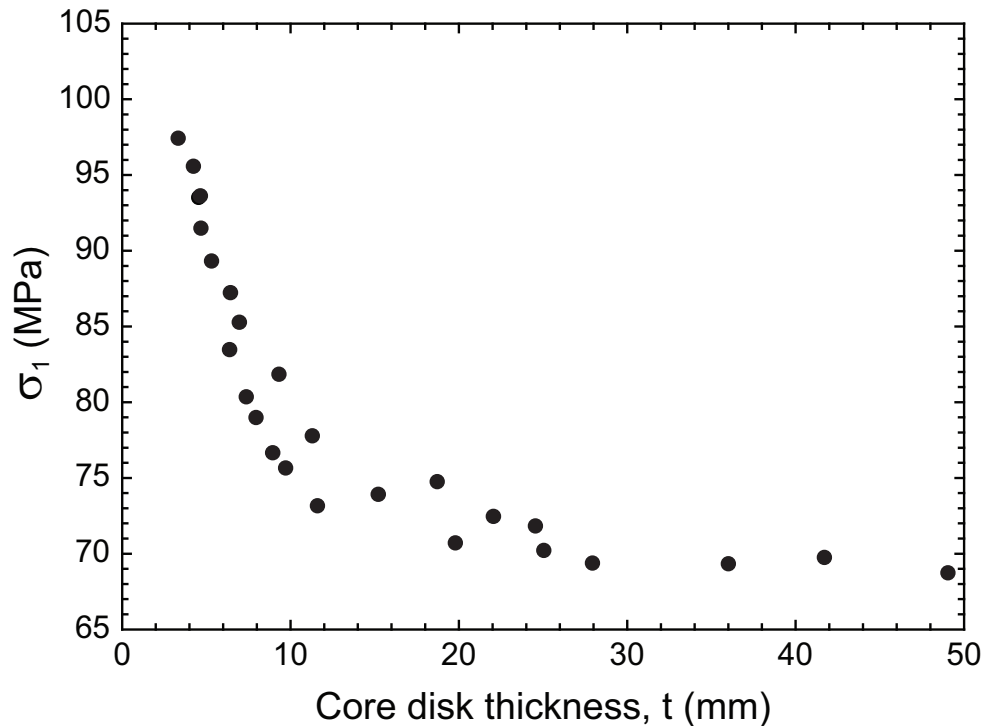
Figure 4.14: The relationship between the magnitude of maximum principal stress, σ_1 and core disk thickness obtained from the MVP8 borehole.

pal stress decreases the core disk thickness increases. When the maximum principal stress decreases to approximately 75 MPa the disk thickness is approximately 10 mm. However, when the maximum principal stress decreases to approximately 68 MPa, the disk thickness increases up to approximately 50 mm.

The technique for establishing the relationship between stress and disk thickness described previously was applied to all the boreholes. The data was also separated into granite and granodiorite. Figure 4.15 provides a summary of all the data for both the granite and granodiorite. As both Figures 4.15a and 4.15b show there is a strong correlation between disk thickness and stress magnitude, regardless of rock type, i.e., grain size. The correlation relating maximum principal stress to the core disk thickness can be expressed using Equation (4.1).

$$\sigma_1 = A + \frac{B}{\exp(\frac{t}{C})} \tag{4.1}$$

where σ_1 is the maximum principal stress (MPa), t is core disk thickness (mm), and A, B and C are curve-fitting parameters. The parameters are A=63.70, B=75.11 and C=3.20 for granite and A=72.73, B=77.66 and C=6.31 for granodiorite respectively. The unit of the first and second terms for the right side of Equation (4.1) is the same as that of maximum principal stress. Figure 4.15 shows the core disking initiation stresses for both rock types as well as parameter A. Based on Figure 4.15 core disking initiation stress for granodiorite is approximately 1.15 times higher than that of granite.

Figure 4.16 shows the relationship between core disk thickness (t) normalized by core diameter (d) and maximum principal stress (σ_1) normalized by Brazilian tensile strength (BT) of intact rock for both granite and granodiorite. According to Figure 4.16, the stress zone could be divided into three; (1) high stress region making thin disking. In this region the stress changes are large with small change of disk thickness and the normalized disk thickness is smaller than 0.2. (2) medium stress region causing medium disk spacing. In this region the stress changes moderately
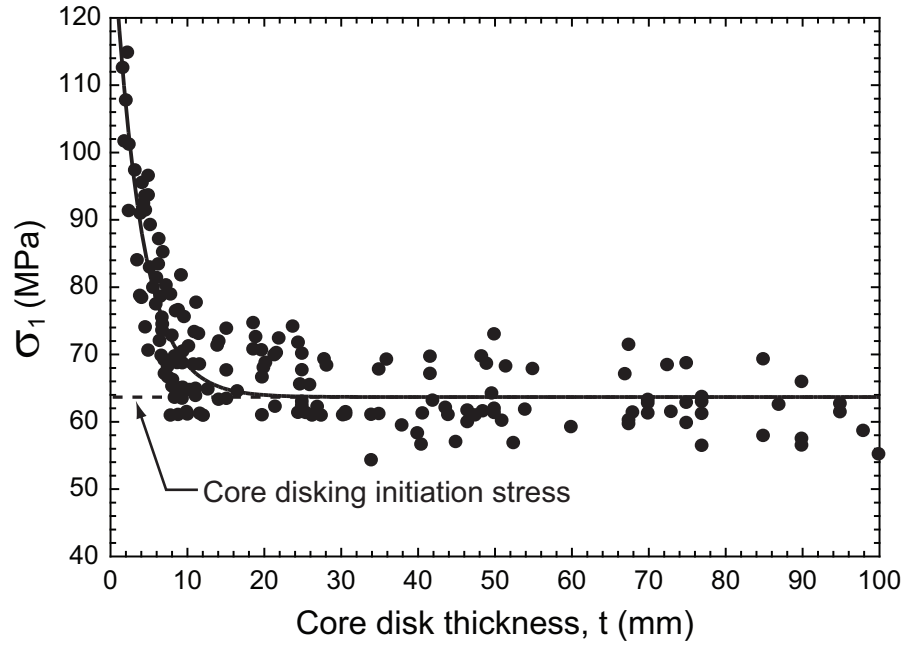
(a)
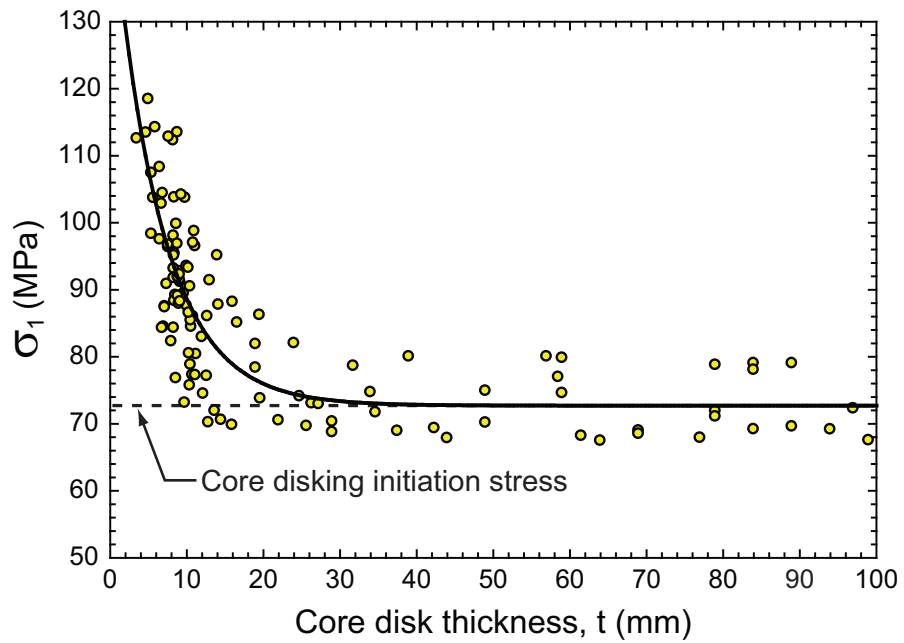
(b)

Figure 4.15: The relationship between core disk thickness and stress magnitude, for (a) granite and (b) granodiorite.
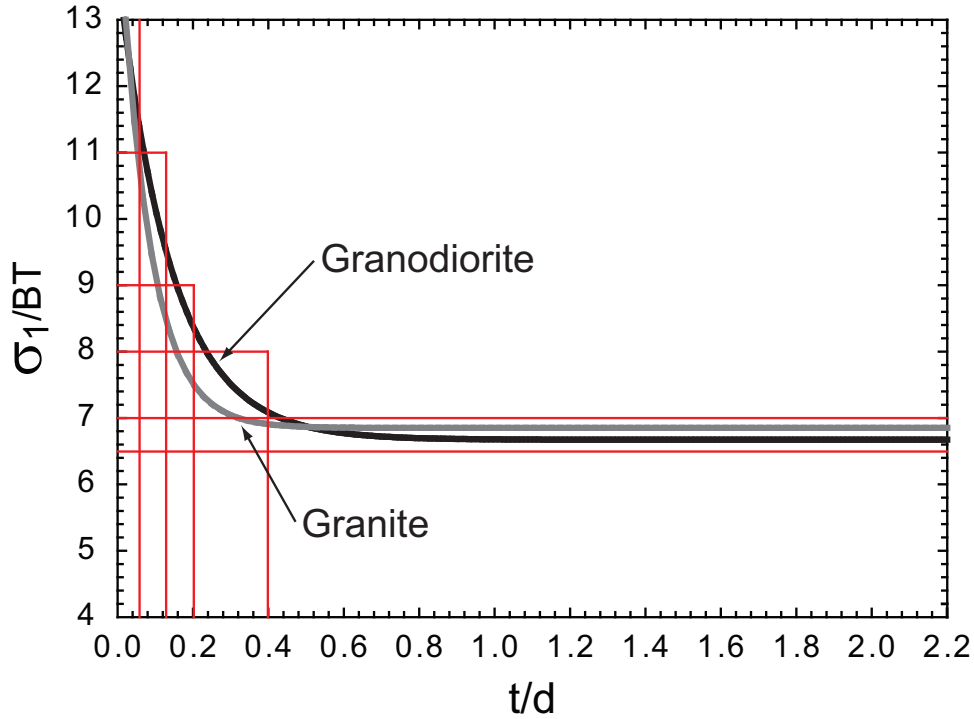
Figure 4.16: Core disk thickness normalized by core diameter versus maximum principal stress normalized by tensile strength of intact rock.

occurred. (3) core disking initiation stress region causing thick and partial disking. Little change of stress with varied disk thickness occurred in this region. If the core disk thickness of this range is observed uniformly in the field, the maximum principal far-field stress normalized by tensile strength of the intact rock could be estimated as higher than 6.5 regardless of disk space. The normalized stress magnitude of 6.5 was analyzed as a core disking initiation stress in this study.

It is clear from Figure 4.16, that there is a gradual increase in normalized disk thickness to about 0.4, as the stress magnitudes decrease. Table 4.3 is an attempt to provide guidelines based on the information in Figure 4.16 and the observations made during the logging of the disking fractures. The observed disking is divided into three general categorizes based on core disk thickness, fracture characteristics and associated stress magnitude: (1) no disking, (2) partial disking, and (3) disking.

96

Table 4.3: Description of core disk thickness for Lac du Bonnet granite and the correlated magnitude of the maximum principal stress normalized to the tensile strength. The core diameter is 45-mm, t = core disk thickness, d = diameter of core, σ_1 = maximum principal stress, BT = Brazilian tensile strength.

Term	Core Photo	Description	Disk Thickness t/d	Stress Condition σ_1/BT
Core Disking		Crushed disking: The disks are crushed due to the extremely high stress.	< 0.05	> 11
		Very thin disking: The majority of the disks are intact but a few are crushed.	0.05 - 0.12	9 - 11
		Thin disking: The shape and spacing of the core disks are uniform.	0.12 - 0.2	8 - 9
		Medium disking: The shape and spacing of the core disks are uniform. Most commonly observed disk thickness.	0.2 - 0.4	7 - 8
		Thick disking: The shape of the core disks is uniform.	0.4 - 2.2	6.5 - 7
Partial Disking		Partially disking: Distinct white lines appear at regular spacings, similar to that observed when the complete disks form, but the core remains intact. Spacing between these lines is similar to that of Medium disking.	0.2 - 0.4	6 - 7
No Disking		No disking: Solid core but the core maybe microcracked which can be seen with the naked eye.	-	-
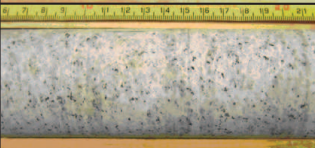
4.6 Discussion

As noted previously the main difference between the granite and granodiorite is grain size. Figure 4.15 shows that this difference is sufficient to increase the average initiation stress for disking from 64 MPa for granite to 73 MPa for granodiorite. Several researchers (Jaeger and Cook, 1963; Sugawara et al., 1978; Li and Schmitt, 1998; Song and Haimson, 1999; Kaga et al., 2003) have shown that core disking is fundamentally a tensile failure phenomenon. Kaga et al. (2003) used a core disking theory based on the concept of a critical tensile stress developed by Matsuki et al. (1997). They found good agreement between their theoretically predicted stress versus disk thickness, and the laboratory core-disking data for Lac du Bonnet granite by Haimson and Lee (1995). Figure 4.17 compares the results predicted by Kaga et al. (2003) with our *in situ* results for Lac du Bonnet granite. As shown in Figure 4.17 there appears to be little agreement between our field data and the prediction by Kaga et al. (2003) based on tensile stress. Obert and Stephenson (1965) found that the Mohr-Coulomb shear failure criterion gave the best fit to the initiation of core disking in various rock types using laboratory tests. Unfortunately they offered no relationship between stress magnitude and disking thickness.

A three dimensional elastic analysis was carried out to examine the stress path experienced by the rock during core drilling. The stress state at the point 2 m from the collar of MVP8 was used for the analysis (see the reference Line R in Figure 4.13). At this location the observed core disking was close to the initiation of disking and the stress gradients are relatively small. Hence at this location the stress condition and the observed disking are relatively unique. The principal stress tensor at this location used for the analysis was: σ_1=70 MPa, dip/dir = 2.6/270.1, σ_2=47 MPa, dip/dir = 0.0/0.0 and σ_3=10 MPa, dip/dir = 87.4/86.7.

Figure 4.18 shows the estimated stress path for three monitoring lines (A, B and C): line A is located in the maximum applied stress direction, line B in the minimum applied stress direction, and line C in the center of the core. The monitoring lines start five core diameter ahead of the hole bottom (A_1, B_1 and C_1) to the free end
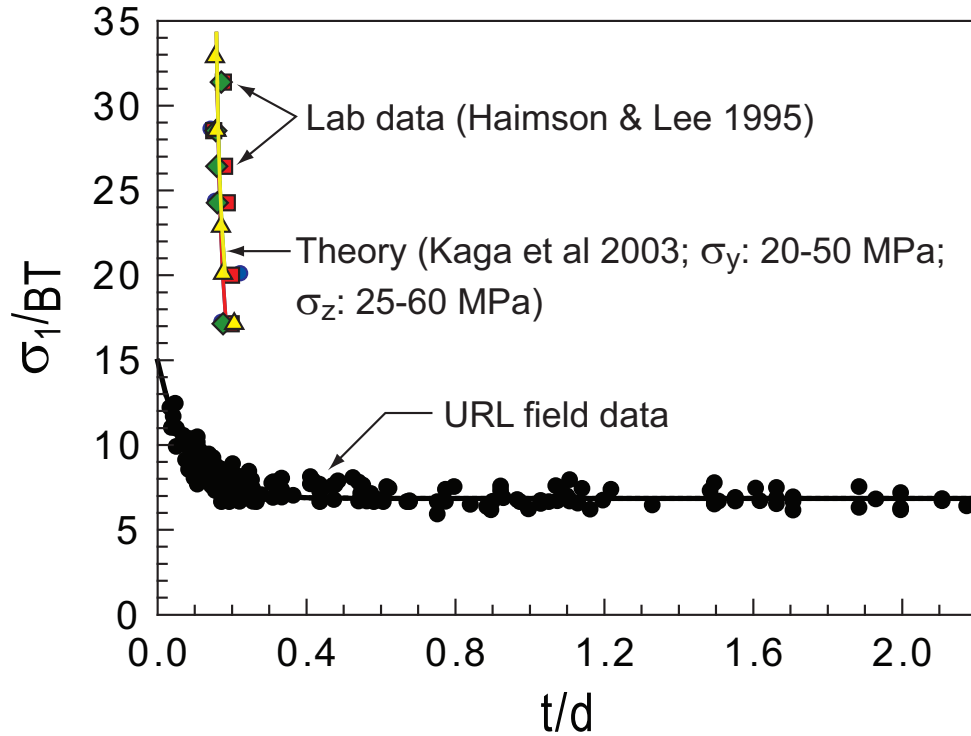
Figure 4.17: Comparison of disk thickness normalized to core diameter (t/d) versus maximum stress normalized to the Brazilian tensile strength (σ_1/BT) based on Kaga et al. (2003), and the disking results obtained experimentally by Haimson and Lee (1995) using Lac du Bonnet granite, with the *in situ* field results from this study.

of core stub (A_3, B_3 and C_3) which is the same distance as the core diameter. Also shown in Figure 4.18 is the Hoek-Brown failure envelope and crack-initiation stress (σ_{ci}) given by Martin (1997) for Lac du Bonnet granite.

The stress paths in Figure 4.18 shows that all the initial stresses are compressive in the core, far from the bit. However, the initial compressional stresses at B_1 and C_1 become tensile in the vicinity of bit (B_2 and C_2). These tensile stresses only occur locally and do not extend to the entire core section as the stress at point A_2 in the core remains compressive. The tensile stresses initiate at the center of the core (line C) and at the edge of the core stub (line B) and cross the Hoek-Brown failure envelope near the location of the drill bit, (B_2 and C_2), indicating that core disking fracture would initiate at these locations. According to the stress path for line A the stress remains compressive at vicinity of drill bit (A_2), but the magnitude
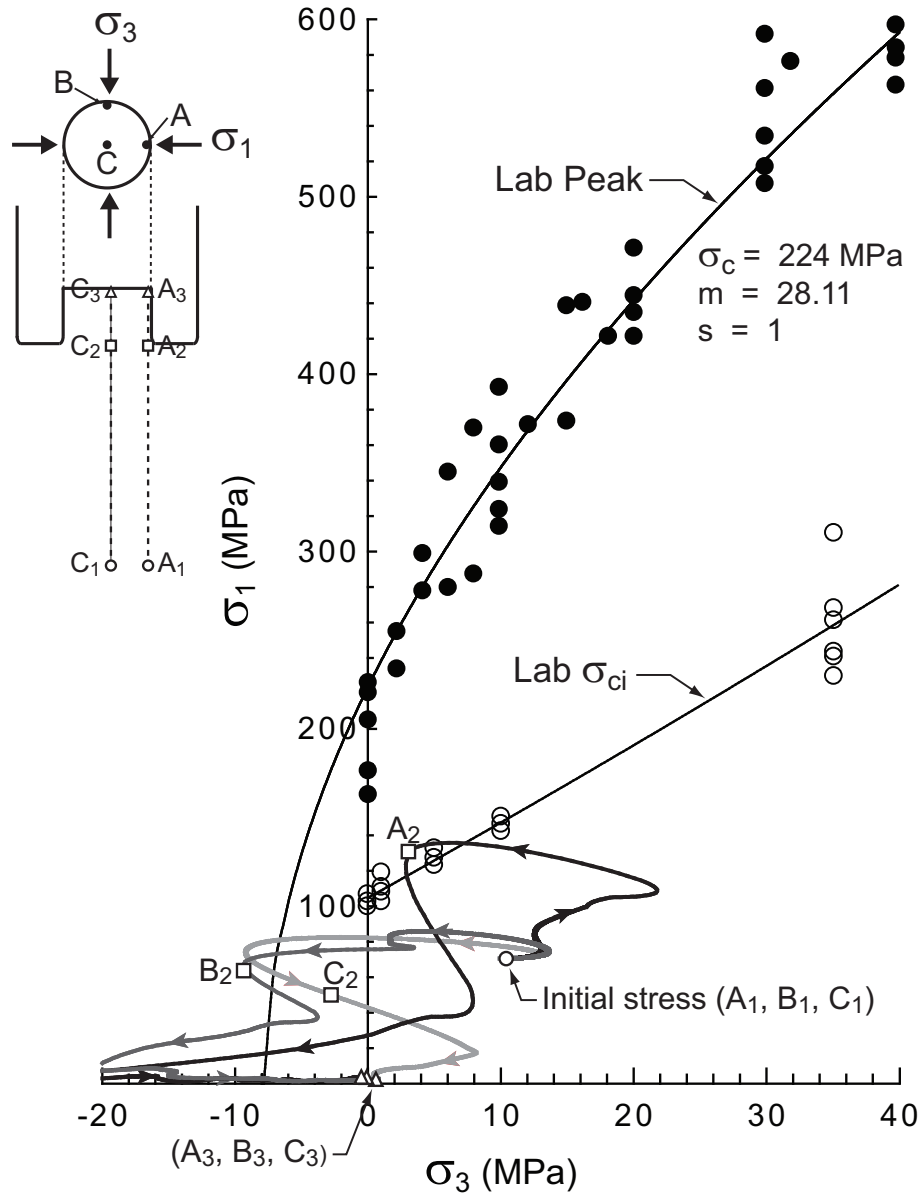
Figure 4.18: Stress path for solid core. The initial stresses (far field stress) are σ_1=70 MPa, σ_2=47 MPa and σ_3=10 MPa. The stress path was traced for the three monitoring lines (A, B and C). The monitoring lines started from 5 times of core diameter ahead of the bottom hole to the free end of core stub of which length is the same as core diameter. Hoek-Brown failure envelope (Martin, 1997) for a reference of failure status and a laboratory *in situ* crack-initiation stress (σ_{ci}) (modified from Lau and Chandler (2004)) for Lac du Bonnet granite are plotted.

of compressive stresses are not sufficient to cause compressive failure. Thus, the main and predominant fracture generation source for core disking will be tensile stress, and tensile strength of the rock could be one of the main material properties to control the core disking initiation and disk thickness.

To check the magnitude of tensile stress and its location the minimum principal stress, σ_3, was plotted versus distance normalized by core diameter in Figure 4.19. The Brazilian tensile strength of the rock is also shown in Figure 4.19 for reference. An interesting point in tracing the stress path is that the core at the location
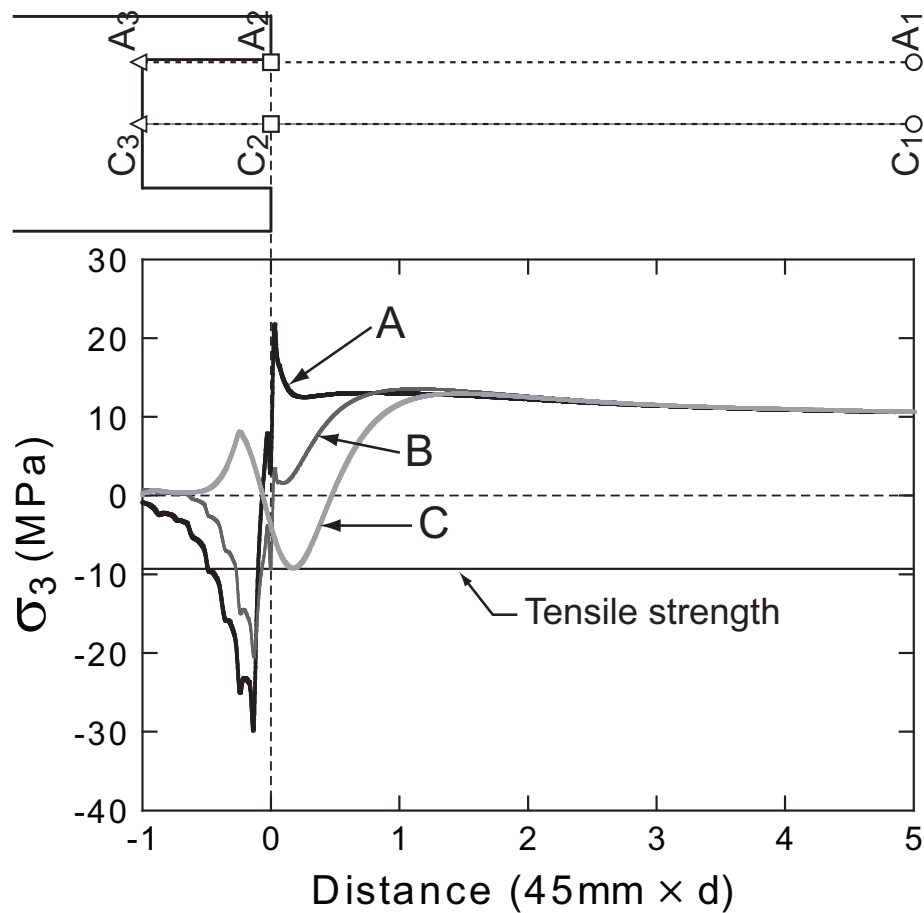
Figure 4.19: Stress path for σ_3 stress component from Figure 4.18. The distance was measured from drill bit bottom and normalized by core diameter, d. Brazilian tensile strength of 9.3 MPa is shown in the figure as a reference for tensile failure.

of three monitoring lines experienced tensile stresses during the drilling process. However the tensile stress magnitudes and the locations of the tensile stress are different. Along the center of core (line C), the maximum tensile stress was generated immediately below the drill bit bottom (i.e., below point C_2) and the magnitude approaches that of tensile strength. On the other hand the maximum tensile stress at outer boundaries of core stub (line A and B) occurred after the drill bit passed the points (A_2, B_2) and the magnitude is considerably greater than the tensile strength of the rock. This suggests that a core disking fracture could be initiated below the drill bit at the center of the core and propagate to outer side of the core stub. However, if a core disking fracture starts at the outer surface of the core stub it could be presumed that the fracture initiated above the bottom of the drill bit. If the magnitude of generated tensile stress in the core center is not sufficient to propagate a disking fracture to the boundary surface of the core stub and the drill bit advances further, passing by the stress measuring points, the higher tensile stress at the outer surface could initiate a new tensile fracture at this location. This may explain the characteristic of fracture initiation and propagation illustrated in Figure 4.8. The fact that most of partial disks are observed at the end of the borehole where the magnitude of maximum principal stress is similar to core disking initiation stress, also supports this hypothesis.

4.7 Conclusion

Core disking is often used as an indicator of elevated stress magnitudes. Extensive core disking was mapped in a series of boreholes drilled from a tunnel located at a depth of 420 m in massive unfractured granite. The thickness of core disks was measured in detail. In addition, the extracted core from the boreholes was categorized using fracture persistence; (1) core disking, (2) partial disking and (3) no disking.

The measured data showed that the disk thickness decreased as the tunnel wall was approached. Three-dimensional elastic numerical analyses were conducted to estimate the stress state around the tunnels and along the boreholes. The maxi-

mum principal stress near the tunnel boundary was approximately 100 MPa and decreased to the far-field maximum stress near the end of the boreholes. A strong correlation was found between core disk thickness and the magnitude of maximum principal stress. It was also found that the grain size influenced the initiation of disking, presumably through its effect on rock strength.

Stress path analyses indicted that the onset of disking was controlled by the minimum principal stress (tensile stress). The location of the disking fracture, during partial-disking, is complex and may appear at the core center or at the core boundary. From the normalization of disk thickness by the core diameter and associated stress magnitude by the tensile strength of the intact rock, it is concluded that core disking occurs when the ratio of maximum principal stress normalized to the Brazilian tensile strength exceeds 6.5. Guidelines are provided for estimating stress magnitudes and disk thickness for Lac du Bonnet granite at the 420 level of AECL′s URL.

Bibliography

Brown, A., Soonawala, N.M., Everitt, R.A., Kamineni, D.C. 1989. Geology and geophysics of the Underground Research Laboratory Site, Lac du Bonnet Batholith, Manitoba. *Can. J. Earth.* 26:404–25.

Doe, T.W., Zieger, M., Enachescu, C., BÖhner, J.B. 2006 In-situ stress measurements in exploratory boreholes. *Felsbau*. 24(4): 39–47.

Dyke C.G. 1989. Core discing: its potential as an indicator of principal *in situ* stress directions. In: *Proceedings of ISRM–SPE International Symposium Rock at Great Depth*, *Pau*. Maury, V., Fourmaintraux, D. *editors*. A.A. Balkema, Rotterdam, vol. II, pp. 1057–1064.

Everitt, R.A. 2001. *The influence of rock fabric on excavation damage in the Lac du Bonnet granite*. Ph.D. thesis, Department of Civil & Geological Engineering, University of Manitoba, Winnipeg, Manitoba, Canada.

Everitt, R.A., Lajtai, E.Z. 2004; The influence of rock fabric on excavation damage in the Lac du Bonnet granite. *Int. J. Rock Mech. Min. Sci.* 41(8):1277–1303.

Haimson B.C., Lee M.Y. 1995. Estimating deep in istu stresses from borehole breakouts and core disking–experimental results in granite. In: *Proceedings of the international workshop on rock stress measurement at great depth, The 8th international congress on rock mechanics*, *Tokyo*, pp. 19–24.

Hakala, M. 1999a. Numerical study of the core disk fracturing and interpretation of the in-situ state of stress. In: *Proceedings Ninth Congress of International*

Society for Rock Mechanics, *Paris*, Vouille, G., Berest, P. *editors*. A.A. Balkema, Rotterdam, vol. 2. pp. 1149–1153.

Hoek, E., Brown, E.T. 1980. Underground Excavations in Rock. The Institution of Mining and Metallurgy, London.

Jaeger, J.C., Cook, N.G.W. 1963. Pinching-off and disking of rocks. *J. Geophys. Res.* 888(6): 1759–1765.

Kaga, N., Matsuki, K., Sakaguchi, K. 2003. The in situ stress states associated with core discing estimated by analysis of principal tensile stress. *Int. J. Rock Mech. Min. Sci.* 40: 653–665.

Lau, J., Chandler, N. 2004. Innovative laboratory testing. *Int. J. Rock Mech. Min. Sci.* 41(8):1427–45.

Li, Y., Schmitt, D. 1998. Drilling-induced core fractures and in situ stress. *J. Geophys. Res.* 103: 5225–5239.

Martin, C.D. 1990. Characterizing *in situ* stress domains at the AECL Underground Research Laboratory. *Can. Geotech. J.* 27:631–46.

Martin, C.D. 1997. Seventeenth Canadian Geotechnical Colloquium: The effect of cohesion loss and stress path on brittle rock strength. *Can. Geotech. J.* 34(5):698–725.

Martin, C.D., Read, R.S. 1996. AECL′s Mine-by Experiment: A test tunnel in brittle rock. In: *Proceedings of 2nd North American Rock Mechanics Symposium*, *Montreal*, Aubertin, M., Hassani, F., Mitri, H., *editors*. A.A. Balkema, Rotterdam, pp. 13–24.

Martin, C.D., Read, R.S., Martino, J.B. 1997. Observations of brittle failure around a circular test tunnel. *Int. J. Rock Mech. Min. Sci.* 34(7):1065–73.

Martino, J.B., Chandler, N.A. 2004. Excavation-induced damage studies at the Underground Research Laboratory. *Int. J. Rock Mech. Min. Sci.* 41(8):1413–26.

Matsuki, K., Hogno, K., Sakaguchi, K. 1997. A tensile principal stress analysis for

estimating three-dimensional in situ stresses from core discing. In: *Rock Stress*, Sugawara, K., Obara, Y., *editors*. A.A. Balkema, Rotterdam, pp. 343–348.

Maury, V.M., Santarelli, F.J., Henry, J.P. 1988. Core discing: a review In: *Proc. 1st Regional ISRM Symposium for Africa: Rock Mechanics in Africa*. Maury, V., Fourmaintraux, D. *editors*. South African National Group on Rock Mechanics, Swaziland, pp. 221–231.

Obert, L., Stephenson, D.E. 1965. Stress conditions under which core discing occurs. *Transactions Sociaty of Mining Engineers*. 232(3): 227–235.

Read, R.S. 1994. *Interpreting excavation-induced displacements around a tunnel in highly stressed granite*. Ph.D. thesis, Department of Civil & Geological Engineering, University of Manitoba, Winnipeg, Manitoba, Canada.

Read, R.S. 2004. 20 years of excavation response studies at AECL′s Underground Research Laboratory. *Int. J. Rock Mech. Min. Sci.* 41(8):1251–75.

Read, R.S., Martin, C.D. 1992. Monitoring the excavation-induced response of granite. In: *Proceedings of 33rd U.S. Symp. on Rock Mechanics*, *Santa Fe*, Tillerson, J., Wawersik, W., *editors*. A.A. Balkema, Rotterdam, pp. 201–210.

Song, I., Haimson, B.C. 1999. Core disking in Westerly granite and its potential use for in situ stress estimation. In: *Proc. 31st U.S. Rock Mechanics Symposium*, *Rotterdam*. Amadei, Kranz, Scoot, *editors*. A.A. Balkema, Rotterdam, pp. 1173-1180.

Stacey, T.R. 1982. Contribution to the mechanism of core discing. *Journal South African Institute of Mining and Metallurgy*. 99: 269-274.

Sugawara, K., Kameoka, Y., Saito, T., Oka, Y., Hiramatsu, Y. 1978. A study on core disking of rock. *Journal of Japanese Association of Mining*. 94: 19-25.

Tsang, C.F., Bernier, F.F., Davies, C. 2005. Geohydromechanical processes in the Excavation Damaged Zone in crystalline rock, rock salt, and indurated and plastic clays in the context of radioactive waste disposal. *Int. J. Rock Mech. Min. Sci.* 42(1):109–25.

Chapter 5

A core disking criterion based on the averaged maximum tensile stress [3]

5.1 Introduction

Core disking is a phenomenon in which the drilled core disks with uniform spacing and shape due to the transient stress changes, and stress release during drilling (Figure 5.1). Investigation of the core disking mechanism and its application to estimating the far-field stress started in the early 1960s'. Since then, mainly three core disking failure mechanisms, (1) shear, (2) extension strain and (3) tensile, have been proposed based on the laboratory tests and/or numerical analyses.

The shear failure mechanism was proposed by Obert and Stephenson (1965) based on the biaxial loading test for five different rock types. Obert and Stephenson (1965) observed that the rupture lines, appearing on the surface of the rock specimen, are very similar to the shear lines observed in highly confined triaxially loaded specimens. They established a linear relationship between the shear strength of rocks and the core disking initiation stress. This shear failure mechanism was later supported by Durelli et al. (1968). Using a photoelastic model Durelli et al. (1968) showed the maximum shear stress concentrated near the bottom of the borehole and concluded

---
[3] This chapter is submitted to Rock Mechanics and Rock Engineering in December 2012
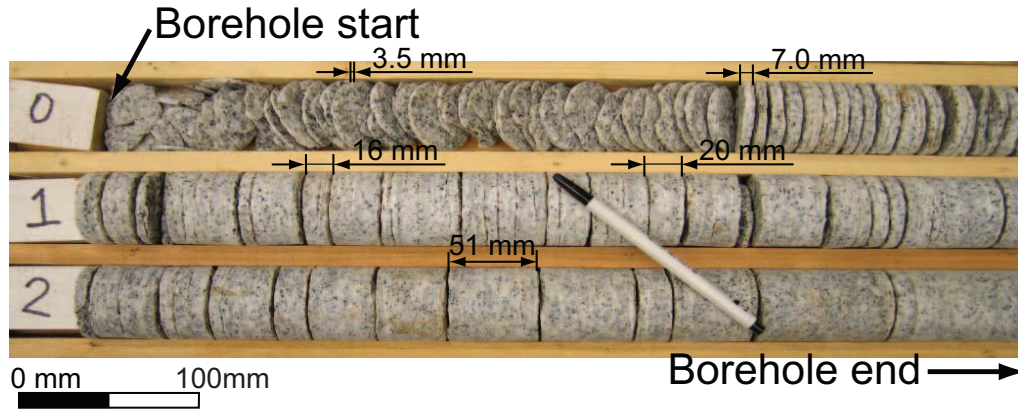
Figure 5.1: Typical core disking observed in 75-mm-diameter boreholes drilled from tunnels at the 420-m depth Level of AECL's Underground Research Laboratory.

that the core disking fracture initiates when the shear stress is greater than the shear strength of the rock. Stacey (1982) proposed that extension strain governed the initiation of and propagation of core disking fractures.

The most frequently suggested mechanism for core disking is tensile failure which was initially proposed by Jaeger and Cook (1963). Jaeger and Cook found from biaxial loading tests that the average applied stresses required to initiate core disking should be higher than 60% of unconfined compressive strength. Supported by the observations that the disked surfaces showed no evidence of shearing, Jaeger and Cook (1963) proposed that core disking is a phenomenon of tensile failure. The tensile failure mechanism was later supported by Sugawara et al. (1978), Dyke (1989), Haimson and Lee (1995), Li and Schmitt (1997), Kaga et al. (2003) and Corthesy and Leite (2008).

Lim and Martin (2010) (Chapter 4 of this thesis) observed extensive core disking in Lac du Bonnet (LdB) granite and granodiorite cores from boreholes drilled from underground openings at the 420-m-Level of AECL's Underground Research Laboratory (URL). The thickness of the core disks varied from several millimeters near the collar of the boreholes and gradually increased in thickness to several centimetres or completely disappeared towards the end of the boreholes (see Figure 5.1). Lim and Martin (2010) analyzed the frequency of the core disks and their

fracture persistency, and established a correlation between core disk thickness and maximum principal stress for the investigated site. The field core disking data was compared with the principal tensile stress criterion proposed by Kaga et al. (2003). A significant discrepancy was observed between the criterion and the field data, with the principal tensile stress criterion over-estimating the magnitude of stresses required for core disking. This study will investigate the tensile stresses in the vicinity of core disking to assess if a better correlation can be found between the observed field data and tensile stresses required for initiating core disking.

5.2   Averaged maximum tensile stress (AMTS)

The stress distribution in the vicinity of an advancing core bit was analysed using the three dimensional boundary element program Examine3D (RocScience, 2004). This program was specifically developed for providing accurate stresses close to the boundary of underground openings. Examine3D runs on a desktop PC in a
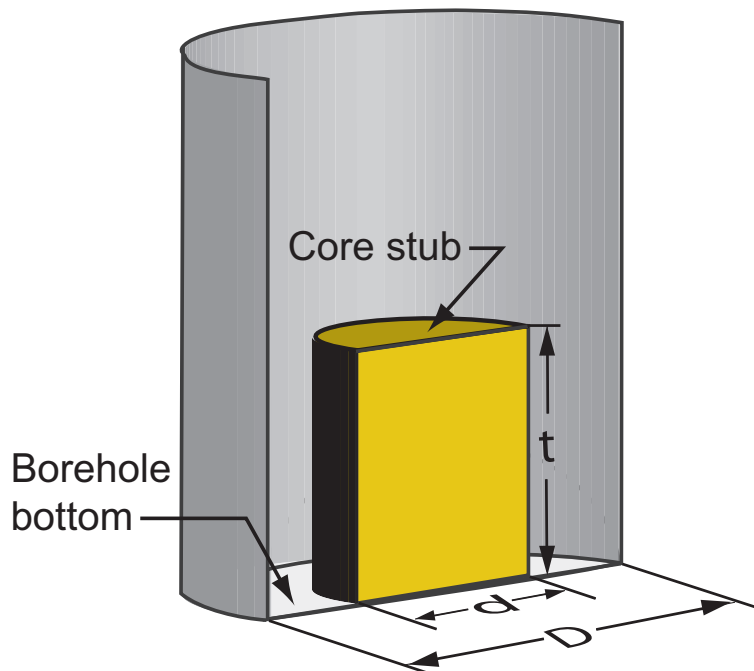
Figure 5.2: Cross section through a cored hole and the core stub. The terminology for this study: D is the diameter of the borehole, t is the thickness of the core stub, d is the diameter of the core.

109

Windows environment and was used for all the numerical analyses in this study. Figure 5.2 shows a cross section through a cored hole and the core, and defines the terminology used in this study.

5.2.1 Stress distribution at the bottom of a borehole

A typical tensile stress distribution near the bottom of a vertical borehole determined from a three dimensional elastic analysis is shown in Figure 5.3 for the case where maximum horizontal stress (σ_H) is greater than the minimum horizon-
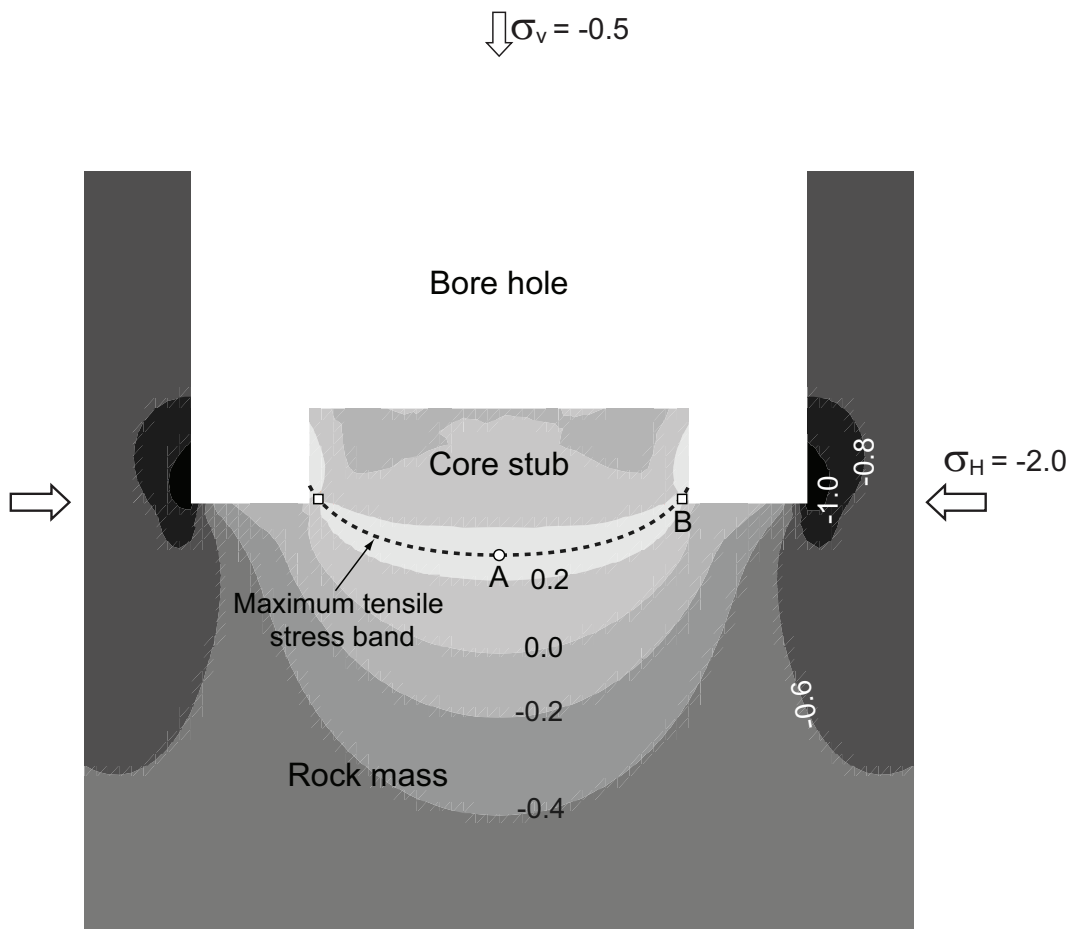
Figure 5.3: An example of the tensile stress distribution near the borehole bottom. The cross section shows the cut through the direction of minimum horizontal *in situ* stress, and the highest tensile stress value (point A) and the lowest tensile stress value (point B) in the maximum tensile stress band are indicated. Applied *in situ* stresses as a boundary condition are σ_H = -2.0, σ_h = -1.0 and σ_v = -0.5 MPa.

tal stress (σ_h), and both of these are greater than the vertical stress (σ_v), i.e., $\sigma_H =$ -2.0, σ_h = -1.0 and σ_v = -0.5 MPa (tensile stress is considered as positive in this chapter). The cross sectional view in Figure 5.3, is taken in the plane of the minimum horizontal and vertical *in situ* stress. In Figure 5.3 the maximum tensile stress appears as a band distributed with a concave shape, starting near the bottom of the borehole on the core stub and extending downward to the core centre. According to the tensile stress criterion based on linear elastic fracture mechanics, the disk fracture would initiate at a point when the magnitude of the tensile stress at the point reaches the tensile strength of the rock. The generated fracture will propagate within the maximum tensile stress band unless a new tensile stress band forms as a consequence of the fracture propagation (Lim et al., 2006). It is realized that the thickness of this tensile stress band is a function of the contouring interval and is simply used here to illustrate the rational for using the averaged maximum tensile stress (AMTS).

If the stress field is considered in 2 dimensions (Figure 5.3), the maximum tensile stress within this maximum tensile stress band is located in the centre of the core at point A (0.23 MPa), and the lowest maximum tensile stress is found near the edge of the core at point B (0.13 MPa). Kaga et al. (2003) adapted the tensile stresses at point B as a core disking stress in their principal tensile stress criterion. However, Lim and Martin (2010) found that this criterion significantly overestimated the stresses required for core disking. An alternative to choosing the tensile stress at Point B, is to base the disking criterion on the greatest tensile stress value in the maximum tensile stress band (stress at point A in Figure 5.3). In this case, however, the fracture initiation would be localized to the centre of the core (Point A) and consequently may not produce a fully separated core disk. Thus the core disking stress could be under-estimated. Detailed examination of the core disking observed in Lac du Bonnet granite showed that the initiation of core disking was quite complex (Figure 5.4). Inspection of Figure 5.4 reveals that disking appears to initiate from both the edge and the centre of the core. Hence, averaging the tensile stresses may more appropriate.
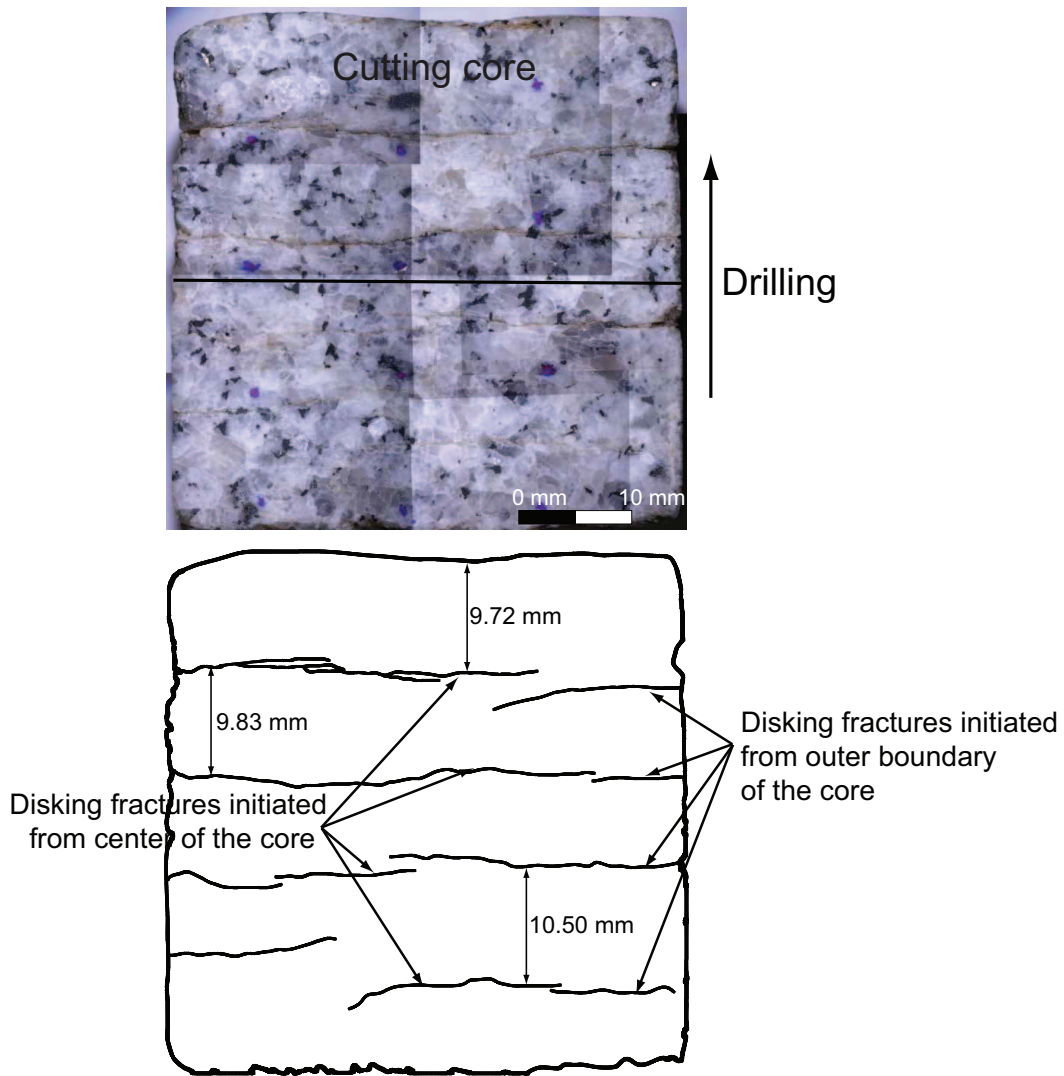
Figure 5.4: Initiation and propagation of core disking fractures. A partially fractured core was cut through the core axis. The sketch shows that some fractures were initiated from the centre of the core, at Point A in Figure 5.3, and others were initiated from the outer boundary of the core, near Point B in Figure 5.3

In this study a simple hypothesis is proposed that the core disking will occur when the AMTS equals the Brazilian tensile strength (BT) of the rock. The AMTS can be calculated in two steps; first, all the contiguous maximum tensile stress points along the entire core width and below the core will be identified (i.e., searching for the maximum tensile stress band) and then the maximum tensile stresses along this band will be averaged. The three dimensional boundary element code was used to

model the geometry of core and borehole, and to calculate the stress components within and below the core stub. Before building the final model the sensitivity of both the number of stress measuring points and the geometry of borehole bottom on the AMTS was tested.

5.2.2 Number of stress measuring points

In Figure 5.5, the AMTS were calculated by increasing the number of stress measuring points. Nine different cases were tested starting from 1 to 256 points per plane perpendicular to core axis. The location of each stress calculation point is a centre of equally divided areas. It is shown in Figure 5.5 that the magnitude of AMTS is unreliable when the stress measuring points are less than 64. When the stress measuring points are greater than 64, however, the magnitude of the AMTS gradually converges to 0.218 MPa, and there is only a 0.3% change in the magnitude of the AMTS when the stress measuring points are greater than 196.
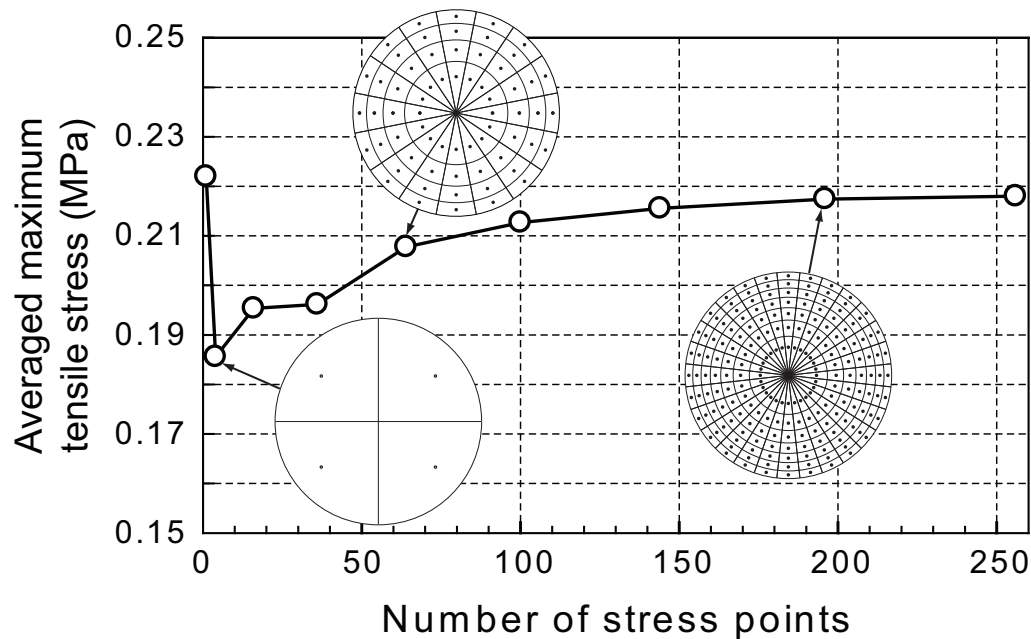
Figure 5.5: Sensitivity of the stress measuring points on the magnitude of averaged maximum tensile stress. Boundary *in situ* stress condition: σ_H = -2.0, σ_h = -1.0 and σ_v = -0.5 MPa.

5.2.3 Geometry of borehole bottom

When simulating core disking numerically, the most significant factor that influences the stress concentration and its distribution is the geometry of the borehole bottom resulting from the shape of the drill bit (Li and Schmitt, 1997; Hakala, 1999b). While many researchers have used a semicircle-shaped borehole bottom for determining their stress distribution (Sugawara et al., 1978; Dyke, 1989; Li and Schmitt, 1997; Kaga et al., 2003), others have used a flat-bottom shape in their numerical models (Stacey, 1982; Corthesy and Leite, 2008). Li and Schmitt (1997) found that the sharp corner of the borehole bottom generates the higher stress concentration than the rounded corner.

The three different geometries of borehole bottom were modelled; i.e., (1) Flat, (2) Round (half circle) and (3) "Model" (flat bottom with rounded edge corner). The AMTS was calculated using these three geometries for the normalized core stub length (t/d) of 0.5 and compared in Figure 5.6. The magnitude of AMTS for Flat shape geometry is approximately 10% higher than the Round shape geometry. For the Model shape geometry, the AMTS falls in between Flat and Round shape models and shows a slightly lower value than the Flat shape (by about 3%). In this study the geometry of borehole bottom is flat with slightly rounded corners. This geometry was based on the drill bit shape used during the coring process.

5.2.4 Stress analysis methodology

The findings from the investigations into the number of stress measuring points required to accurately determine the AMTS and different borehole geometries described in the previous sections resulted in the numerical model geometry and the location of the stress monitoring points illustrated in Figure 5.7. The tensile stresses are calculated at 196 points per plane with each plane separated by 0.025d. This results in up to 19,796 stress monitoring points per model depending on the core stub length. The stress points extend to a maximum depth below the bottom of the hole to 0.5d. This depth was found to be adequate for all boundary *in situ* stresses
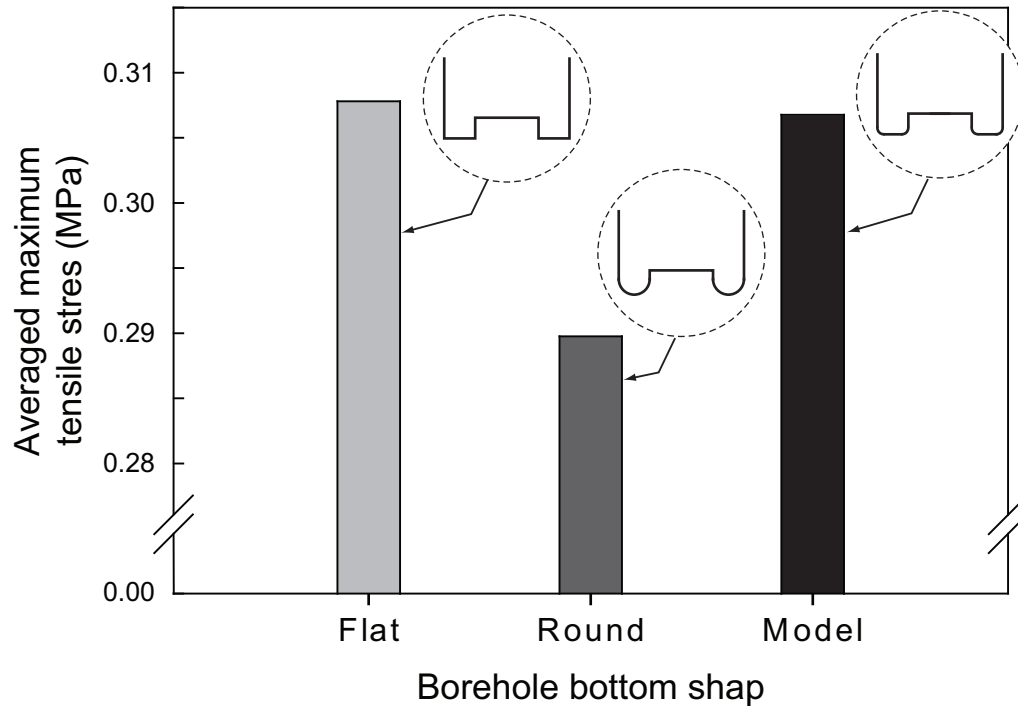
Figure 5.6: The effect of borehole bottom shape on the averaged maximum tensile stress. Three different geometries were tested: Flat, Round and Model using the applied boundary condition for the analyses are σ_H = -2, σ_h = -1 and σ_v = 0 MPa.

used in this study.

Figure 5.8 shows the location of the maximum tensile stress distribution from the numerical analysis given in Figure 5.7 using the applied *in situ* stresses of σ_H = -2.0, σ_h = -1.0 and σ_v = -0.5 MPa, and a core stub length was 0.25d. The location of maximum tensile stresses are highlighted in the sectional views, and the magnitudes of the maximum tensile stresses are projected to the circular plane in the centre of Figure 5.8. The highest magnitude of the maximum tensile stress is generated at the edge of the core near the inner side of borehole bottom, in the direction of the minimum horizontal *in situ* stress. The region of relatively low magnitude of maximum tensile stress appears in the maximum horizontal *in situ* stress direction, between the centre and the edge of the core. These stress points in the circular plane

115
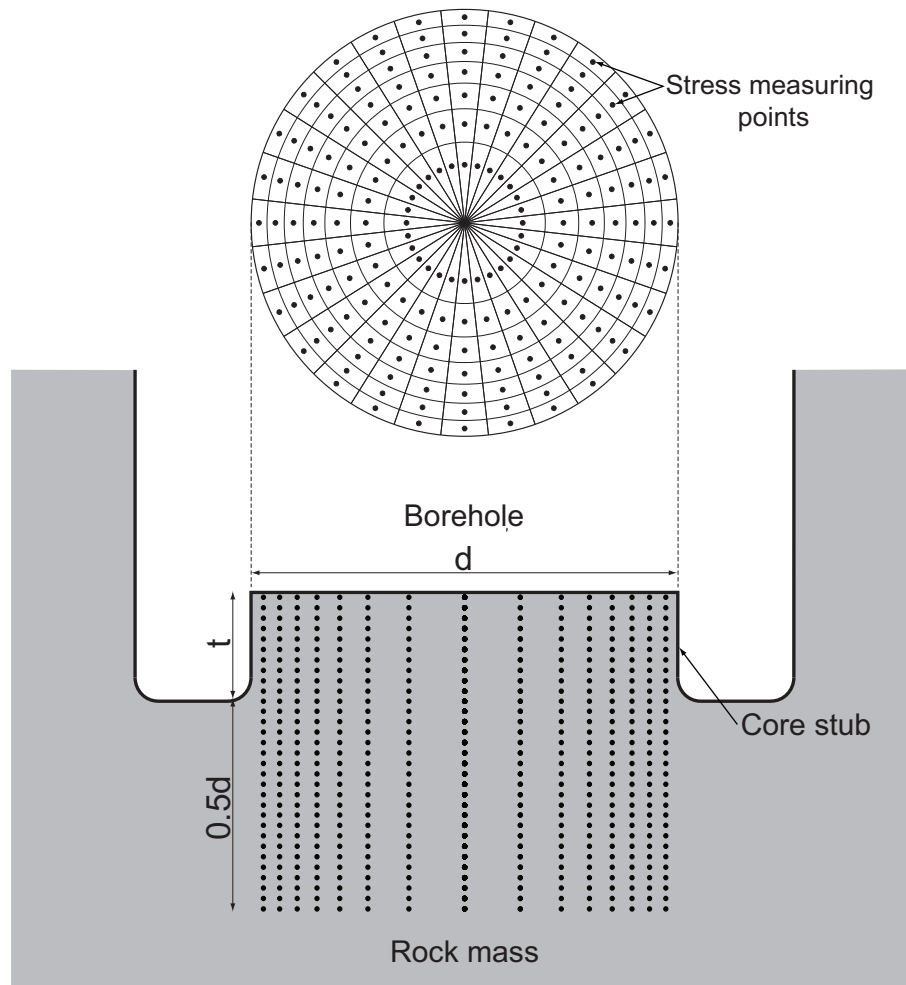
Figure 5.7: Illustration of the numerical model geometry of borehole bottom and the location of stress measuring points (d: core diameter, t: core stub length).

shown in Figure 5.8, can be used to determine the highest, lowest and average value of the maximum tensile stress. In this study these three stress values will be defined as; the maximum of maximum tensile stress, MTSmax, the minimum of maximum tensile stress, MTSmin and averaged maximum tensile stress, AMTS.

5.2.5 AMTS and disk thickness

It is well known that the thickness of core disks decreases as the far-field stresses increases. To assess if this trend is observed using the maximum tensile stress criterion, the core stub length (t) in Figure 5.7 is increased while keeping the boundary
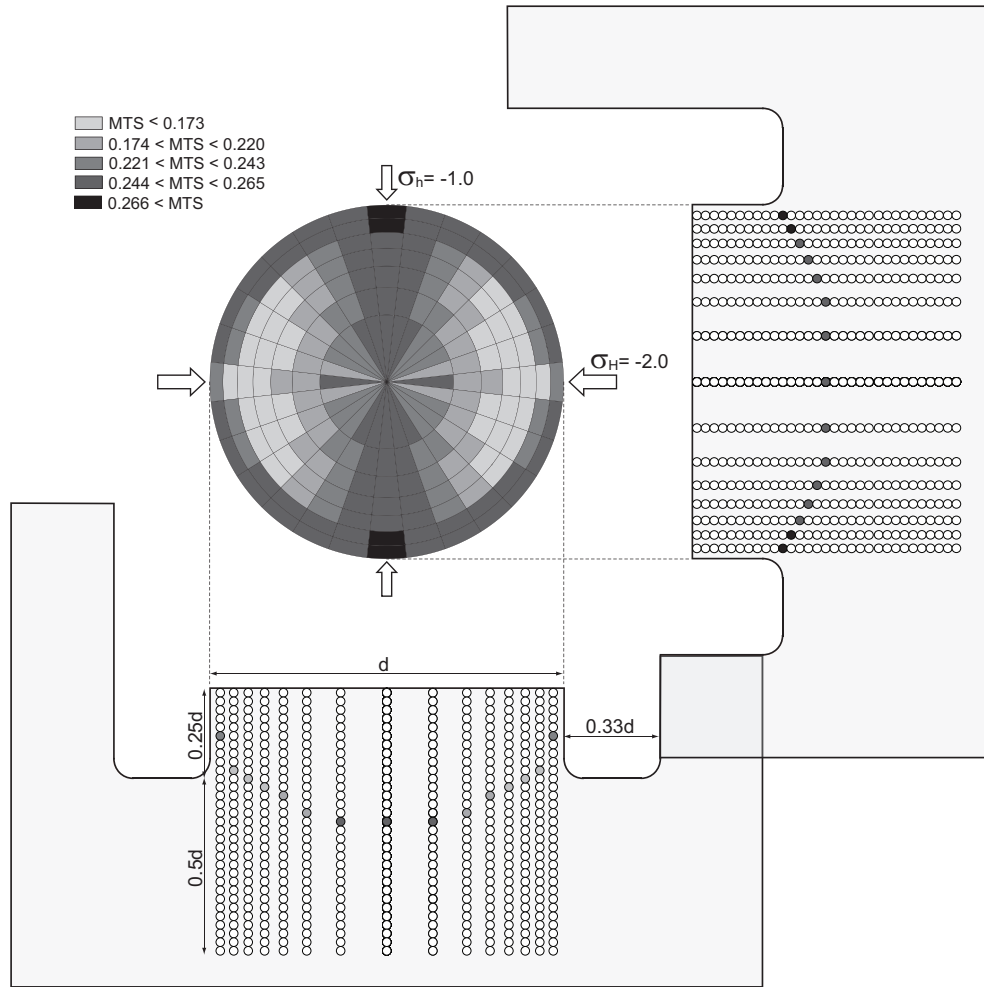
Figure 5.8: An example of the location of the maximum tensile stresses (MTSes). The applied boundary condition for the analyses are $\sigma_H = -2.0$, $\sigma_h = -1.0$ and $\sigma_v = -0.5$ MPa).

stresses the same. The model uses the same borehole geometry as in the previous section with 9 different core-stub lengths. The magnitude of MTSmax, MTSmin and AMTS was calculated for each core-stub length and the results compared in Figure 5.9. In Figure 5.9, the length of the core stub (t) is normalized to the core diameter (d). Initially MTSmax, MTSmin and AMTS increase when t/d is less than 0.15. While the magnitude of AMTS continues this increasing trend between 0.15t/d and approximately 1.0t/d, the magnitudes of MTSmax and MTSmin do not display this gradual increasing trend, particularly between 0.15 and 0.4t/d. Be-
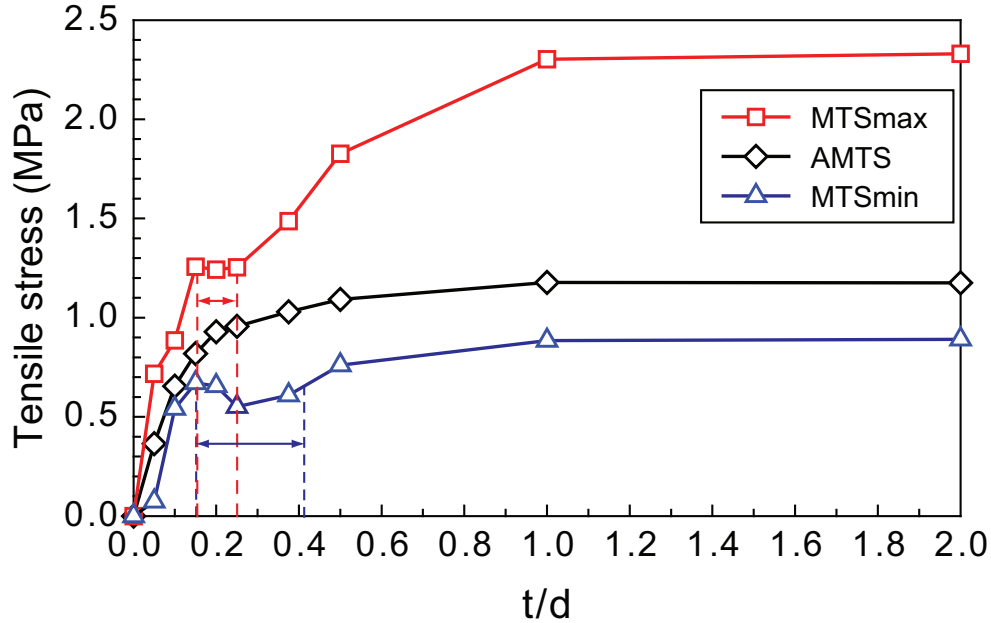
Figure 5.9: The magnitude of MTSmax, AMTS and MTSmin versus core stub length normalized by core diameter. The applied boundary stress condition: σ_H = -8, σ_h = -4 and σ_v = -1 MPa).

yond 1.0t/d there is essentially no change in the stress magnitude for any of the methods used to establish the maximum tensile stress. The MTSmax and MTSmin show essentially no change or a decrease in the stress to change the thickness of the core disk when the normalized core stub lengths are in 0.015<t/d<0.025 and 0.15<t/d<0.042 range respectively (see reference lines in Figure 5.9). This is not supported by the field evidence from Lim and Martin (2010) where a significant change in tensile stress was required to change the disk thickness over the range between 0.03t/d and 2.2t/d (see Figure 4.17 in Chapter 4).

The core disking criteria MTSmax, MTSmin and AMTS, were evaluated using the field core disking data in Figures 4.15a from Chapter 4. The known far-field stress conditions for nine t/d values for the field core disking data, were applied to the model shown in Figure 5.7. The relationship between core disk thickness and corresponding maximum horizontal *in situ* stresses from three different criteria (MTSmax, MTSmin and AMTS) was established and compared with field data in Figure 5.10. Inspection of Figure 5.10 shows that while AMTS criterion provides
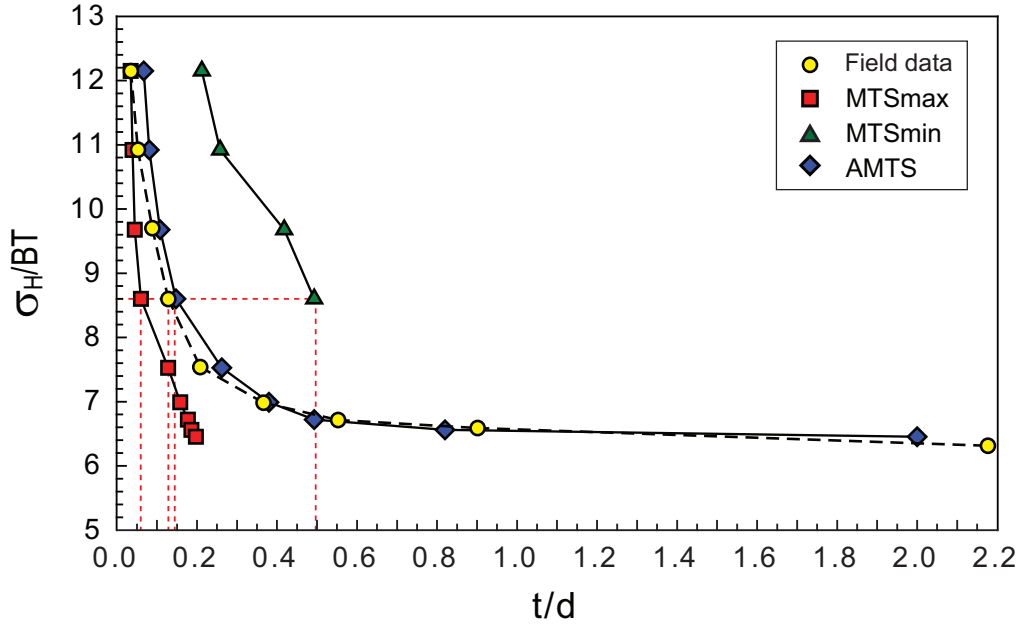
Figure 5.10: Comparison between MTSmax, MTSmin and AMTS criteria from numerical analysis, and the field core disking data for Lac du Bonnet granite at 420-m Level of URL. The AMTS criterion shows a best fit with the field core disking data. σ_H: maximum horizontal *in situ* stress (MPa), BT: Brazilian tensile strength (MPa), t: core disk thickness (mm), d: core diameter (mm).

good agreement with field core disking data, the MTSmin criterion over-estimates the core disking stress and the MTSmax criterion tends to under-estimates the core disking stress. For example, when the boundary condition of σ_H/BT = 8.6, σ_h/BT = 5.4 and σ_v/BT = 1.1 applied as a far-field *in situ* boundary condition the normalized core disk thickness is 0.06 for MTSmax criterion, 0.5 for MTSmin criterion, 0.15 for AMTS criterion, and the field observation was 0.13 (see reference lines in Figure 5.10).

From the numerical analyses based on the maximum tensile stress concept and the comparison of different criteria with field core disking data it is suggested that the AMTS may provide a reasonable core disking criterion. In the following section the core disking for AMTS criterion will be investigated using data from two field sites.

5.3 Application of AMTS as a core disking criterion

In this section the disking criteria based on the AMTS is applied to two field sites: (1) AECL′s Underground Research Laboratory (URL), Canada and (2) Forsmark, Sweden. At both sites extensive stress measurement campaigns were carried out to establish the far-field *in situ* stresses to a depth of approximately 1000 m. At Forsmark all investigations were carried out in surface collared boreholes, while at the URL the drilling was carried out from the surface and underground excavations. The laboratory properties of the intact rocks encountered at the URL and Forsmark are given in Table 5.1.

Table 5.1: Laboratory geotechnical properties of Lac du Bonnet (LdB) granite and Forsmark granite (σ_c = uniaxial compressive strength, BT= Brazilian tensile strength, E = Young′s modulus, ν = Poisson′s ratio).

Rock Type	σ_c (MPa)	BT (MPa)	E (GPa)	ν
LdB Granite	213 ± 2	9.3 ± 1.3	65 ± 5	0.25 ± 0.05
Forsmark Granite	226 ± 2	13 ± 2.0	76 ± 3	0.23 ± 0.03

5.3.1 Core disking and far-field *in situ* stresses

AECL′s Underground Research Laboratory (URL) is located within the Lac du Bonnet (LdB) granite batholiths near the western edge of the Canadian Shield, 150 m northeast of Winnipeg, Canada (Brown, 1989). The cores were obtained from both surface drilled vertical boreholes and boreholes drilled from underground openings at 420-m-depth Level (Lim and Martin, 2010). The 96-mm-diameter surface hole produced 62-mm core, and the 76-mm diameter holes drilled from underground produced 45-mm core. All holes were drilled with triple tube core barrels. While extensive core disking was obtained from boreholes drilled from the underground excavations due to the stress concentrations around the openings, only extensive microcracking was observed in surface drilled cores at a depth equivalent to the 420 Level.

The geometry of a vertical 96-mm-diameter borehole was modelled to establish

the core disking criterion for the site. A total of 92 simulations under a variety of far-field stress combinations were carried out and the results are illustrated in Figure 5.11. The applied *in situ* stress components, σ_H, σ_h, and σ_v, are normalized by the Brazilian tensile strength (BT). Figure 5.11 shows the solid core disking initiation diagram under three different σ_v conditions ($\sigma_v/\text{BT} = 0$, 1 and 2). The core disking lines represent the *in situ* stress combination that can initiate core disking. If an *in situ* stress combination falls above this core disking initiation lines core disking will occur. For example, at Point A in Figure 5.11 core disking would be expected at a relatively shallow depth if the far-field *in situ* stresses were $\sigma_H/\text{BT} = 6$, and $\sigma_h/\text{BT} = 4$.

The stress region where core disking can occur in Figure 5.11 can be divided into two geological fault regimes using the fault classification of Anderson (1951). An-
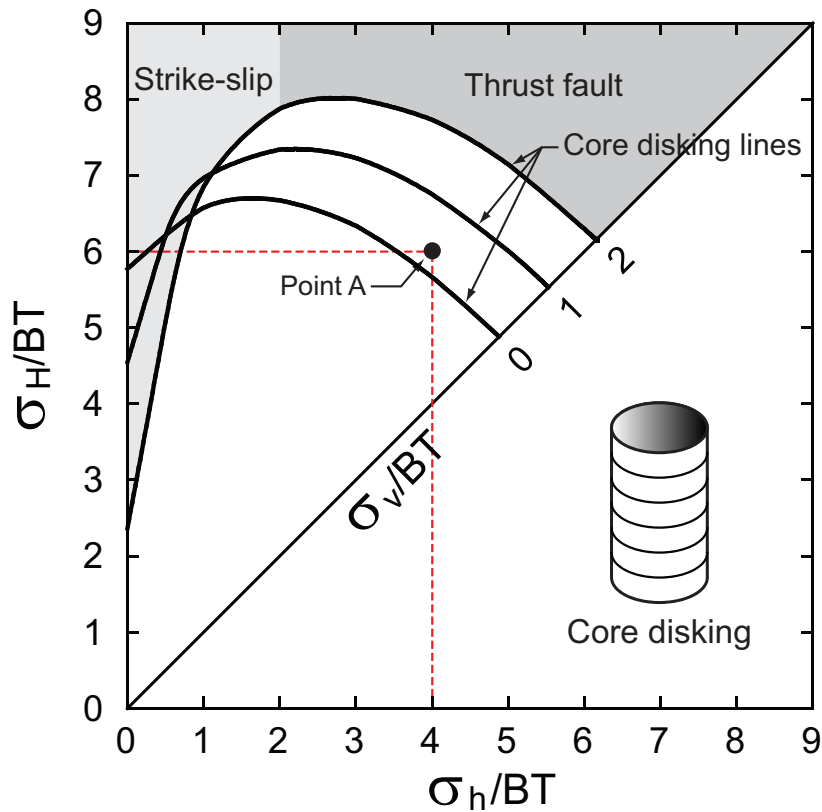
Figure 5.11: Core disking initiation diagram based on the AMTS concept for Lac du Bonnet granite at URL.

derson (1951) proposed that for a thrust fault both horizontal stresses must be greater than the vertical stress leading to $\sigma_H > \sigma_h > \sigma_v$. For the strike-slip fault the minimum stress must be in the horizontal plane leading to $\sigma_H > \sigma_v > \sigma_h$. These two fault regimes for the stress condition of $\sigma_v/\text{BT} = 2$ are illustrated in Figure 5.11. An interesting point in Figure 5.11 is that the σ_H required for core disking decreases as σ_h increases in the thrust fault stress region. Hence in a thrust fault regime disking in vertical boreholes is influenced not only by the magnitude of the horizontal stress but also by the horizontal deviatoric stresses. For example, from Figure 5.11, the horizontal stress magnitudes required for disking is at a minimum if ratio of σ_H to σ_h is approximately 1, i.e., no horizontal deviatoric stress. However in the strike slip fault regime the maximum horizontal stress required for core disking is at a minimum when the horizontal deviatoric stresses are at a maximum. This implies that core disking in vertical boreholes is affected not only by the deviatoric stress between σ_H (or σ_h) and σ_v but also by the deviatoric stress between σ_H and σ_h.

Kaga et al. (2003) also established a core disking criterion based on the principal tensile stress concept and applied it to LdB granite. The criterion showed a good agreement with the laboratory core disking results by Haimson and Lee (1995). Figure 5.12 provides a direct comparison between the disking criterion proposed by Kaga et al. (2003) and the AMTS criterion introduced in this study. The comparison was carried out using a vertical stress of 25 MPa. Figure 5.12 illustrates a large discrepancy between the two criteria. For example, when the normalized minimum horizontal stress is 3, the principal tensile stress criterion estimated the maximum horizontal disking stress about 73% higher than the disking stress predicted by the AMTS criterion (see reference line in Figure 5.12). In addition, the trends in the two criteria are also not in agreement. The required maximum horizontal stress increases as the minimum horizontal stress decreases over the entire stress range in the principal tensile stress criterion. While the AMTS criterion in the strike-slip stress environment shows the opposite. This opposite trend for the AMTS in the strike-slip stress condition in Figure 5.12 is in agreement with the results from the laboratory core disking experiment by Sugawara et al. (1978). The over-estimation

of the core disking stress by the principal tensile stress criterion is due to the fact that the criterion uses the MTSmin as a core disking stress.
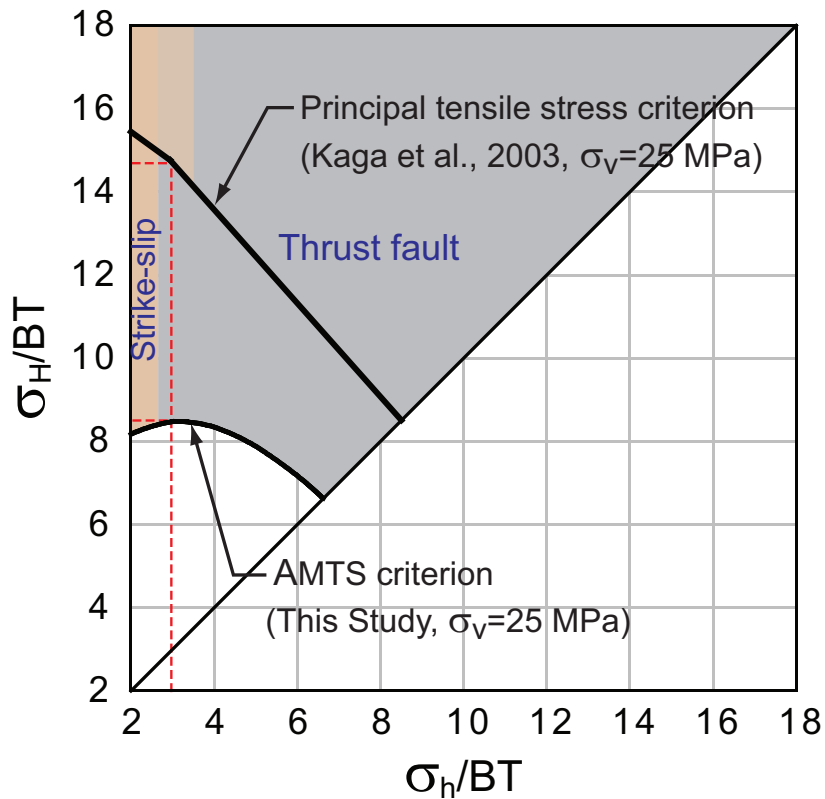
Figure 5.12: Comparison of core disking criteria for Lac du Bonnet granite using the principal tensile stress criterion proposed by Kaga et al. (2003) and the averaged maximum tensile stress (AMTS) criterion established in this study.

5.3.2 Comparison of disking criteria and far-field *in situ* stress

The stress profile at URL was established based on measurements from the traditional USBM overcoring method, the large scale under-excavation method and the modified door stopper technique (Martin et al., 1997; Thompson and Chandler, 2004). The results from those tests are given in Figure 5.13b. The *in situ* stress condition at five different depth (A: 250m, B: 350m, C: 420m, D: 675m and E: 960m) were plotted on the core disking initiation diagram in Figure 5.13a to check whether core disking will occur. In Figure 5.13a, if the horizontal stress combination (σ_H,
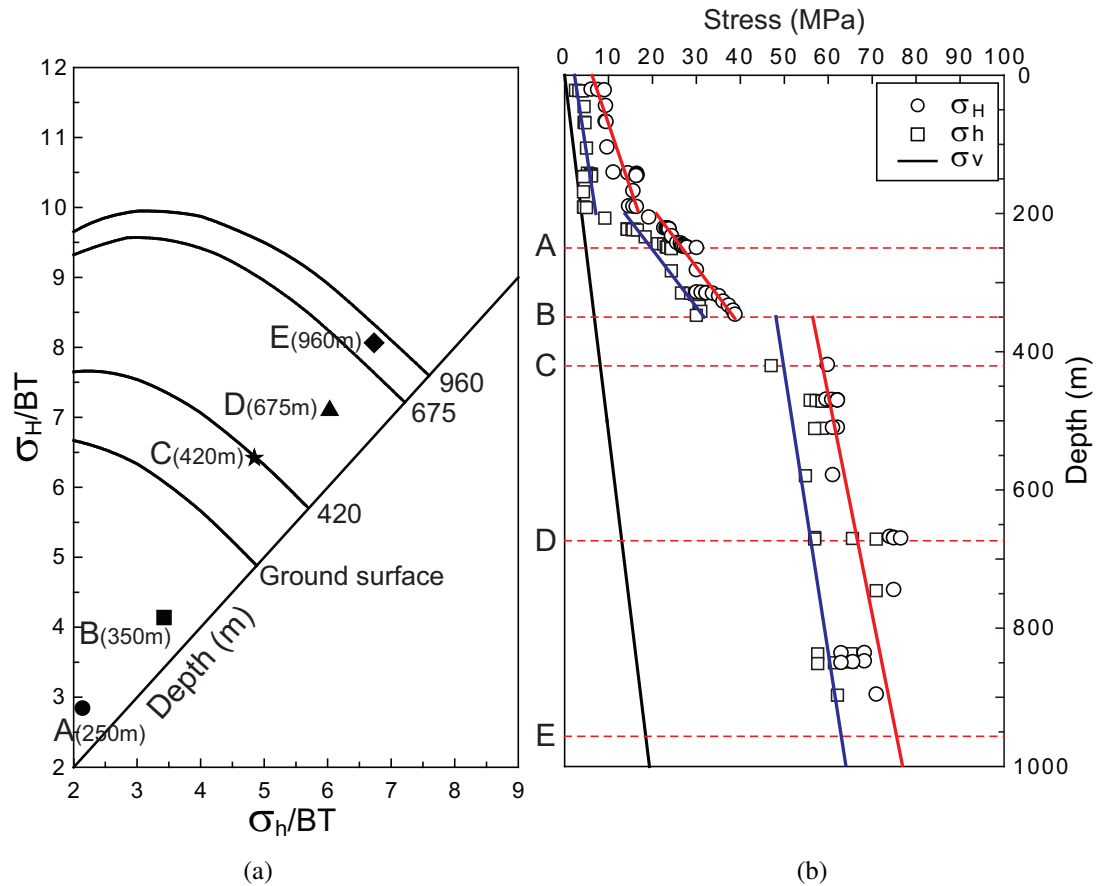
Figure 5.13: Evaluation of the potential for core disking for Lac du Bonnet granite at URL using the AMTS criterion. (a): Core disking initiation diagram at different depth (ground surface, 420m, 675m and 960m). (b): *In situ* stress profile at URL. The *in situ* stress conditions at A, B, C, D and E, are indicated on the core disking initiation diagram.

σ_h) at each depth falls above the core disking initiation lines for the depth, core disking should be observed. All of the *in situ* stress points however fall below the core disking criteria. This implies that no core disking should be observed for the entire investigated depth, and this result is consistent with field core observation. It is worth noting that extensive stress-induced microcracks were observed in the core extracted from surface-drilled borehole at 420-m depth, and also the *in situ* stress condition at C (420m) falls very close to the core disking initiation diagram in Figure 5.13a.

Forsmark is the candidate site recommended for construction of the nuclear used fuel repository for Sweden (SKB, 2005). At the Forsmark site extensive *in situ* stress measurement campaigns were carried out using surface drill holes (SKB, 2008). The *in situ* stress magnitudes and orientations were obtained using overcoring and hydraulic fracturing techniques, including hydraulic testing of pre-existing fractures (Sjöberg et al., 2005). The *in situ* stress magnitude profile for the Forsmark site is illustrated in Figure 5.14b.

A series of three dimensional numerical analyses were carried out to establish the core disking initiation diagram for Forsmark. The 76-mm hole diameter borehole
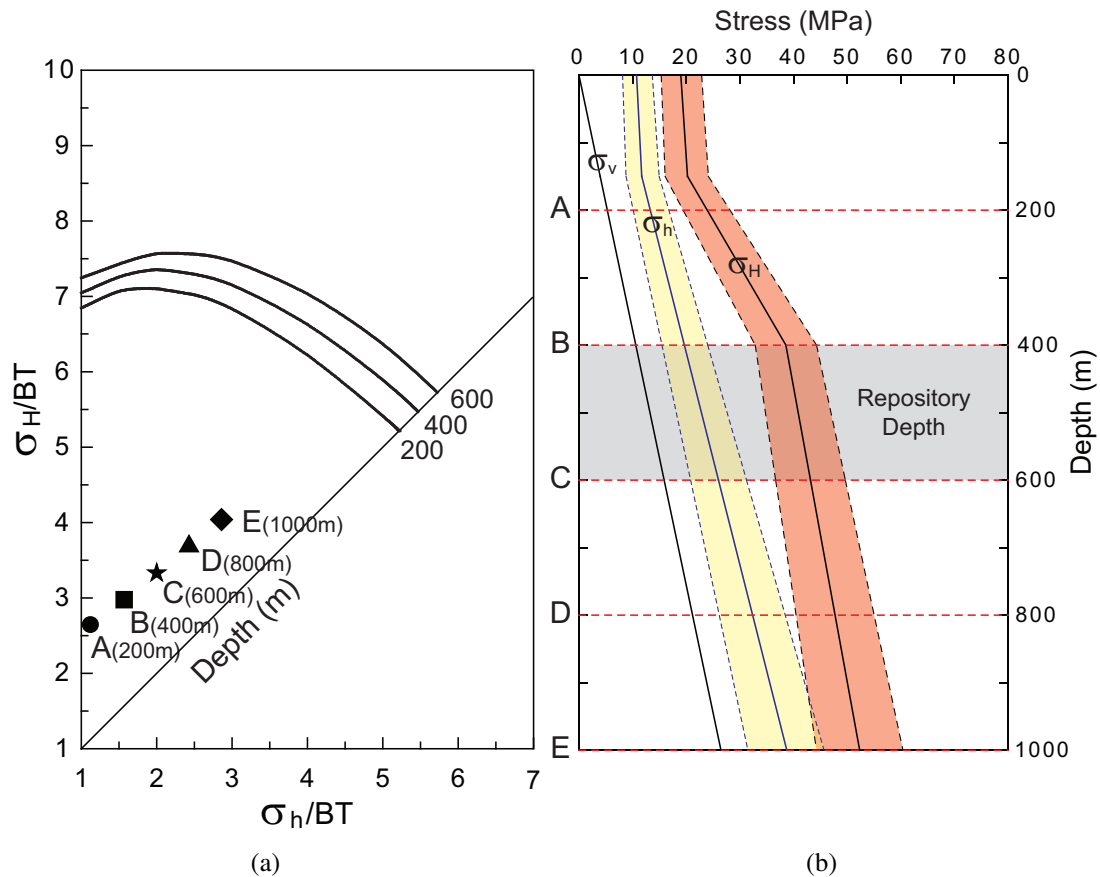
Figure 5.14: The potential of core disking at the Forsmark site. (a): Core disking diagram at different depth (200m, 400m and 600m). (b): *In situ* stress profile at Forsmark site (data from SKB (2008)). The *in situ* stress conditions at A, B, C, D and E, are plotted on the core disking initiation diagram.

and the 51-mm-diameter core were modelled in all the numerical analyses. A total of 63 analyses were conducted and the AMTS calculated for each far-field boundary *in situ* stress combinations. From the numerical analyses the solid core disking initiation diagram for three vertical *in situ* stress conditions (200m, 400m and 600m) was established in Figure 5.14a. In Figure 5.14a the *in situ* stress conditions at different depth (A: 200m, B: 400m, C: 600m, D: 800m, E:1000m) were plotted on the core disking diagram. As shown in Figure 5.14a, all *in situ* stress conditions for five different depths fall well below the core disking initiation lines. That means no solid core disking would be observed in the depth between ground surface and 1000 m. This prediction is consistent with field observations noted by Sjöberg et al. (2005) that to the depths of 1000 m the only solid core disking observed was localized to short (less than 10 cm) sections and often associated with pegmatites.

In comparing Figure 5.13 and Figure 5.14, it is clear that in all cases at Forsmark the far-field stress magnitudes are well below those needed to initiate disking, while at the URL the stress magnitudes are much closer to the magnitudes needed for disking. Despite the granite at Forsmark and URL having similar unconfined compressive strength, 226 MPa and 213 MPa, respectively; the tensile strengths of these granites are quite different. The tensile strength of the Forsmark granite is approximately 40% greater then that of Lac du Bonnet granite. This tensile strength difference and the slightly different *in situ* stress profiles combine to provide the contrasting core disking environments.

5.3.3 Comparison of criteria with observed disking

Lim and Martin (2010) compiled core-disking observations from the boreholes drilled from tunnels at the 420-m Level of URL. Because these boreholes were drilled from underground tunnels the stress concentrations due to the tunnels were sufficient to cause the core disking. Also, because the boreholes are collared at the tunnel wall, and the disking initiates at the collar (see Figure 5.1) the vertical stress, i.e, the stress along the borehole axis, normalized to the tensile strength was between 0.0 and 2.0. Lim and Martin (2010) determined the *in situ* stress mag-

126

nitudes associated with the observed core disking. These far-field *in situ* stresses are plotted on the core disking diagram in Figure 5.15 which was developed in Figure 5.11. Figure 5.15 provides a direct comparison between the core disking criteria established using the AMTS methodology and the field core disking data. In Figure 5.15, all the disking data points falls above the core disking lines which is in agreement with the field observations (see Figure 5.1), suggesting that the AMTS methodology is a useful predictive tool for core disking.
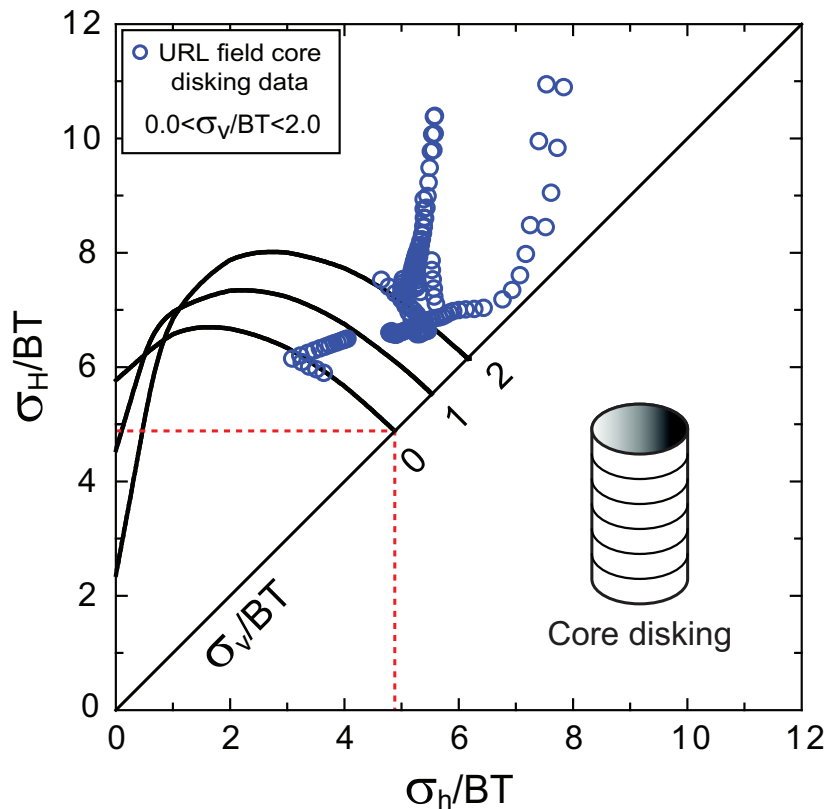
Figure 5.15: Comparison between core disking initiation diagram based on the AMTS criterion and field core disking data for Lac du Bonnet granite at URL.

5.3.4 Ring-disking

It is well known that a pilot hole in a core reduces the stresses required for disking (Sugawara et al., 1978; Lim et al., 2006). This form of disking is referred to as ring-disking and is sometimes encountered when attempting to use an overcoring

stress measurement technique. The numerical models used to develop Figure 5.11 were re-analyzed for the effect of a 38-mm-diameter pilot hole. Figure 5.16 shows the stress diagram for initiation of ring-disking. The general trends are the same as those observed for the solid core disking stress criterion in Figure 5.11, however the magnitude of the horizontal stresses required for ring disking is about 40% lower than the magnitude required for solid core disking under the same vertical stress.
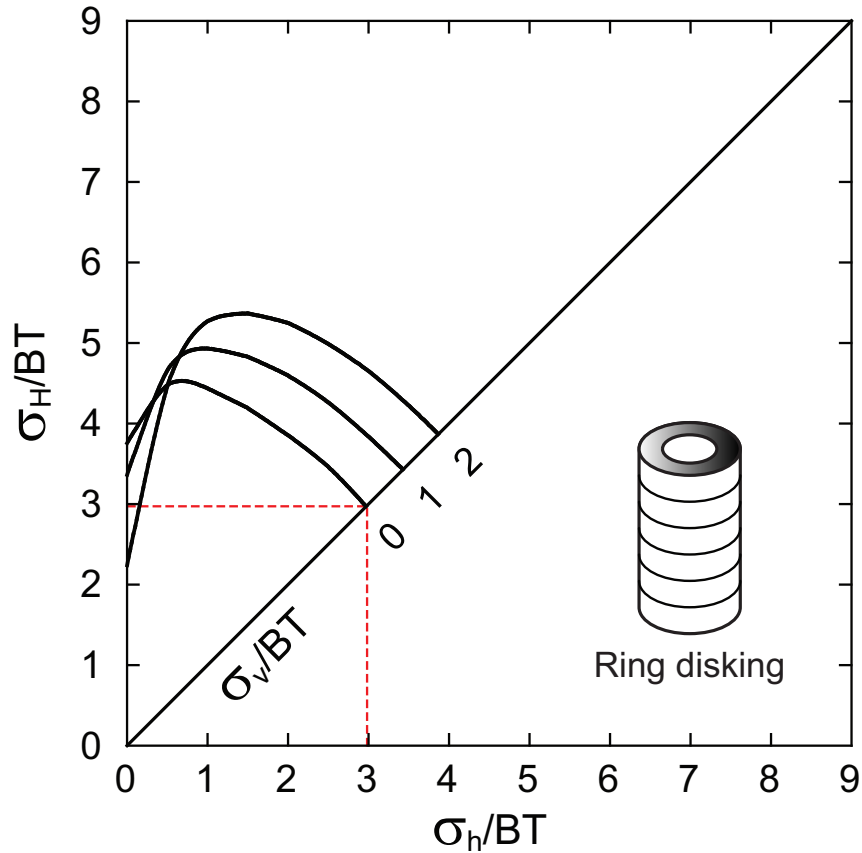
Figure 5.16: Stress magnitudes required to initiate ring disking.

5.3.5 Effect of drill hole diameter and drill core diameter on core disking

When core disking is encountered in exploratory surface based boreholes, it can be disruptive to a stress measurement and sampling program. It has already been shown that simply drilling a pilot hole reduces the stress magnitudes necessary to

cause disking. Hence, one of the questions that is often posed; can core disking be eliminated if the size of the borehole and core are changed?

Numerical analyses were carried out using the model for five different industry standard drill bit sizes producing the hole dimensions (AQ:48mm, BQ:60mm, NQ:76mm, HQ:96mm and PQ:123mm). As the drill hole diameter changes the ratio of drill core diameter (d) to drill hole diameter (D) also changes. Figure 5.17 shows the change in the disking stress using the AMTS methodology for each drilling bit size. As the ratio of core diameter to borehole diameter (d/D) increases, the stress causing core disking decreases. A 25% increase in the d/D ratio can reduce the AMTS stress by about 11%. It is also shown in Section 5.2.3 that the rounded-edge shape drill bit, compared to the sharp-edge shape could reduce the AMTS about 10% (see
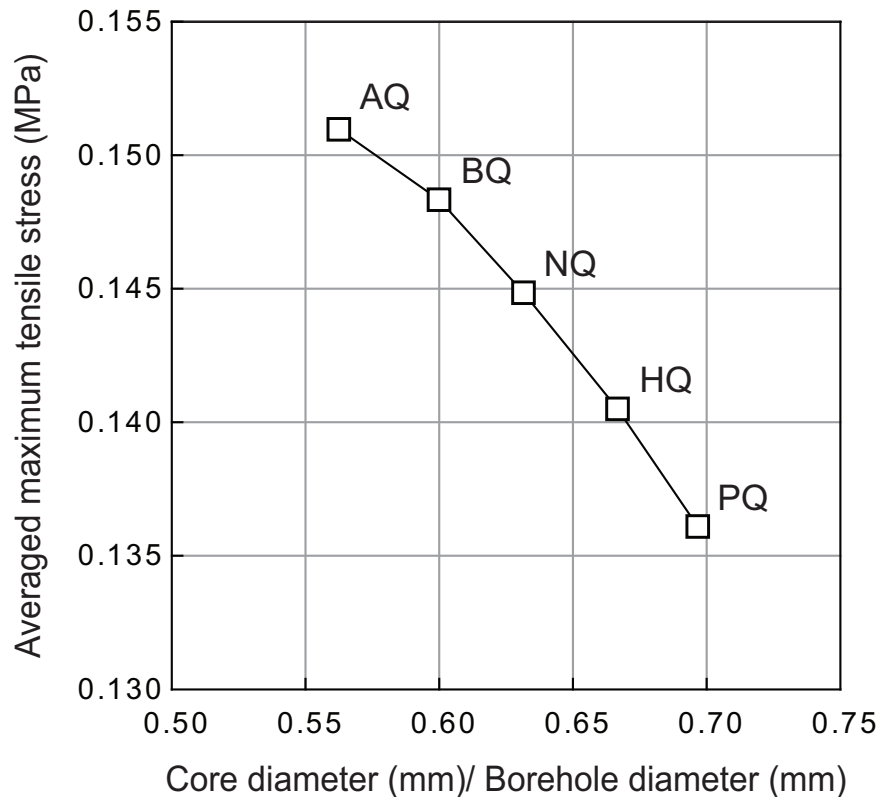
Figure 5.17: Effect of the ratio of core diameter (d) to borehole diameter (D) on the averaged maximum tensile stress. Five different drill bit diameters were tested under the same core stub dimension (t/d = 1.0) and *in situ* stress ($\sigma_H = \sigma_h = $ -1 MPa and $\sigma_v = $ -0.5 MPa).

Figure 5.6). Thus, it can be concluded that if a large diameter hole with a rounded shape bit is used for drilling at significant depth the potential for drilling-induced core damage and core disking can be reduced. However, the merits for using a larger diameter borehole are only warranted if the core diameter also increases.

5.4 Conclusion

Three dimensional elastic numerical analyses were carried out to estimate the stress conditions required for core disking. The numerical models were used to calculate the tensile stresses in and around the core stub using the as-built geometry of the borehole bottom. These tensile stresses vary spatially in the core stub and hence a range of tensile stresses is obtained depending on its spatial location relative to the borehole centre. A sensitivity study was carried out to determine the number of sampling points needed to establish the tensile stresses in this core stub. Three approaches were used to quantify the magnitude of these maximum tensile stresses: 1) the maximum, 2) the minimum and 3) the average of the maximum tensile stress. These three approaches were applied to core disking field data to determine which of the three approaches could be used for establishing the core disking stress. The maximum tensile stress under-estimated the core disking stress and the minimum tensile stress over-estimated the core disking stress while the averaged maximum tensile stress (AMTS) showed good agreement with the field data.

The AMTS criterion was used to develop core disking nomograms based on the maximum and minimum horizontal stress, and vertical stress. The criterion showed marked changes in the trend of the criterion, depending on the nature of the far-field stress regime. The approach was used to estimate the core disking stresses for LdB granite at URL and Forsmark granite at Forsmark. The core disking criterion was found to be in general agreement with the core disking observations at both sites. The analyses showed that, for the same vertical stress, the horizontal *in situ* stresses required for solid disking are about 40% higher than the *in situ* stresses required for ring-disking.

The stress distribution around the borehole bottom is complex and a variety of fac-

tors, such, the geometry of the borehole and core, and *in situ* stress condition, influence the magnitude of maximum tensile stress. Thus, the estimation of *in situ* stress by using only a single formula will have some limitations. However, it is shown in this study that if core disking analyses are carried out using site specific drilling geometry, the disking criteria may be useful for estimating the *in situ* stress magnitudes, should core disking be encountered.

Bibliography

Anderson, E.M. 1951. *The dynamics of faulting*. Oliver & Boyd, Edinburgh.

Brown, A., Soonawala, N.M., Everitt, R.A., Kamineni, D.C. 1989. Geology and geophysics of the Underground Research Laboratory Site, Lac du Bonnet Batholith, Manitoba. *Can. J. Earth* 26: 404–425.

Corthesy, R., Leite, M.H. 2008. A strain-softening numerical model of core discing and damage. *Int. J. Rock Mech. Min. Sci.* 45(3): 329–350.

Durelli, A.J., Obert, L., Parks, V. 1968. Stresss required to initiate core discing. *Transactions Sociaty of Mining Engineers*. 241: 1065–1073.

Dyke C.G. 1989. Core discing: Its potential as an indicator of principal *in situ* stress directions. In: *Proceedings of ISRM–SPE International Symposium Rock at Great Depth*, *Pau*. Maury V., Fourmaintraux D. *editors*. A.A. Balkema, Rotterdam, vol. II, pp. 1057–1064.

RocScience 2004. *Examine3D version 4.0*.

Haimson B.C., Lee M.Y. 1995. Estimating deep in istu stresses from borehole breakouts and core disking – experimental results in granite. In: *Proceedings of the International Workshop on Rock Stress Measurement at Great Depth, The 8th International Congress on Rock Mechanics*, *Tokyo*, pp. 19–24.

Hakala, M. 1999b. Numerical study on core damage and interpretation of in-situ state of stress, *Technical Report POSIVA–99–25*, Posiva Oy, Helsinki, Finland.

Jaeger, J.C., Cook, N.G.W. 1963. Pinching-off and disking of rocks. *J. Geophys. Res.* 888(6): 1759–1765.

Kaga, N., Matsuki, K., Sakaguchi, K. 2003. The in situ stress states associated with core discing estimated by analysis of principal tensile stress. *Int. J. Rock Mech. Min. Sci.* 40: 653–665.

Li, Y., Schmitt, D. 1997. Effects of poisson′s ratio and core stub length on bottom-hole stress concentrations. *Int. J. Rock Mech. Min. Sci.* 34(5): 761–773.

Lim, S.S., Martin, C.D. 2010. Core disking and its relationship with stress magnitude for Lac du Bonnet granite. *Int. J. Rock Mech. Min. Sci.* 47(2), 254–264.

Lim, S.S., Martin, C.D., Christiansson, R. 2006. Estimating in-situ stress magnitudes from core disking In: *Proceedings of International Symposium on In-situ Rock Stress*, *Trondheim*. Lu, M., Li, C.C., Kjorholt, H., Dahle, H. *editors*. A.A. Balkema, Rotterdam, pp. 159–166.

Martin, C.D., Read, R.S., Martino, J.B. 1997. Observations of brittle failure around a circular test tunnel. *Int. J. Rock Mech. Min. Sci.* 34(7): 1065-1073.

Martin, C.D., 2007. Quantifying in-situ stress magnitudes and orientations for Forsmark - Forsmark stage 2.2. *SKB P–07–26*, Swedish Nuclear Fuel and Waste Management Co., Stockholm.

Obert, L., Stephenson, D.E. 1965. Stress conditions under which core discing occurs. *Transactions Sociaty of Mining Engineers* 232(3): 227–235.

Sjöberg, J., Lindfors, L., Perman, F., Ask, D. 2005. Evaluation of the state of stress at the Forsmark site. *SKB P–05–35*, Swedish Nuclear Fuel and Waste Management Co., Stockholm.

SKB, 2005. Preliminary site description Forsmark area – version 1.2. *SKB R–05–18*, Swedish Nuclear Fuel and Waste Management Co., Stockholm.

SKB, 2008. Site description of Forsmark at completion of the site investigation

phase. SDM-Site Forsmark. *SKB TR–08–05*, Swedish Nuclear Fuel and Waste Management Co., Stockholm.

Stacey, T.R. 1982. . *Journal South African Institute of Mining and Metallurgy* 99: 269–274.

Sugawara, K., Kameoka, Y., Saito, T., Oka, Y., Hiramatsu, Y. 1978. A study on core disking of rock. *Journal of Japanese Association of Mining* 94: 19–25.

Thompson, P.M., Chandler, N.A. 2004. In situ rock stress determinations in deep boreholes at the Underground Research Laboratory. *Int. J. Rock Mech. Min. Sci.* 41(8): 1305–1316.

Chapter 6

Summary and Conclusion

6.1 Stress-induced microcracking

Extracting cores from deep bore holes can significantly increase microcrack porosity, or what is commonly called sample disturbance or stress-induced core damage. Chernis (1984) noted that the origin and types of microcracks are influenced by microcrack porosity, and that microcrack volume strongly affects the physical properties of the rock samples.

After using image analysis combining both fluorescent and polarized microscopy techniques to quantify microcracking in two different granites, this study measured and analyzed the microcrack types, densities, lengths, orientations, and grain sizes for each granite sample. Most of these microcracks were grain boundary cracks, naturally occurring among samples at shallow depth ($<$200 m). While the density of all three types of microcracks (grain boundary, intragranular, and transgranular) increased with depth, a significant increase in density of transgranular microcracks signaled an association with elevated stress magnitudes. Because most of these microcracks formed perpendicular to the core axis, the ratio of horizontal to axial transgranular microcracks could indicate the degree of stress-induced core damage.

The characteristics and quantity of microcracks measured in core samples can provide indirect evidence on *in situ* stress magnitudes. Carlson and Wang (1986) found

a linear correlation between mean *in situ* stress and microcrack porosity with depth. It remains unclear whether the linear trend will occur in thrust fault geological conditions, in which horizontal *in situ* stress is at maximum. The microcrack volume in laboratory samples can be estimated using the total microcrack volumetric strain. This was measured for 87 granite samples from the study sites. It was found that the volume of microcracks for LdB granite was approximately one order of magnitude greater than the volume found in Forsmark granite, even though the total number of microcracks is similar for both granites. Because the crack volumes tend to be dominated by grain boundary cracks it appears that the difference in the microcrack volumetric strain is related to the larger grain size in LdB granite (approximately 5 times larger than the Forsmark granite). Linear trends were established between the normalized mean *in situ* stress and total microcrack volumetric strain for both LdB granite and Forsmark granite.

6.2   Field core disking observation

Core disking is a frequently-used indicator of elevated stress magnitudes. Researchers have been investigating core disking since the early 1960s′ using laboratory testing and numerical analysis. While their studies have provided insight into the core disking mechanism, there is still uncertainty as to the relationship between core disking and the stress magnitudes required to cause it. This uncertainty arises because of the lack of core-disking field data where the *in situ* stress magnitudes are reliably known.

This study mapped extensive core disking in a series of bore holes drilled from a tunnel located at a depth of 420 m in massive, unfractured Lac du Bonnet (LdB) granite, and measured the thickness of the core disks in detail. Using fracture persistence, they grouped the extracted cores from the bore holes into three categories: core disking, partial disking, and no disking. Having characterized the *in situ* stress magnitudes using previous studies, the researchers sought to relate those magnitudes to core disking.

This study estimated stress states around the tunnels and along the boreholes us-

ing 3D elastic numerical analyses. The maximum principal stress near the tunnel boundary was approximately 100 MPa and decreased to the far-field maximum *in situ* stress near the end of the boreholes. Having found a strong correlation between core disk thickness and the magnitude of maximum principal stress, this study concluded that core disking occurs when the ratio of maximum principal stress, normalized to Brazilian tensile strength, exceeds 6.5. Guidelines are provided for estimating stress magnitudes and disk thickness for LdB granite at the 420 level of AECL′s URL.

Stress path analyses indicated that minimum principal stress (tensile stress) caused the onset of disking. Core disking fracture is complex, and may be initiated at core centre or boundary.

6.3 Core disking criteria

Tensile stress plays a critical role in the creation of core disking. Kaga et al. (2003) proposed a single formulation as a core disking criterion applicable for any core disk length or shapes. The principal tensile stress criterion proposed by Kaga et al. (2003) appears to agree well with laboratory core disking data for LdB granite tested by Haimson and Lee (1995). However, the criterion shows a large discrepancy with the field core disking data obtained by Lim and Martin (2010).

Three dimensional numerical analyses were carried out to figure out the core disking stress condition. The analyses show that the maximum tensile stress plays a critical role in core disking. Three stress values of maximum tensile stress could be used as a threshold of core disking stress: maximum, minimum, and the average of the maximum tensile stress. The principal tensile stress criterion proposed by Kaga et al. (2003) adapted the minimum value of the maximum tensile stresses as a core disking stress. That criterion highly over-estimated the core disking stress. Because averaged maximum tensile stress (AMTS) shows excellent agreement with field core disking data, this study proposes it as a core disking criterion.

This study used the AMTS criterion to develop core disking nomograms based on

the maximum and minimum horizontal stress, and vertical stress. The approach provided estimates for core disking stresses of LdB granite at URL and Forsmark granite at Forsmark. The core disking criteria were in general agreement with core disking observations at both sites. The analyses showed that, for the same vertical stress, the horizontal *in situ* stresses required for solid disking are about 40% higher than the *in situ* stresses required for ring-disking. While increased maximum and minimum horizontal stresses accelerates core disking, vertical stress shows an inverse relationship with the magnitude of AMTS. Higher horizontal stresses with lower vertical stress generate thinner core disks.

The criterion showed marked changes in its trend, depending on the nature of the far-field stress regime. The orientation of maximum tensile stress rotates from parallel (or sub-parallel) to horizontal *in situ* stresses, to the direction of vertical *in situ* stress when the stress condition changes from thrust fault to strike-slip fault. Therefore, stress estimation based on core disk thickness is applicable only for thrust fault stress environments. The scale effect test with standard drill bits demonstrated that bigger, round bits can significantly reduce core disking.

6.4 Future research

As part of the core disking study, this study attempted the fracture mechanics approach and discrete element method approach to simulate fracture initiation, propagation, and networking of multiple fractures. However, the study was unsuccessful in this aim due to the following limitations of the software used for the simulations:

1. Fracture mechanics approach using FRANC3D (a fracture analysis code for simulating an arbitrary non-planar three dimensional crack growth (CFG, 2003):

   - Initial fracture initiation point(s) should be indicated by the modeler, which has a high potential to mislead the fracture initiations point(s) and may result in changing the persistence and shape of the fracture.

   - Fracture propagation stops when the tangential stress at the fracture tip

138

is negative (compressive) at least one point. The fracture-induced dilation will not be considered properly in this situation.

2. Discrete element method (DEM) approach using PFC3D (PFC is particle flow code using circular or spherical elements, developed to mimic the micro-processes of the particle interactions in actual rocks (Potyondy and Cundall, 2004).

   - The tensile strength to compressive strength ratio is considerably greater than that measured in the laboratory tests, which is a fundamental limitation of the code. During the core disking modeling using PFC3D, this study found extensive compressive fractures began before the tensile fractures did. The compressive fractures softened the model and the core disking fracture never began.

When limitations are addressed with numerical codes, this study recommends core disking simulation using fracture mechanics approach or DEM approach, as well as research to resolve those limitations.

This study compared the characteristics of stress-induced microcracks to natural microcracks, and investigated the measurement of those microcrack volumes, and established a linear correlation between mean *in situ* stress and microcrack volume. However, the measurement of stress-induced microcrack volume did not distinguish between stress-induced microcracks caused by the release of *in situ* stress and drilling-induced microcracks generated by drilling. The author suspects that the former may correlate with mean *in situ* stress, whereas the latter will be affected more by maximum deviatoric stress.

In many cases, the strain recovery methods (ASR, DSCA) and acoustic methods show unreliable results, because those methods assume that stress-induced microcracks are primarily aligned with the direction of *in situ* stress (Strickland and Ren, 1980; Teufel, 1982), without considering that drilling-induced microcracks are dominant in high horizontal stress conditions. This study therefore rec-

ommends quantification work for microcracks generated by two different stress sources (stress-induced and drilling-induced).

Bibliography

Carlson, S.R., Wang, H.F. 1986. Microcrack porosity and in-situ stress in Illinois borehole UPH 3. *J. Geophys. Res.* 91: 10421–10428.

Connel Fracture Group, 2003. *FRANC3D version 2.6 manual*. 118.

Chernis, P.J. 1984. Comparison of the pore-microstructure of shallow and deep samples of the Lac du Bonnet granite. *Technical Record 223*, Atomic Energy of Canada Limited, Onterio.

Haimson B.C., Lee M.Y. 1995. Estimating deep in istu stresses from borehole breakouts and core disking - experimental results in granite. In: *Proceedings of the international workshop on rock stress measurement at great depth, The 8th international congress on rock mechanics, Tokyo*, pp. 19–24.

Kaga, N., Matsuki, K., Sakaguchi, K. 2003. The in situ stress states associated with core discing estimated by analysis of principal tensile stress. *Int. J. Rock Mech. Min. Sci.* 40: 653–665.

Lim, S.S., Martin, C.D. 2010. Core disking and its relationship with stress magnitude for Lac du Bonnet granite. *Int. J. Rock Mech. Min. Sci.* 47(2): 254–264.

Potyondy D.O., Cundall P.A. 2004. A bonded-particle model for rock. *Int. J. Rock Mech. Min. Sci.* 41: 1329–1364.

Strickland F.G. Ren, N.K. 1980. Use of differential strain curve analysis in predicting the in-situ stress state for deep wells. In: *Proc. 11the Cong. Int. Soc. Rock Mech. (ISRM)*. Ribeiro e Sousa, Olalla, Grossmann, *editors*. Taylor & Francis Group, London, pp. 55–58.

Teufel, L.W. 1982. Prediction of hydraulic fracture azimuth from anelastic strain recovery measurements in oriented core. In: *Proc. 23th U.S. national rock mechanics symposium*, pp. 238–245.

Appendix A

In situ stress estimation using crack closure energy in crystalline rock [4]

A.1 ABSTRACT

Under high horizontal *in situ* stress conditions traditional stress measurement method such as hydraulic fracturing and overcoring often do not give reliable values for the horizontal *in situ* stress magnitudes. Under such conditions additional information is required to constrain the *in situ* stress magnitudes. In this study, a correlation between the magnitude of crack closure energy and the maximum *in situ* stress magnitude was established at a site where the stress magnitudes were known with accuracy to depth of 900 m. The crack closure energy was measured on standard uniaxial tests. The correlation was used to estimate the possible range of the maximum horizontal stress at depths between 400 and 700 m at a site in central Sweden. The predicted maximum *in situ* stress was in agreement with estimates made using over-core measurements at shallower depths.

---

[4] This chapter has been published in the Proceedings of International Symposium on In-situ Rock Stress, *Trondheim*. Lu, M., Li, C.C., Kjorholt, H., Dahle, H. *editors*. A.A. Balkema, Rotterdam, pp. 159–166

A.2   INTRODUCTION

The Swedish Nuclear Fuel and Waste management Co. (SKB) is currently conducting extensive site investigations at Forsmark, Sweden, one of the candidate sites for construction of a nuclear waste repository. One of the parameters required for the design of the underground openings associated with the nuclear waste repository is the *in situ* stress magnitudes and orientations. The repository is currently planned for a depth between 400 and 700 m and hence the *in situ* stress magnitudes are required at these depths. Extensive stress measurements were conducted in the 1970s′ and 1980s′ in the Forsmark area to a maximum depth of 500 m for the construction of the nuclear Power Plants and the final repository for reactor waste, SFR. The SFR Facility includes a series of underground caverns and a 70 meter high underground silo that was constructed in the mid 1980s. This construction experience and the previous stress measurements indicated that the horizontal stress magnitudes at the Forsmark site were greater than the weight of the overburden which is common in the Scandanivain Shield at shallow depths.

The current stress measurement campaign began in 2003 and consisted of hydraulic fracturing in boreholes to depth of 1000 m and overcoring using the Borre Probe (Sjöberg and Klasson, 2003) to the target depth of a repository for spent fuel (500 m). Those campaigns have established the stress magnitudes and orientation to a depth a approximately 400 m. Below this depth the confidence in the *in situ* stress magnitudes is significantly reduced.

It is well known that extracting core samples at depth can lead to a significant increase in crack porosity (Chernis, 1984; Martin and Stimpson, 1994). This crack porosity can occur from two sources: (1) new stress-induced microcracks associated with the coring process, and (2) naturally closed pores that open when the *in situ* stress magnitudes are released. In all cases the increase in crack porosity will lead to an increase in nonlinear stress-strain behaviour in unconfined compression tests. Martin and Stimpson (1994) established that the amount of nonlinearity in the stress-strain curve was a function of the maximum principal stress. In this paper

a relationship between the crack closure energy measured in uniaxial compression tests and the *in situ* stress magnitudes is established for Lac du Bonnet granite. This relationship is then applied to the Forsmark site in Sweden to predict the maximum horizontal stress at depths between 400 and 700 m. The results from this methodology are compared to the results from hydraulic fracturing and overcoring.

A.3   CRACK CLOSURE ENERGY

In the stress-strain curve during the compression loading of the rock specimen, the specimen behaviour can be divided into four sections (Figure A.1), O-A: Non-linear microcrack and pore closure, A-B: Linear elastic behaviour, B-C: Stable fracture initiation and propagation, C-D: Unstable fracture propagation and strain hardening. In the stage O-A, the nonlinear behaviour is a function of the pore space in the sample. If there was no porosity the stress-strain response would only be a function
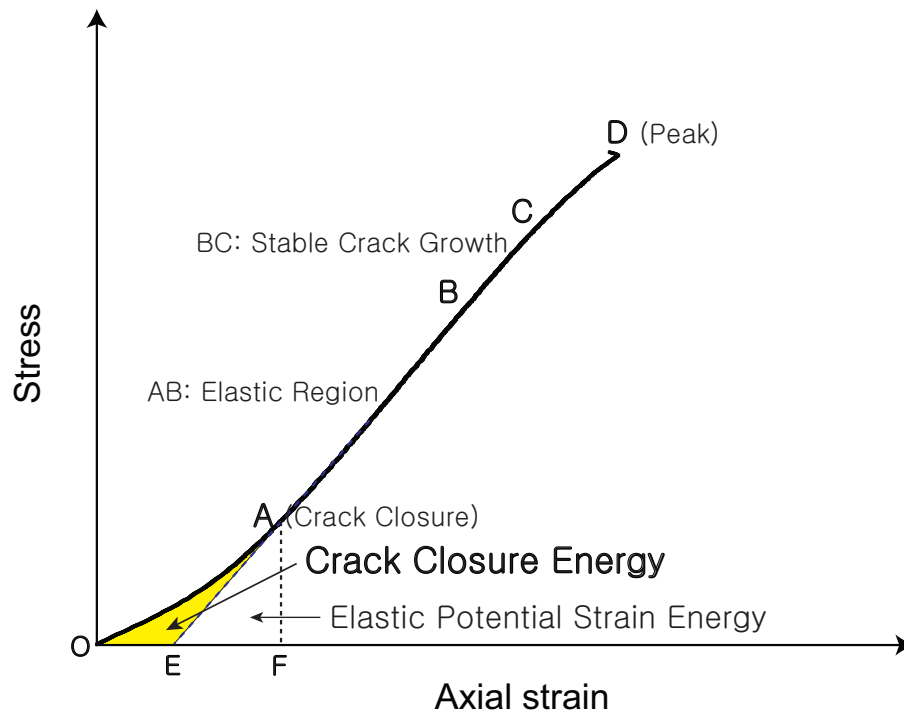
Figure A.1: Illustration of the axial stress-strain response of a uniaxial compression test for a sample of hard rock containing open pores. The crack closure energy is highlighted.

145

of the solid particles and their contact stiffness. In hard rocks this contact stiffness is essentially the same as the stiffness of the intact particles and hence the stress-strain response is linear. As the porosity increases, the stress-strain response is composed of two parts: (1) the stress-strain response of the volume of rock containing the pore and (2) the stress-strain response of solid rock volume. It is intuitive that as the volume of the porosity increases so should the nonlinearity of the stress-strain response.

The nonlinearity of the stress-strain response in compression is controlled not only by the volume of pores but also the shape of the pores (Figure A.2). In hard rocks natural pores tend to have polygonal shapes and these pores in Lac du Bonnet granite create a porosity of 0.04% for samples from the depth of 809 m (Chernis, 1984). Stress-induced microcracks tend to have long-parallel walls and in Lac du Bonnet granite can create an increase in porosity of 0.28%. Figure A.2, suggests that the amount of nonlinearity should be dominated by the stress-induced microcracks because of their shape. However, if there are no stress-induced microcracks the nonlinearity will be controlled by the natural porosity which in natural granites is very low (<0.1%, Schild et al. (2001)).

When samples are cored at various depths the stress redistribution that occurs around the coring bit creates a complex stress path that may or may not exceed the threshold for inducing new microcracks. Nonetheless, any closed natural pores will be unloaded and this stress release will increase the pore volume. The larger the amount of stress release the greater the potential for an increase in pore volume. There is a triggering point when stress-induced microcracking occurs. It is likely that the pore volume from this process would be so large that it would quickly mask the nonlinearity associated with the natural pore response. Hence when a sample is tested in the laboratory and nonlinear stress strain response is recorded, it is difficult to determine if the nonlinear response is due to natural pores or stress-induced microcracks. However, what can be determined is the stress magnitude required to close these pores. Based on this pore closure point, the crack closure energy can be defined.
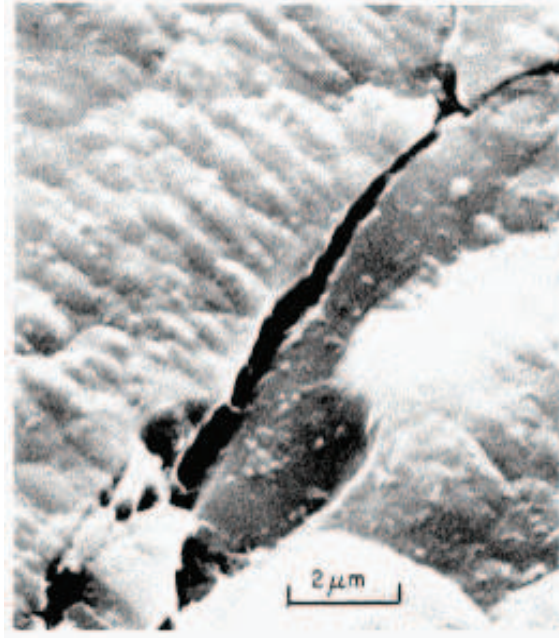
(a)

(b)

Figure A.2: Photos of pore structure in Lac du Bonnet granite, from Chernis (1984). (a) natural pore, (b) stress induced microcrack.

The potential strain energy stored in the material in case of principal stresses and strains is defined as (Saada, 1974):

$$U_t = \int_{q_0}^{q_1} Q dq \tag{A.1}$$

where, U_t is the total strain energy, Q and q are the generalized forces and displacements respectively. Based on Figure A.1, this equation can be rewritten as:

$$W_{t,A} = \int_0^F \sigma \varepsilon d\varepsilon \tag{A.2}$$

where, $W_{t,A}$ is the total potential strain energy stored in the rock specimen at the point A, σ is the applied stress and ε is the generated strain associated with the stress. And for the elastic behavior section:

$$W_{e,A} = \int_E^F \sigma \varepsilon d\varepsilon \tag{A.3}$$

For the nonlinear stress-strain behavior in Figure A.1, the associated energy can be divided into two parts: (1) elastic portion (EAF) called elastic strain potential energy and (2) anelastic portion (OAE). In Figure A.1, the linear portion A–B can be extended to the axial strain axis, and the area OAE defined as the crack closure energy, W_{cc}. The crack closure energy at point A can be calculated by subtracting the elastic potential strain energy from the total strain energy:

$$W_{cc} = W_{t,A} - W_{e,A} \tag{A.4}$$

The unit of the crack closure energy is the same as that of stress. Figure A.3 show the examples of the stress-strain curve and the magnitude of crack closure energy for the rock core samples of Lac du Bonnet granite taken from (a) ground surface, (b) 240-m Level and (c) 420-m Level of AECL′s Underground Research Laboratory respectively. The increasing trend of the crack closure energy is observed with

increasing depth.
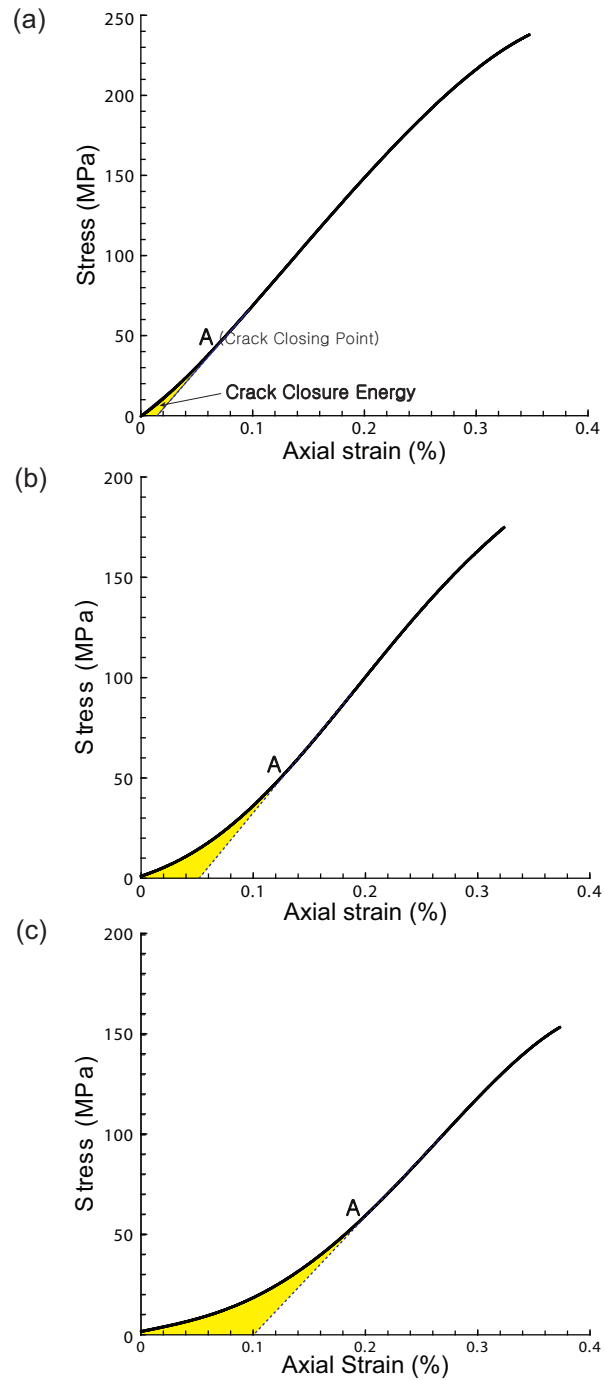
Figure A.3: Compression of the magnitude of crack closure energy for three rock core specimens from different depth: (a) ground surface, (b) 240-m Level and (c) 420-m Level, URL, Canada.

A.4 INFLUENCING FACTORS FOR THE MEASUREMENT OF CRACK CLOSURE ENERGY

To use the crack closure energy parameter for the evaluation of the *in situ* stress magnitude, the parameter should be independent of different test conditions such as testing machine, loading rate, measuring equipment, sample condition and the scale of the sample. If the test result can be affected by those conditions, a standard measuring procedure would also need to be developed. Four influence factors: (1) effect of sample condition, (2) effect of loading rate, (3) effect of measuring equipment and (4) effect of scale, were investigated. The results from the loading rate and scale effects are described below. The effects of the remaining influence factors are still under investigation.

A.4.1 *The influence of loading rate*

Hoek and Brown (1980) and more recently Jackson (1991) concluded that the uniaxial compressive strength of the intact rock cores increases with increasing loading rate. To determine if there is an influence of the loading rate on the crack closure energy, the magnitude of crack closure energy was measured and analyzed for four different loading rates using 24 rock core samples of Lac du Bonnet granite. These samples were the same samples used by Jackson (1991) to examine the effect of loading rate on the uniaxial compressive strength. Figure A.4 shows the influence of loading rate on the magnitude of crack closure energy. The axial strain increased as the loading rate increases from 0.00075 MPa/sec to 0.075 MPa/sec and little change occurred when the loading rate is higher than 0.075 MPa/sec. It can be concluded that the magnitude of crack closure energy can be influenced by the loading rate. But if the uniaxial compressive tests are carried out using the ISRM suggested loading rate of 0.5–1.0 MPa/sec, (Brown, 1981), the influence of loading rate on the crack closure energy is negligible.
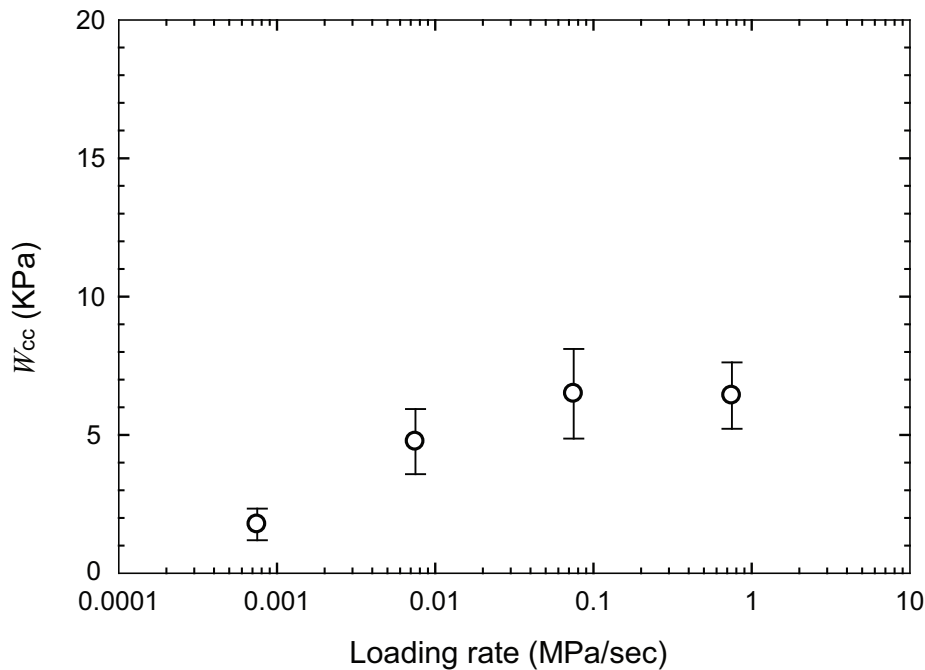
Figure A.4: The magnitude of crack closure energy as a function of loading rate.

A.4.2 *The effect of sample scale*

Hoek and Brown (1980) also insisted that the uniaxial compressive strength of rock cylinders decreases with increasing specimen size. Jackson (1991) also observed a similar trend for samples that varied from 33 mm to 294 mm diameter. A total 55 uniaxial compressive test data were analyzed by Jackson and these samples were re-analyzed to determine the effect of scale on the crack closure energy. Figure A.5 shows the magnitude of crack closure energy with increasing specimen diameter. From Figure A.5, there appears to be an effect of scale on the crack closure energy that is removed beyond a diameter of approximately 96 mm-diameters. There also appears to be little effect of scale for diameters between 33 mm and 63 mm. Thus, from this study crack closure energy induced damage is considered to be relatively consistent if the specimen size is between 33 mm and 63 mm and if the specimen size is greater than 100 mm diameter.
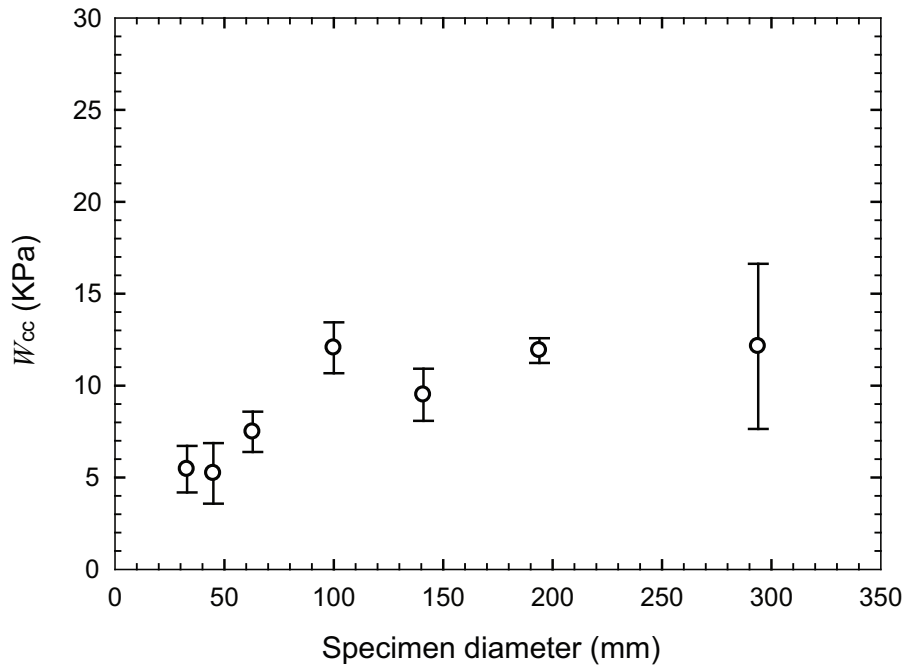
Figure A.5: The magnitude of crack closure energy as a function of loading rate.

A.4.3 *Summary*

Based on these studies it appear that providing the samples are tested at a loading rate between 0.5 and 1 MPa/sec and the diameters of the samples are between 33 mm and 63 mm, the magnitude of the crack closure energy should be relatively consistent. All of the specimens used for measuring the crack closure energy to evaluate the *in situ* stress magnitudes in the following section, had the range of diameters of 45 mm to 63 mm, hence it is unlikely that the results would be significantly affected by scale or loading rate effects. In addition all the samples were tested using the Suggested Methods of the ISRM (Brown, 1981; Fairhurst and Hudson, 1999).

A.5 *IN SITU* STRESS AND CRACK CLOSURE ENERGY

A.5.1 *Lac du Bonnet Granite*

The *in situ* stress at AECL′s Underground Research Laboratory (URL) was initially characterized using traditional triaxial overcoring, hydraulic fracturing and back analysis of convergence measurements (Martin, 1990). Large scale *in situ* experiment was later used to confirm and refine the variability in the *in situ* stress magnitudes to a depth of 420 m (Martin et al., 1997). More recently Thompson and Chandler (2004) reported the stress magnitudes at the URL to a depth of approximately 1000 m.

A series of uniaxial compression tests of Lac du Bonnet granite were analyzed to determine the crack closure energy. These samples are selected from different depths at the URL in the vicinity of the stress measurements. A total of 34 samples were analyzed. The crack closure energy as a function of depth is given in Figure A.6.
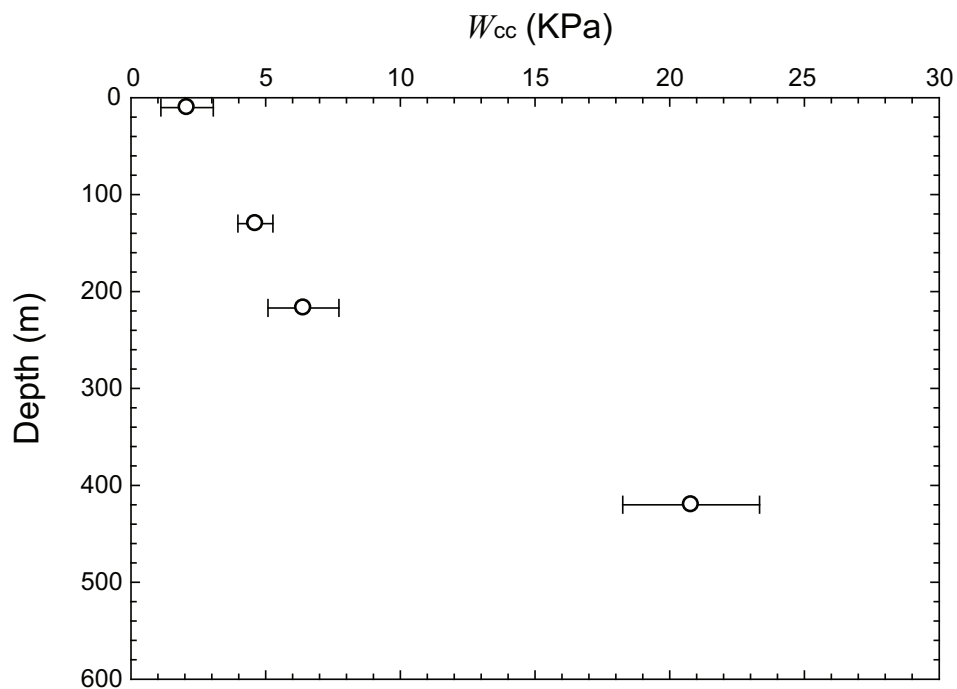
Figure A.6: Crack closure energy versus depth for Lac du Bonnet granite.
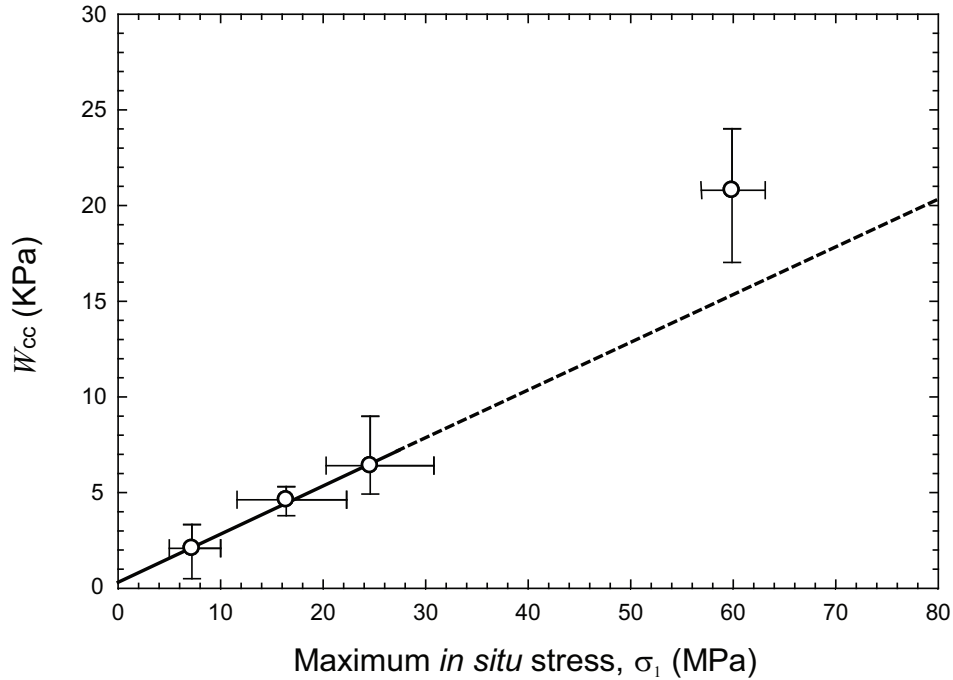
Figure A.7: Crack closure energy as a function of maximum *in situ* horizontal stress for Lac du Bonnet granite.

The mean value as well as the standard deviation is shown in Figure A.6. The correlation between the maximum *in situ* stress and crack closure energy is given in Figure A.7. The variability in the maximum *in situ* stress was determined using the approach given by Walker el al. (1990).

The solid line in Figure A.7 represents the best fit for the relationship between the crack closure energy when the maximum stress magnitudes are less than 25 MPa. Figure A.7 also shows the projected crack closure energy when the stress magnitude is 60 MPa. It is clear from Figure A.7, that the measured crack closure energy for a maximum *in situ* stress of 60 MPa exceeds the predicted crack closure energy. Martin and christiansson (1991) showed that when the maximum stress magnitudes approached 25 to 30 MPa, stress-induced microcracks were readily observed in overcore samples. Hence it appears that beyond 30 MPa the potential for stress-induced microcracks increases significantly. Everitt (2001) also noted that the stress-induced microcracks in cores obtained from the 420 Level of the

Table A.1: Comparison of laboratory geotechnical properties of Lac du Bonnet Granite (LdB) and Forsmark Granite.

Rock Type	σ_c (MPa)	σ_t (MPa)	γ (kg/cm^3)	E (GPa)	ν
LdB Granite	210	9.3	2.64	69	0.26
Forsmark Granite	225	13	2.75	76	0.24

URL (maximum horizontal stress 60 MPa) contained a significant number of stress induced microcracks. Hence it appears that below 30 MPa there is a linear relationship between *in situ* stress and crack closure energy and that this relationship does not hold when the maximum stress magnitude reaches 60 MPa. It can not be determined from Figure A.7 the stress magnitude at which the linear crack closure energy versus stress magnitude does not apply. What is clear from Figure A.7 is that once the stress magnitudes are sufficient to induce a large volume of stress-induced microcracks, it clearly exceeds the response established for the low stress magnitudes.

A.5.2 *Forsmark granite*

SKB has conducted an extensive site investigation at the Forsmark site located approximately 130 km North of Stockholm. The site investigation used 76-mm-diameter drill bits with triple tube for core samples. The nominal core has a diameter of 51 mm. The maximum drilled depth is 1000 m.

The Forsmark granite is similar in age to the Lac du Bonnet granite and the average uniaxial compressive strength is also similar. The average values of mechanical properties for Lac du Bonnet granite and Forsmark granite were compared in Table A.1.

Twenty four specimens of 51 mm diameter from two boreholes, KFM04A and KFM05A, were analyzed for crack closure energy. Figure A.8 shows the magnitude of crack closure energy with increasing depth for Forsmark site. From Figure A.6 and Figure A.8 it is observed that the magnitude of crack closure energy for Forsmark granite was much smaller than that of Lac du Bonnet granite. This implies

that the granite in Forsmark is stiffer and thus stores less potential strain energy than that of Lac du Bonnet granite.

Figure A.8 shows that the linear relationship between crack closure energy and depth is maintained to the depth of 700 m at Forsmark. The solid line shows the best fit and the error bars indicate the standard deviation. From the core observations it was found that the visible microcracks did not occur in the samples until depths are greater than 850 m. Thus, it is possible that the linear relationship between crack closure energy and maximum *in situ* stress magnitude observed at the URL could be applied to the Forsmark site to a depth of 850 m.

A.6   FORSMARK *IN SITU* STRESS ESTIMATION

The geology of the Forsmark site is given in the Site Descriptive model in (SKB, 2005) and simplified in Figure A.9. The granite is located in the nose of a fold and bounded on the north and south by major subvertical deformation zones. At Fors-

Figure A.8: Crack closure energy versus depth for Forsmark, Sweden. The error bars refer to the standard deviation from the mean.

156
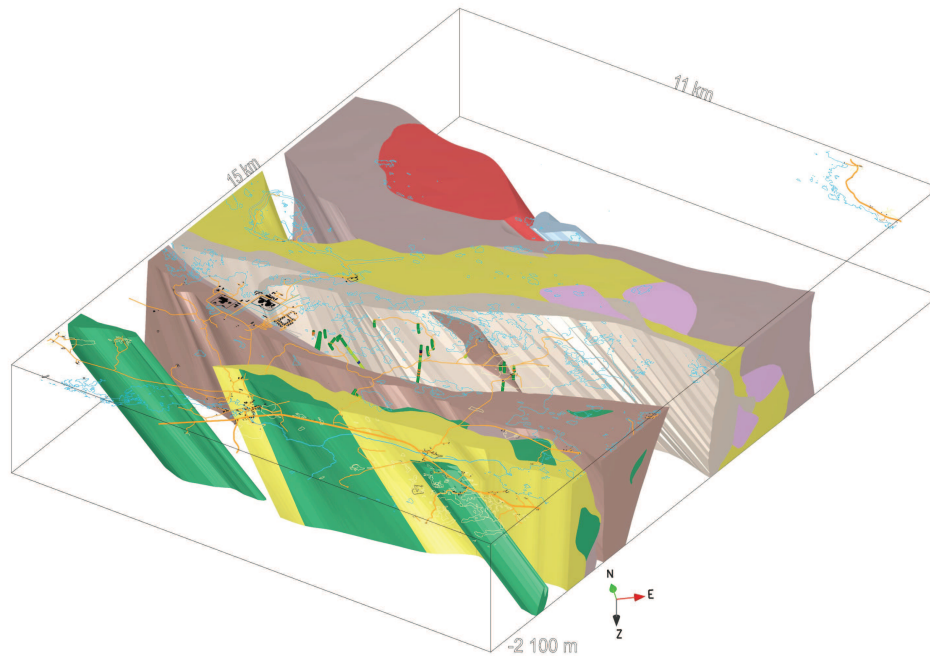
Figure A.9: Geology model for the Forsmark site The granite is removed from the centre of the block model. Surrounding rocks are gneiss and mafic rocks.

mark two major fracture domains have been identified. Fracture domain FFM02 can be classed as a blocky rock that extends to a depth of approximately 300 m. Below this depth the open fracture frequency decreases and rock mass quality improves. This domain FFM01 is considered similar to the rock mass conditions at the URL. To estimate the increase in *in situ* stress magnitudes with depth at the Forsmark site using the crack closure energy measurement method, the state of stress must be known at one location. The stress magnitudes at Fosmark have been measured in 76-mm-diamter boreholes drilled from the ground surface using hydraulic fracturing and overcore methods. The overcore method was successful in fracture domain FFM02, but below a depth of 300 m, ring disking was commonly observed and hydraulic fracturing only provided the weight of the overburden. Eight successful *in situ* stress overcore measurements obtained from three different depths were used to establish the correlation between *in situ* stress magnitude and crack closure

157
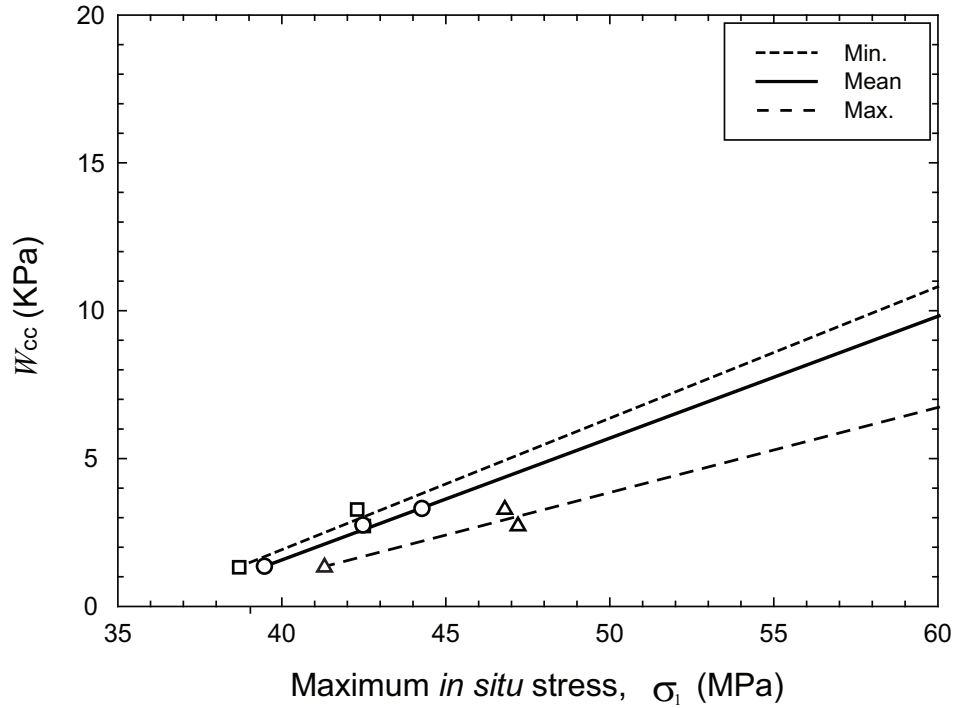
Figure A.10: The relationship between crack closure energy and maximum *in situ* stress for Forsmark site

energy. Figure A.10 shows the mean, the maximum and the minimum values of the maximum *in situ* stress calculated based on confidence stress measurement (Walker el al., 1990) and the magnitude of average crack closure energy was measured at the same depth.

From the relationship between crack closure energy versus depth in Figure A.8 and the maximum *in situ* stress versus the magnitude of crack closure energy in Figure A.10, the maximum *in situ* stress was estimated for the potential repository depth between 400 and 700 m. Figure A.11 shows the estimated maximum *in situ* stress to the depth of 850 m where it is expected that microcracking will reduce the confidence in the predicted magnitude.
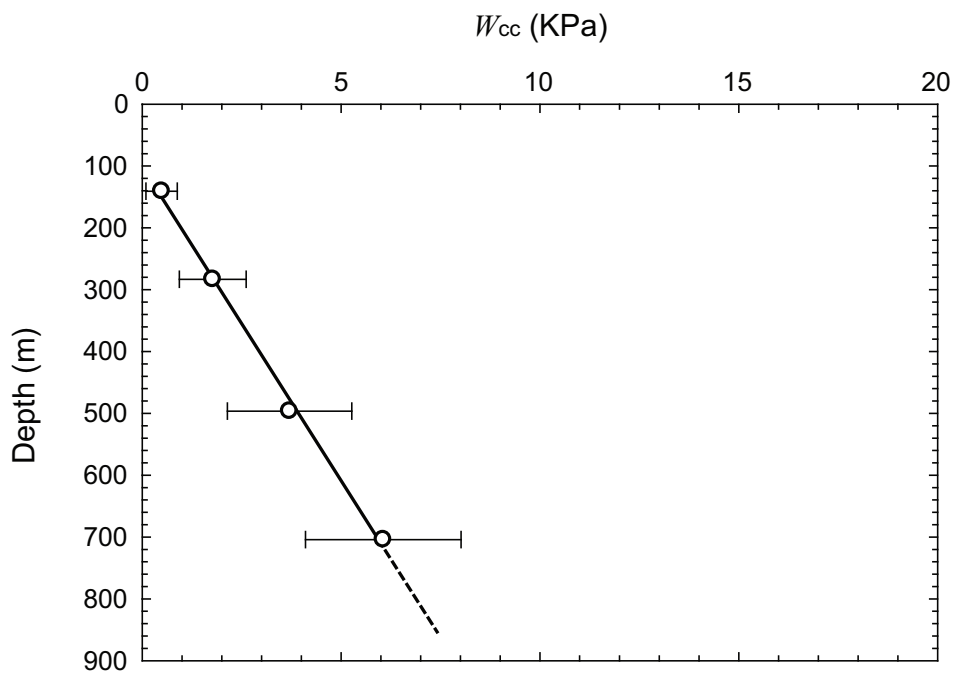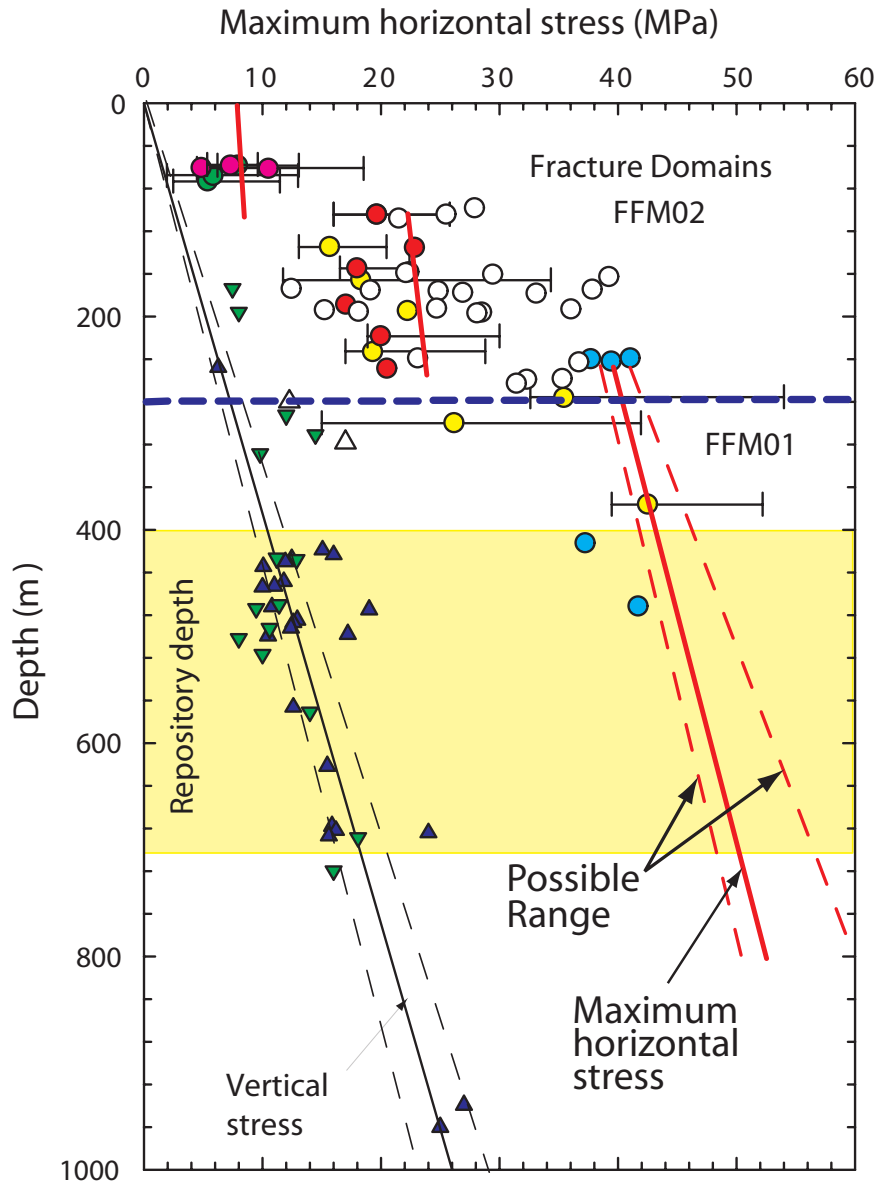
Figure A.11: Crack closure energy versus depth for Forsmark, Sweden. The error bars refer to the standard deviation from the mean.

A.7   CONCLUSION

When both horizontal stress magnitudes exceed the weight of the overburden, e.g., in a geological thrust environment, traditional stress measurement techniques such as hydraulic fracturing and overcoring often do not provide reliable stress mag-

nitudes at depth. For such situations additional information from indirect measurements and observations may be needed to constrain the stress magnitudes. In this study, the crack closure energy has been introduced as an indirect measurement linking energy to stress magnitudes. The methodology uses the crack closure energy obtained from standard uniaxial compressive strength tests correlated with stress magnitudes. Once the correlation is established a linear projection can be carried out for those depths where stress magnitudes cannot be obtained using the traditional methods. The methodology breaks down when the stress magnitudes are so large that stress-induced microcracks significantly influences the crack-closure energy. The methodology was used to predict the maximum stress magnitudes at the Forsmark site at depths between 400 and 700 m and appears to provide reasonable results. Work is ongoing to evaluate this methodology.

Bibliography

Brown, E.T. 1981. *Rock characterization testing and monitoring*. International Society for Rock Mechanics–the Commission on Testing Methods, Pergamon.

Chernis, P.J. 1984. Comparison of the pore-microstructure of shallow and deep samples of the Lac du Bonnet granite. *Technical Record 223*, Atomic Energy of Canada Limited, Onterio.

Everitt, R.A. 2001. *The influence of rock fabric on excavation damage in the Lac du Bonnet granite*. Ph.D. thesis, Department of Civil & Geological Engineering, University of Manitoba, Winnipeg, Manitoba, Canada.

Fairhurst, C.E., Hudson, J.A. 1999. Draft ISRM suggested method for the complete stress-strain curve for intact rock in uniaxial compression. *J. Basic Engng.* 85: 519–527.

Hoek, E., Brown, E.T. 1981. *Underground Excavation in Rock*. The institution of mining and metallurgy, London.

CANMET, 1990. Scale effects testing on rock samples from Lac du Bonnet. Manitoba. *Division Report MRL 90–058(TR)*, CANMET, Energy, Mines and Resources Canada.

CANMET, 1991. The effect of loading rate on the uniaxial mechanical properties of Lac du Bonnet granite. Manitoba. *Division Report MRL 90–058(TR)*, CANMET, Energy, Mines and Resources Canada.

Martin, C.D. 1990. Characterizing in situ stress domains at the AECL Underground Research Laboratory. *Can. Geotech. J.* 27: 631–646.

Martin, C.D., Christiansson, R. 1991. Overcoring in highly stressed granite – The influence of microcracking. *Int. J. Rock Mech. Min. Sci.* 28(1): 53-70.

Martin, C.D., Read, R.S., Martino, J.B. 1997. Observations of brittle failure around a circular test tunnel. *Int. J. Rock Mech. Min. Sci.* 34(7):1065–1073.

Martin, C.D., Stimpson, B. 1994. The effect of sample disturbance on laboratory properties of Lac du Bonnet granite. *Can. Geotech. J.* 31(5): 692–702.

Saada, A.S. 1974. *Elasticity: theory and applications*. Pergamon press, Inc.

Schild, M., Siegesmund, S., Vollbrecht, A., Mazurek, M. 2001. Characterization of granite matrix porosity and pore-space geometry by in situ and laboratory methods. *Mech. and Mining Sci.* 40: 1205–1224.

Sjöberg, J., Klasson, H. 2003. Stress measurements in deep boreholes using the Borre (SSPB) probe. *Int. J. Rock Mech. Min. Sci.* 40(8): 1205–1223.

SKB, 2005. Preliminary site description Forsmark area – version 1.2. *SKB R-05-18*, Swedish Nuclear Fuel and Waste Management Co., Stockholm.

Thompson, P.M., Chandler, N.A. 2004. In situ rock stress determinations in deep boreholes at the Underground Research Laboratory. *Int. J. Rock Mech. Min. Sci.* 41(8): 1305–1316.

Walker, J.R., Martin, C.D., Dzik, E.J. 2004. Confidence intervals for in situ stress measurement. *Int. J. Rock Mech. Min. Sci.* 27(2): 139–141.

Appendix B

Estimating *in situ* stress magnitudes from core disking [5]

B.1   ABSTRACT

It is well known that elevated stress magnitudes will cause core disking during drilling. During recent site investigation drilling at Forsmark, Sweden, to depths of 1000 m localized core disking was encountered. The disking was observed in short (<1-m long) sections of solid core, and as ring-disking in overcore cylinders. Three dimensional elastic numerical analyses were carried out to estimate the stress magnitudes required to initiates both ring- and solid-core disking. Three-dimensional fracture mechanics approach was used to investigate the relationship between disk thickness and disk shape as a function of stress magnitudes. A series of analyses were also carried out to determine the relationship between tensile strength and horizontal stress magnitudes. The results indicate that core disking can be used to constrain the stress magnitudes but that the tensile strength can have a significant impact on the stress magnitudes determined from core disking.

B.2 INTRODUCTION

The estimation of *in situ* stress is essential in the design of deep underground excavations. Various methods have been developed to investigate the far-field state of stress, with hydraulic fracturing (Haimson and Fairhurst, 1967) and overcoring (Leeman and Hayes, 1966) being the most widely used methods. Over the past 20 years the technology for both of these methods has advanced such that both methods can be used in small diameter boreholes to depth exceeding 500 m.

Both of these methods assume that the rock behaves as a linear elastic continuous homogeneous material. In many geological environments this assumption is violated and in a thrust fault environment where the minimum principal stress is the vertical stress, hydraulic fracturing can only provide, with confidence, the weight of the overburden. In addition, once the stress magnitudes exceed a critical value core disking is frequently observed when over coring is attempted. Hence, there are certain stress states where the measurement of *in situ* stress becomes very difficult. In such situations, it is important to make use of additional information that may be used to constrain the stress magnitudes and directions.

Core disking is a phenomenon in which the drilled core disks with uniform spacing and shape due to the transient stress changes, and stress release during drilling (Figure B.1). The investigation of the core disking mechanism and its application to estimate the far-field stress state was started in 1963 by Jaeger and Cook (1963). Jaeger and Cook (1963) discovered an inverse relationship between the applied principal stress and disk thickness through laboratory experiments conducted with cylinderical cores. Obert and Stephenson (1965) suggested a criterion which provides the threshold of axial and lateral stress for inducing core disking by biaxial loading for various rock types. Most recently, Haimson and Lee (1995) developed a set of testing equipment which can apply stresses triaxialy and showed the correlation between applied stress and disk thickness with limited applied stress combination.

A variety of numerical modeling has also been completed to investigate the core
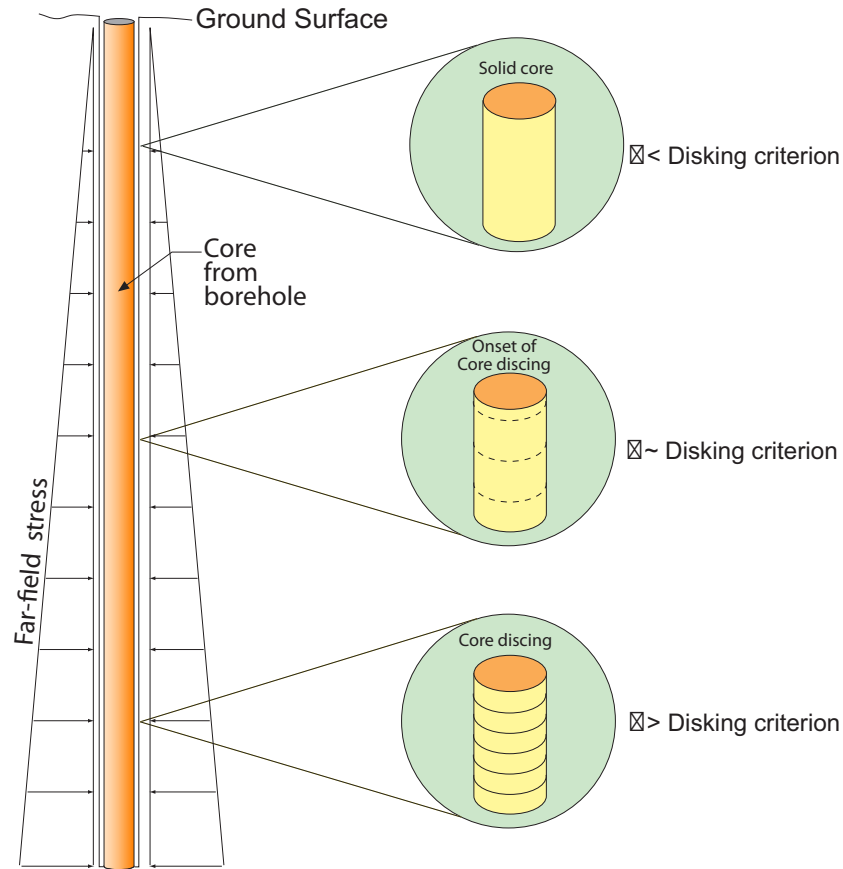
Figure B.1: Core disking as a function of *in situ* stress magnitudes, i.e., borehole depth.

disking phenomena. The results of numerical analysis have been used to develop interpretation techniques. Finite element modeling was carried out by Sugawara et al. (1978) and Stacey (1982) suggesting a tensile failure mechanism and an extension strain theory respectively. Dyke (1989) calculated the stress and extension strain path using a three dimensional elastic boundary element analysis and concluded that tensile stresses were the dominant cause of core disking. Extensive finite element analyses have been conducted by Li (1997) and Kaga et al. (2003). Li (1997) considered rock properties, cutting geometries, drilling pressure, fluid pressure, and core stub length to be important factors that influence the stress concentrations in the bottom of the wellbore. Kaga et al. (2003) suggested that core disking could be predicted using a principal tensile stress failure criterion.

Despite the advances in our understanding of the core disking process, core disking is still only used as an indicator of stress magnitudes, i.e., when disking occurs stress magnitudes are considered to be large. In this study a fracture mechanics approach was used to establish relationships between the thickness of core disk and stress magnitudes.

B.3   OBSERVATIONS AT FORSMARK, SWEDEN

During recent site investigation drilling at Forsmark, Sweden, to depths of 1000 m localized core disking was encountered. The disking was observed in short ($<$1-m long) sections of solid 50-mm-diameter core, and as ring-disking in 62-mm-diameter overcore cylinders. During the overcoring process, the core obtained from drilling the 36-mm-diameter pilot hole was retrieved as solid core with no visible evidence of damage. However, during the drilling of the overcore cylinder, ring disking was sometimes observed (Figure B.2).

At Forsmark, overcoring using the Borre probe (Sjöberg and Klasson, 2003) has

Figure B.2: Core disking in overcored sample at a depth of 255 m in Forsmark site investigation borehole.

been carried out at depths between 239 and 473 m. The results have been compiled for two measuring levels; level 1, 239 to 242 m and level 2, 413 to 473 m. The results from these tests indicate high horizontal stress magnitudes. For level 1, a reasonable estimate of stress magnitudes and orientations was obtained through three successful measurements. The average stress indicates a major sub-horizontal principal stress magnitude of around 40 MPa.

For Level 2, ring-core disking was observed for almost all tests. Out of 11 attempts for testing only two were successful. Those tests were located in the vicinity of sparsely fractured rock. Figure B.3 shows the estimated range of the vertical, and maximum horizontal and minimum horizontal stress. The focus of this study was to determine if the core disking information could be used to further constrain the stress magnitudes.

B.4 CORE DISKING BACKGROUND

B.4.1 *Failure mechanisms*

To estimate relationships between *in situ* stress magnitudes and core disking, it is essential to understand the failure mechanism leading to core disking and to establish a disking criterion. Figure B.4 shows that core disking is not influenced by the diameter of the core. Hence a core disking criterion should be independent of core diameter for cores larger than 75 mm diameter. At smaller core diameters a scale dependence is expected.

Jaeger and Cook (1963) reported that the average applied stresses required to initiate core disking are less than uniaxial compressive strength of the material. It was also suggested that core disking resulted from a tensile failure mechanism due to the observation of clean, unsheared failure surfaces. Obert and Stephenson (1965) concluded that the fractured disks are created by either tension or shear stresses and noted that the initiation point could be the surface of the core stub or the centre of the core axis. According to the experimental results, Obert and Stephenson (1965) suggested that the horizontal stress must be greater than one-half of the unconfined
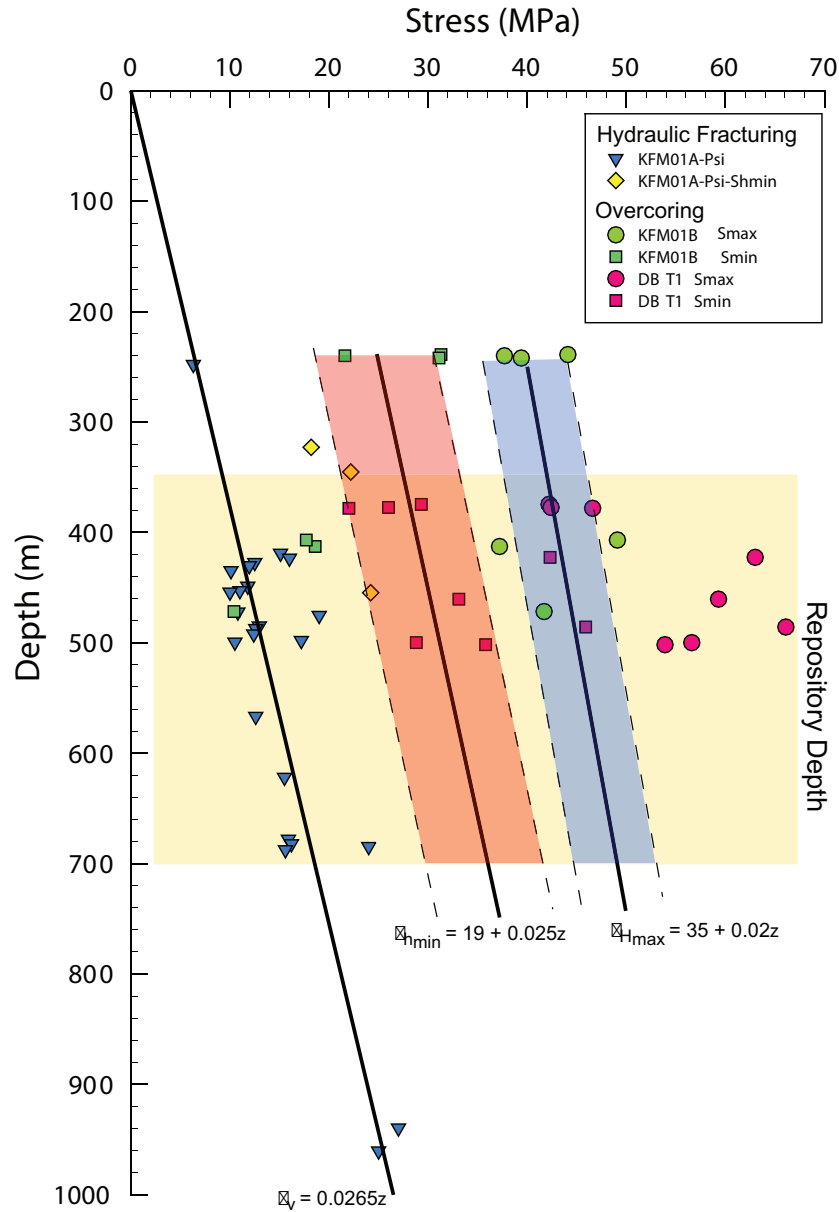
Figure B.3: Suggested stress profiles for Forsmark based on overcore and hydraulic fracturing measurements (SKB, 2005).

compressive strength of the rock.

Durelli et al. (1968) showed that core disking initiates near the bottom of the bore-hole by the concentrated maximum shear stress and this shear stress must be higher than the shear strength of the rock. Stacey (1982) suggested an extensional strain
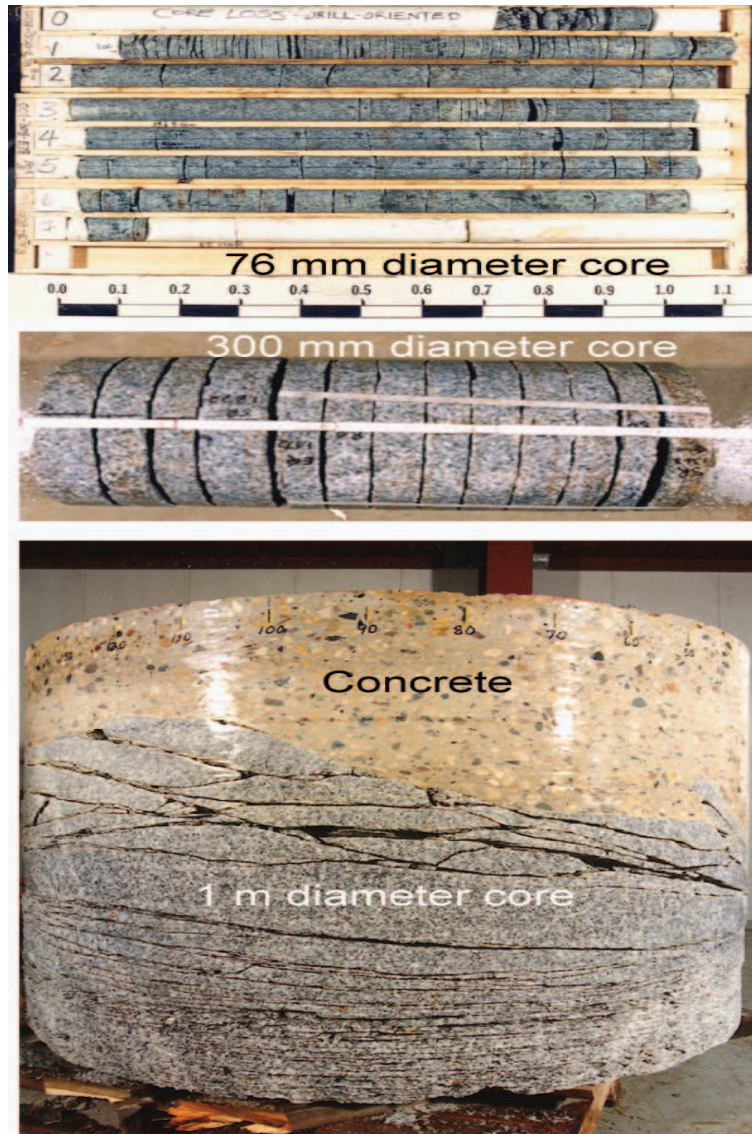
Figure B.4: Examples of core disking at various scales. All core drilled from the 420 Level of AECL′s Underground Research Laboratory, $\sigma_1 = 59$, $\sigma_2 = 45$, $\sigma_3 = 11$ MPa.

failure criterion with an observation that the maximum extension strain moves from the centre of the core to the outer boundary, just below the core, with increasing core stub length. It was also reported that failure was initiated when the extension strain was greater than the critical value. Dyke (1989); Li (1997); Matsuki et al. (2004) carried out extensive numerical analysis and suggested a tensile failure mechanism and explained that the failure is likely to be initiated at the core surface or interior of

169

the core or both simultaneously. And all three studies concluded that the initiation point varies depending on the applied principal stress conditions.

B.4.2 *Interpretation of disk thickness and shapes*

If core disking occurs, the spacing and the shape of the disk could be an indicator of the *in situ* stress state. Jaeger and Cook (1963) first suggested that the ratio of the thickness to the diameter of the disk decreased as the stress increased and that the disk shape was slightly concave. This concaved disk shape was also observed by Obert and Stephenson (1965) and Stacey (1982) who concluded that the disking phenomenon would not provide a reliable estimation of the absolute stress magnitude. Maury et al. (1988) concluded from the review of previous experimental work by Massieu and Durville, that saddle shaped disks were produced by biaxial horizontal stress condition. They suggested that the low points in the disk indicated the direction of maximum horizontal stress. The shapes of disk and their relationship with horizontal stress condition were suggested through numerical analysis by Dyke (1989) and Li (1997), and by experimental laboratory results by Haimson and Lee (1995). Recently Kaga et al. (2003) and Matsuki et al. (2004) proposed the stress criteria which can be applied to any disk length and shapes based on a tensile principal stress criterion.

B.4.3 *Summary*

While there is general agreement that core disking is observed when the stress magnitudes are elevated, there are no guidelines that can be used to estimate the stress magnitudes from core disking. It is also unclear if the stress state that produces core disking is unique. In the following sections numerical analyses are used to simulate core disking.

B.5 *STRESS PATH DURING PILOT HOLE AND OVER-CORE DRILLING*

The overcoring system at Forsmark used a 76-mm hole diameter with a pilot hole diameter of 36 mm. Overcoring equipment includes a conventional Craelius T2-76 core barrel and coring bit, producing a nominal core diameter of 61.7 mm (Figure B.5). The latter is a requirement for being able to fit overcored samples into the biaxial test cell. In the numerical model described below the bit had a flat bottom with slightly rounded edges (Figure B.5). This geometry was based on the bit designed and also reduced the potential to cause unrealistic stress concentrations in the numerical model.

As already mentioned, most of the core disking at Forsmark occurred as ring-disking, i.e, the disking occurred during the drilling of the overcore and not during the drilling of the pilot hole. A series of three dimensional elastic analyses were carried out to examine the stress path experienced by the rock during (1) the drilling of the normal core and (2) during the drilling of the overcore. The analyses were carried out using the boundary element program Examine3D. For all the analyses discussed in this paper the following material properties were used: Young′s modulus of 60 GPa, Poisson′s ratio of 0.25, Brazilian tensile strength of 14.8 MPa, Direct tensile strength of 10 MPa. Mode I fracture toughness of 3.8 $MPa.m^{1/2}$ and a density of 2.6 $tonnes/m^3$. These rock properties have been obtained by laboratory testing of the granodiorite, the dominant rock type at a depth of 500m in the Fosmark area. Based on Figure B.3, it is assumed that the minimum principal stress is the same as overburden stress and acts parallel to the borehole axis. The applied principal stress for these analyses was 10 MPa for the vertical stress. And the applied uniaxial horizontal stress to estimate the stress path was 40 MPa.

Figure B.5 shows the three monitoring lines chosen to trace the stress path as the drilling advanced. Line O, M and C were located outside, midway and center of the solid core stub respectably and Line E, B and N represent the edge, midway and inside of overcore stub, respectively. The reference lines were located relative to
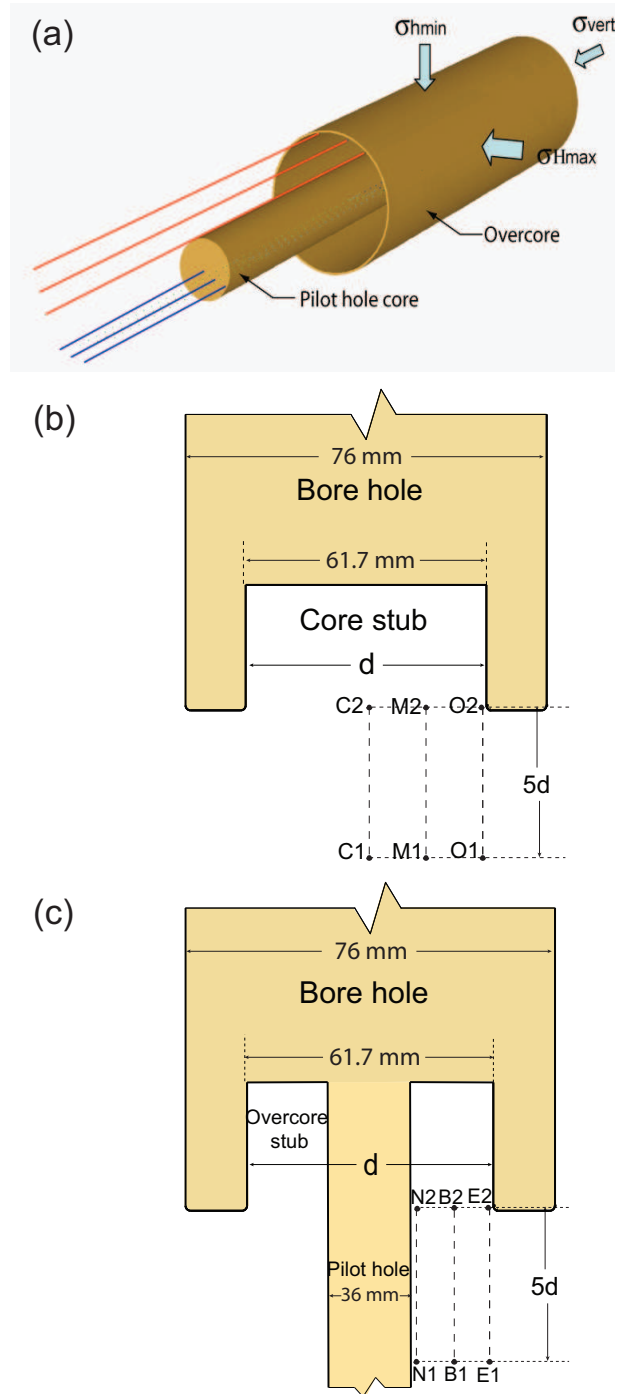
Figure B.5: Model geometry and reference points used in the stress path analyses. (a) Overall geometry and reference lines, the dimension and reference points for (b) coring and (c) overcoring.

the core diameter. The reference lines start 5 times the core diameter (5d) ahead of the 76-mm hole bottom. For the overcore example, the stress path is only shown after the pilot has been drilled.

Figure B.6 shows the results from these analyses. Also plotted on Figure B.6 is the tensile strength based on direct tension and the onset of damage initiation based on the results from uniaxial and triaxial compressive strength results. Figure B.6a shows that the all the stresses are compressive stresses in the core, far from the bit. However, stresses at lines M and O which start compressive become tensile in the vicinity of bit but that these tensile stresses only occur locally and do not extend into the centre of the core, i.e., the stresses in the center of the core (line C) remain compressive. Figure B.6b shows the stress path for overcoring process. At the end of the pilot hole drilling the stresses next to the pilot hole are already tensile, while the stresses at lines B and E remain compressive. As overcoring advances, all the stresse at lines E, B and N become tensile and eventually exceed the 10 MPa tensile strength of the rock. Comparing the stress paths for the solid core and the overcore, it is clear that the overcoring process causes tensile stresses throughout the overcore sample and hence will be more prone to disking than the solid core, resulting in ring disks. This is also in keeping with the observations at Forsmark. In these analyses the ratio k of the maximum to minimum horizontal stress was one. Additional analyses were carried out for $k>1$ and similar stress path results were observed. Hence for many stress states, ring-disking will be observed before disking of solid core is observed.

In the solid core Figure B.6a, the tensile stresses initiate at the edge of the core bit and it is assumed that disking would also initiate at this location. However, it must be realized that the magnitude of tensile stresses is a function of the bit geometry and therefore it is important that geometry in the numerical model accurately replicate the geometry of the hole produced by the coring bit. During overcoring, the tensile stress was initially generated in the inside of overcore near the pilot hole. So the failure may start from the interior of overcore which is already damaged by pilot hole drilling and propagate across the overcore as drilling advances. In all

173
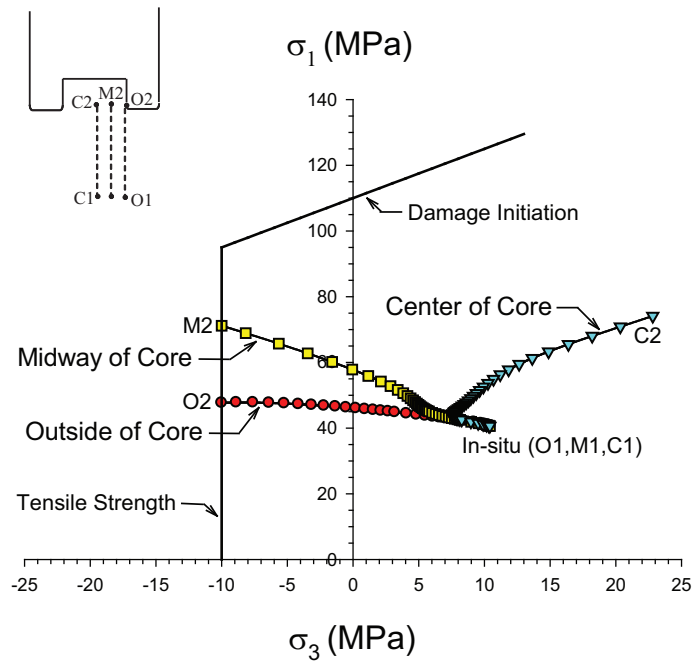
(a) Stress path for solid core.
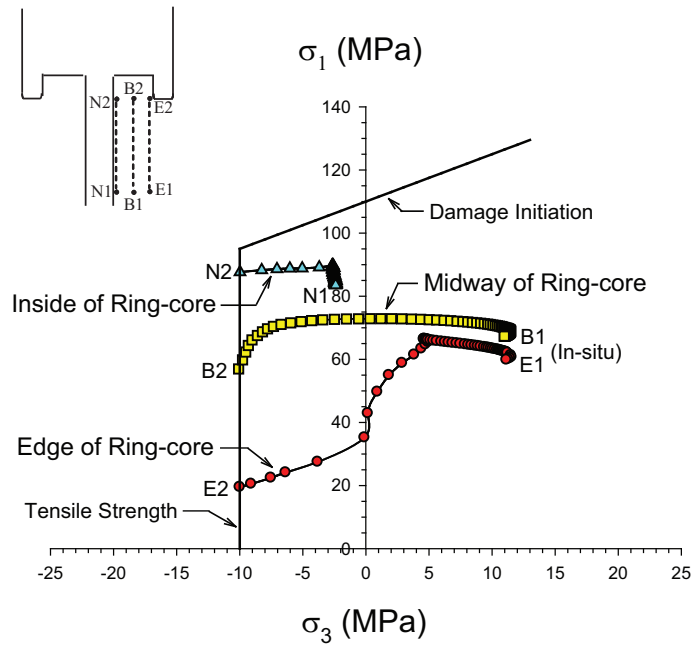
(b) Stress path for overcore.

Figure B.6: Stress path for solid core and the overcore. Notice that in the overcore sample tensile stress are experienced by the entire wall of the overcore sample. While the tensile stresses for the solid core are localized.

174

these analyses no attempt is made to simulate the growth of the fracture. In the next section this aspect is investigated.

B.6 FRACTURE MECHANICS APPROACH

FRANC3D is a Fracture Analysis Code for simulating an arbitrary non-planar three dimensional crack growth (CFG, 2003). It combines real geometry and topology with automated local meshing in the vicinity of crack propagation. FRANC3D utilizes linear elastic fracture mechanics to determine the fracture growth and its direction. In FRANC3D the fracture has a finite width while traditionally in linear elastic fracture mechanics, the fracture has zero width. This finite width is important in core disking because as the disk fracture forms the fracture induces dilation which can contribute to fracture growth. In the FRANC3D, mode I and mode II Stress Intensity Factors (SIF) are calculated based on a displacement correlations technique; so called Displacement Extrapolation Technique (DET) (Lim et al., 1992). SIF is estimated by extrapolating the nodal displacements along the crack face. The expression is given as,

$$K_I = \lim_{r^{*i} \to 0} K_I^{*i} \tag{B.1}$$

$$K_{\mathrm{II}} = \lim_{r^{*i} \to 0} K_{\mathrm{II}}^{*i} \tag{B.2}$$

and,

$$K_I^{*i} = \frac{G}{k+1} \sqrt{\frac{2\pi}{r^{*i}}} v'\left(r^{*i}\right) \tag{B.3}$$

$$K_{\mathrm{II}}^{*i} = \frac{G}{k+1} \sqrt{\frac{2\pi}{r^{*i}}} u'\left(r^{*i}\right) \tag{B.4}$$

where,

K_I^{*i} = Mode I SIF computed from ith nodal pair along crack face

K_{II}^{*i} = Mode II SIF computed from ith nodal pair along crack face

r^{*i} = distance between ith node and the crack tip

G = shear modulus

k = material constant: $k = 3 - 4\nu$ for plane strain, $k = (3 - 4\nu)/(1 + \nu)$ for plane stress

ν = Poisson's ratio

v', u' = local displacement along and normal to crack axis

The initial fracture propagates when the calculated Mode I SIF at the fracture tip is higher than the critical SIF of the rock. The propagation direction of the fracture is evaluated by using either the maximum tangential stress theory, the maximum strain energy release rate or the minimum strain energy density. In this study the direction of the fracture extension is determined by the maximum tangential stress theory (Erdogan and Sih, 1963). Thus, the fracture propagates in the direction parallel to the maxmum tangential stress at the fracture tip. The maximum amount of extension is controlled by the user and the extension along the entire fracture front is determined based on the relative values of SIF along the fracture front. So the new fracture front is determined by combination of the direction and the amount of propagation at points along the existing fracture front.

B.6.1 *Disk Thickness*

It is generally observed that the thickness of the core disks is related to the stress magnitudes. For example core drilled from the surface of underground openings will have the thinnest disks near the collar of the hole where the tangential stresses are the greatest. The thickness of the disks will increase away from the hole collar as the stress magnitudes decrease.

A series of analyses were carried out to determine the effect of stress magnitudes on the thickness of the core disks assuming the solid core drilling conditions shown in Figure B.5b. For these analyses the magnitude of vertical stress (σ_v) was assumed to be 10 MPa, i.e., equivalent to an overburden thickness of about 500 m and the maximum horizontal stress is equal to the minimum horizontal stress. Both the Brazilian and direct tension tensile strength values were used as the critical stress values causing core disk, and core disking was assumed to occur when the tensile

176

stress magnitudes across 2/3 of the core cross sectional area exceeded the tensile strength values.

Figure B.7 shows the results from these analyses and indicates that in order to create thin disks the horizontal stress magnitudes must be high. This is in keeping with observations made when drilling from underground openings. From Figure B.7 when the t/d>0.4 (t>25mm) the effect of the magnitude of the horizontal stresses is significantly reduced. However, the authors experiences suggest that most core disking in crystalline rocks shows disk thickness <25 mm. Hence the *K* ratio for t/d = 0.4 may indicate an approximate lower limit for solid core disking.

According to Figure B.7, it is difficult to determine the exact stress values from the core disk thickness only because a small change of disk thickness causes a large change of stress in the very high stress zone (region A in Figure B.7) and yet there is little change in the horizontal stress magnitude despite the large change in disk
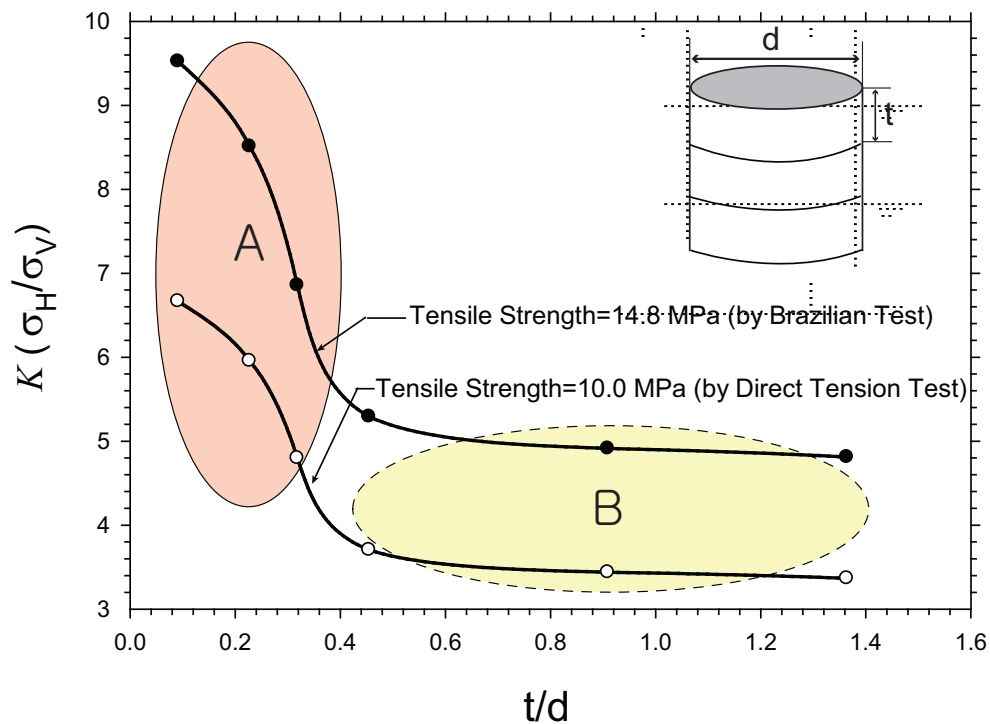

Figure B.7: Relationship between the ratio of core disk thickness t to the core diameter d and *K* (ratio of horizontal stress ($\sigma_H = \sigma_h$) to vertical stress (σ_v)). For these analyses d = 61.7 mm.

thickness in region B in Figure B.7. Figure B.7 suggests that when the thickness of core disk is 1.3 times the core diameter disking or partial disking will not occur. These findings are similar to those reported by (Li, 1997). Li (1997) concluded that if tensile stress causes core disking, the disks would occur at a spacing of no more than 0.25 the core diameter. Maury et al. (1988) suggested that the thickness of core disks could average 9 cm but the partial disk was not considered in this average. The effect of $k1$ will obviously affect these results and will be investigated in additional work.

B.6.2 *Disk Shape*

The shape of the core disk may be non-uniform. For some stress states the disk surface is flat while for other stress states researchers have reported saddle shapes (Maury et al., 1988). To investigate the effect of the anisotropy of horizontal stress magnitudes on the core disk shapes, a series of solid core analyses were carried out using FRANC3D. The initial fracture was made in the circumference of the core stub where the maximum tensile stress occurred. The disk fracture begins to propagate when the stress intensity factor in the initial fracture tip around the core is higher than the Mode I fracture toughness. The fracture propagates until the stress intensity factors at all fracture tips are reduced below the fracture toughness of the rock.

Figure B.8a shows a flat shape fracture when the horizontal stresses are equal. Figure 8b shows the saddle shape of core disk when the maximum horizontal stress exceeds the minimum horizontal stress by factor of 2. The low point in Figure B.8b indicates the direction of the maximum horizontal stress. It is clear from Figure B.8 that the shape of the disk surface can be used to constrain the horizontal stress anisotropy.

B.7   ESTIMATION OF *IN SITU* STRESS

The results reported in this paper show that both the thickness and shape of the core disks can be used to constrain the stress magnitudes. A series of stress analyses

(a) (σ_v =10MPa, σ_h =50MPa and σ_H=50MPa)
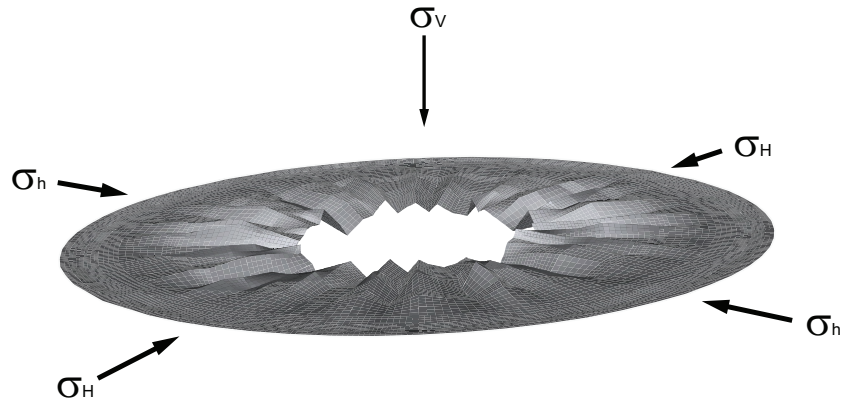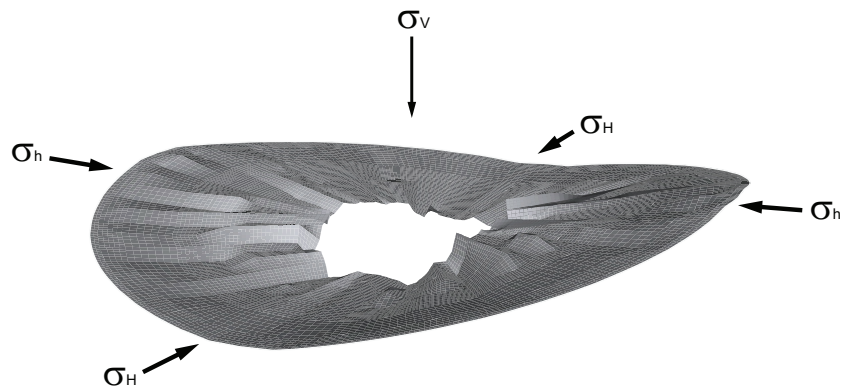
(b) (σ_v =10MPa, σ_h =30MPa and σ_H=60MPa)

Figure B.8: Shape of the disk surface for two horizontal stress ratios. The saddle shape becomes more pronounced as the stress ratio increases.

were carried out using Franc3D to develop a relationship between tensile stress and horizontal stress magnitudes. For all analyses the vertical stress is 10 MPa. The magnitude of tensile stress considered sufficient to cause core disking was defined as the maximum tensile stress generated in the entire core stub surface. If this tensile stress is higher than the tensile strength of the rock, the core is assumed to disk. Figure B.9 shows the variation of maximum tensile stress at the core stub surface with various combinations of horizontal stresses. The tensile stress required to initiate disking increases as the horizontal stresses increase. However, the increasing rate of tensile stress depends more on the ratio between horizontal stresses (σ_H/σ_h) than the absolute magnitude of mean horizontal stress.
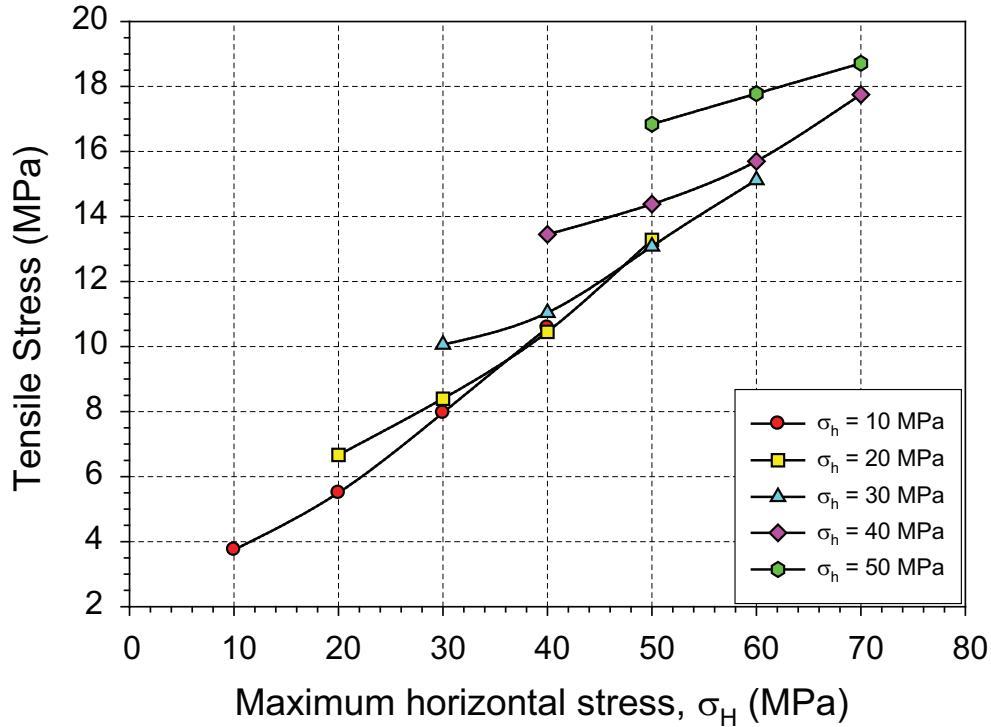
179

Figure B.9: Limits for core disking in terms of tensile stress and horizontal stress.

Figure B.9 shows that the horizontal stress magnitudes can be estimated if the tensile strength of the rock mass is known with reasonable confidence. However, the tensile strength is normally determined using the Brazilian test. The direct tension test typically gives tensile strength magnitudes that are approximately 70% of the Brazilian strength values. The Brazilian strength for the Forsmark rock is 14.8 MPa which would reduce to approximately 10 MPa in direct tension. At this stage it is not clear if the core disking process results from Brazilian or direct tension loading conditions. Considering the tensile strength of rock in this area the presumable area of stress state could be decided. Using 14.8 MPa, the estimated maximum horizontal stress magnitudes could range between 50 and 60 MPa with the minimum horizontal stress ranging between 30 and 40. However, using 10 MPa tensile strength, estimated magnitudes for the maximum horizontal stress ranges between 30 and 40 MPa and the minimum horizontal stress ranges between 20 and 30 MPa. Clearly knowing the representative tensile strength is important in constraining the stress magnitudes.

B.8 CONCLUSIONS

Three-dimensional elastic and three-dimensional fracture mechanic numerical analyses were used to investigate the failure mechanism of solid core and overcore ring-core disking. The following conclusion arise from these analyses:

- From the stress paths examined, the overcoring generates more uniform tension throughout the core and hence is more susceptible to disking then solid core for the same stress state.

- Core disking in solid core initiates in the circumference of the core stub near the bottom of the hole or below the bottom hole under uniform horizontal stress condition.

- Core disking during the overcoring process is likely to be initiated on the wall of the pilot hole and propagates to the outside as drilling advances.

- The thickness of the core disks may be suitable for estimating the horizontal stress magnitudes if t/d < 0.4 (disk thickness <25 mm).

- The shape of the core disk surface may be used to indicate the anisotropy of the horizontal stress magnitudes. The direction of the maximum horizontal stresses can also be determined from the saddle shape of the disk surface.

- A relationship was established between horizontal stress magnitudes and tensile strength for a vertical stress of 10 MPa. The estimated *in situ* horizontal stresses are sensitive to the magnitude of the tensile strength of the rock mass.

Bibliography

Connel Fracture Group, 2003. *FRANC3D version 2.6 manual*. 118.

Durelli, A.J., Obert, L., Parks, V. 1968. Stresss required to initiate core discing. *Transactions Sociaty of Mining Engineers*. 1065–1073.

Dyke C.G. 1989. Core discing: Its potential as an indicator of principal *in situ* stress directions. In: *Proceedings of ISRM–SPE International Symposium Rock at Great Depth*, *Pau*. Maury, V., Fourmaintraux, D. *editors*. A.A. Balkema, Rotterdam, vol. II, pp. 1057–1064.

Erdogan, F., Sih, G.C. 1963. On the crack extension of plates under plane loading and transverse shear. *J. Basic Engng.* 85: 519–527.

Haimson, B., Fairhurst, C. 1967. Initiation and extension of hydraulic fractures in rocks. *Socitey of Petroleum Engineers Journal*. 310–318.

Haimson B.C., Lee M.Y. 1995. Estimating deep in istu stresses from borehole breakouts and core disking - experimental results in granite. In: *Proceedings of the International Workshop on Rock Stress Measurement at Great Depth, The 8th International Congress on Rock Mechanics, Tokyo*, pp. 19–24.

Jaeger, J.C., Cook, N.G.W. 1963. Pinching-off and disking of rocks. *J. Geophys. Res.* 888(6): 1759–1765.

Kaga, N., Matsuki, K., Sakaguchi, K. 2003. The in situ stress states associated with core discing estimated by analysis of principal tensile stress. *Int. J. Rock Mech. Min. Sci.* 40: 653–665.

Leeman, E.R., Hayes, D.J. 1966. A technique for determining the complete state of stress in rock using a single borehole. In: *Proc. 1st Int. Congn. On Rock Mech.Lisbon.*, vol. 2 pp. 17–24.

Li, Y. 1997. *Drilling-induced core damage and its relationship to crustal in situ state of stress and rock properties.* Ph.D. thesis, University of Alberta, Edmonton, Alberta, Canada

Lim, I.L., Johnston, I.W., Choi, S.K. 1992. Comparison between various displacement-based stress intensity factor computation techniques.. *International Journal of Fracture* 58: 193–210.

Matsuki, K., Kaga, N., Yokoyama, T., Tsuda, N. 2004. Determination of three dimensional in situ stress from core discing based on analysis of principal tensile stress. *Int. J. Rock Mech. Min. Sci.* 44: 1167-1190.

Maury, V.M., Santarelli, F.J., Henry, J.P. 1988. Core discing: a review In: *Proc. 1st Regional ISRM Symposium for Africa: Rock Mechanics in Africa*. Maury, V., Fourmaintraux, D. *editors*. South African National Group on Rock Mechanics, Swaziland, pp. 221–231.

Obert, L., Stephenson, D.E. 1965. Stress conditions under which core discing occurs. *Transactions Sociaty of Mining Engineers*. 232(3): 227–235.

Sjöberg, J., Klasson, H. 2003. Stress measurements in deep boreholes using the Borre (SSPB) probe. *Int. J. Rock Mech. Min. Sci.*

SKB, 2005. Preliminary site description Forsmark area - version 1.2. SKB R-05-18, Swedish Nuclear Fuel and Waste Management Co., Stockholm.

Stacey, T.R. 1982. Contribution to the mechanism of core discing. *Journal South African Institute of Mining and Metallurgy* 99: 269-274.

Sugawara, K., Kameoka, Y., Saito, T., Oka, Y., Hiramatsu, Y. 1978. A study on core disking of rock. *Journal of Japanese Association of Mining* 94: 19-25.